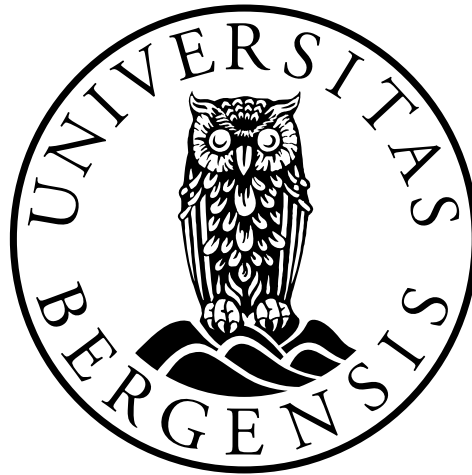# UNIVERSITY OF BERGEN

GEOPHYSICAL INSTITUTE

Master Thesis in Energy

Specialization in Energy Technology

Electrical Power engineering

Dynamic Modelling of Squirrel Cage Induction Motors for Studying Motor Current Signature Analysis

---

By: Andreas Askvik

June 1, 2018

Abstract

This study investigates dynamic modelling of induction motors with a variety of different defects and condition monitoring of these. The focus is directed at squirrel cage induction motors(SCIM) which is the most used electric motor in the world. A motor with this importance needs to be monitored to decrease downtime. The condition monitoring technique used in this study is known as motor current signature analysis(MCSA). MCSA is an on-line condition monitoring technique which uses the frequency spectrum to detect abnormalities. One of its advantages is that measuring the supply current is enough, releasing the need for extra sensors with the motor. This gives the technique an edge, especially in hazardous or difficult accessible areas.

There are four main categories of failure in the SCIM, these are modelled separately before being integrated to a generic model which can be used as a tool in SCIM diagnostics. The models are based on direct-quadrature(DQ) transformation in an ideal and symmetrical machine before being modified in a way that introduces different defects. Every aspect of the model is thoroughly explained with the following assumptions. The results are validated against proven scientific papers on MCSA. Since MCSA is a promising technique in monitoring of subsea induction motors, a cable model with transformers and a pulse-width modulator(PWM) source is also tested with the generic model.

Preface

This master thesis marks the end of my five year education in electrical power engineering. The thesis is a part of the master's degree at the University of Bergen(UiB) in collaboration with Western Norway University of Applied Sciences(HVL).

I would like to thank my supervisor, Assistant Professor Lasse Sivertsen for finding the topic of the thesis and for advising me along the way. I would also like to thank Associate Professor Shujun Zhang for helping with different simulation troubles.

Last but not least, a great thanks to my fellow students with our endless discussions where I always exit a bit brighter.

Table of Contents

List of Figures

List of Tables

List of Abbreviations

BRB   Broken rotor bar

CSI   Current source inverter

DC   Direct current

DFT   Discrete Fourier transform

DQ   Direct quadrature

EMF   Electromotive force

FFT   Fast Fourier transform

GUI   Graphical user interface

IGBT   Insulated-gate bipolar transistor

MCSA   Motor current signature analysis

MMF   Magnetomotive force

MWFA   Modified winding function approach

PID   Proportional-integral-derivative

PWM   Pulse-width modulation

SCIM   Squirrel cage induction motor

VSD   Variable speed drive

VSI   Voltage source inverter

1   Introduction

Electric motors consume more than half of the end-user electricity in the world, 30% of which is used in industrial electric motor-driven systems[1]. The demand in the industrial sector is expected to increase with 70% by 2040[2]. Most of these motors are of the type induction motors. The society is absolutely dependent on the induction motor and consequently it needs to be monitored to decrease downtime.

Dynamic modelling have many great benefits, but the modelling of electric machinery is not straightforward. To make it more comprehensible, a transformation on the variables are often used. This transforms the variables from one reference frame to another. There have been used several different reference frames in analysis of electric machinery over the years, a general approach was not introduced until 1960's[3]. With this approach the reference frame can be rotating in a arbitrary speed, when a specific speed is determined it can be easily assigned.

Motor current signature analysis(MCSA) is an on-line condition monitoring technique which has been developed since the late 1970's[4]. This technique can diagnose faults in the induction motor at a cheap cost and early stage[5]. MCSA may give the operator a chance to get the necessary parts and do maintenance before the fault is developed to a critical stage.

In the offshore oil and gas industry, new resources within distances from 20 - 50 kilometers can be accessed with only subsea components[6]. The pumps and compressors are often driven by squirrel cage induction motors(SCIM) which again is driven by variable speed drives(VSD). Monitoring these motors can be challenging with the ever increasing distances and hopefully this study will give an realistic model when simulating similar cases.

1.1 Background

There have been developed several computer models to study faults in induction motors. These can be divided into categories such as; multiple couple circuit(MCC) models, DQ models, magnetic equivalent circuit(MEC) models and finite element method(FEM) models[7].

In this study the DQ model is used. There are multiple studies on how to modify this model to include stator, rotor and eccentricity fault. A simplified stator fault model which includes inter-turn short circuit or stator unbalance in general is described in[8] and integrated to Simulink in[9]. This is the same case for the rotor, where it is described in[10] and integrated to Simulink in[11]. A simplified model for eccentricity fault based on how the air-gap varies is described in[12]. Mechanical faults in general such as misalignment, unbalance and mechanical looseness are studied in [13]. Using MCSA to test the faulted models were done in all the studies. A specific study on bearing fault modelling and combining any of the other faulted models are not documented as far as the author knows.

As mentioned earlier, the MCSA is a promising technique in the oil and gas industry. There have been done multiple studies on how long cables, transformers and VSDs affect the performance of the SCIM[6, 14]. Using MCSA in this context has also been studied[15], but not a combination of both long cable and VSD. These were also practical tests, using a dynamic simulation to study these concepts has not been documented as far as the author knows.

1.2 Object of Thesis

The goal of this study is to develop a dynamic model of the induction motor with its typical failures. There are several purposes with the model: studying condition monitoring techniques, studying how different failures affect the performance of the motor and to be used as a tool for motor diagnostics. It is well documented that different faults have different frequency response in the stator currents[16]. The faulty models are validated in the frequency domain against approved scientific papers on MCSA. The developed model should also be tested for a cable model and

PWM controller to look at its capabilities for subsea installations. A dynamic model to simulate failure gives several advantages: reducing resources, both in manpower and equipment, reducing time consumption, easier to monitor and avoiding health risks. The model should be realistic, yet simple and easy to manipulate and control.

1.3 Method

The author will carefully examine the DQ model, finding its strength and weaknesses for modelling of faulty induction motors. All the relevant equations will be thoroughly derived and all the taken assumptions will be stated.

The process of developing the faulty models are strategic. First a healthy model is developed and tested, then the faulted models are derived and tested individually against MCSA. The faulty models are developed from both earlier studies and innovative ideas related to how the faults affect the motor. The tested faulty models will be integrated to a generic model. A graphical user interface(GUI) will also be developed to make it easier for an operator.

The last part of this study is to test the generic model in a simulation with subsea components such as PWM, cable model and transformers. This will clarify if the model is capable in a subsea context.

1.4 Structure

The second chapter presents the basics of the induction motor as well as a brief history of its development. Condition monitoring in general is described in this chapter before going into details on MCSA. The spesific response to each of the typical failures are also described in this chapter.

The third chapter develops the dynamic model of the induction motor. Starting with a healthy one and then the faulted ones. Every faulted model are first described by the equations before being integrated in to Simulink. This chapter ends with a generic model and GUI of the Simulink program.

The results are presented in the fourth chapter and discussed in the fifth. The conclusions are made in the sixth chapter with a subsection describing possible future work.

2 Induction Motor

This section will provide the principles of the induction motor by looking at the physical structure and a short look at the electromagnetic physics. The induction motor has its name from how its torque is obtained, by electromagnetic induction. This motor is also known as the asynchronous motor as a result of the speed which lies behind the rotating magnetic field.

2.1 Brief History

The first induction motors were invented separately by Galileo Ferraris and Nikola Tesla, both publishing their findings in 1888[17, 18]. Both Ferraris and Teslas motors relied on two-phase induction. The better three-phase induction motor was invented by Mikhail Dolivo-Dobrovolsky in 1889[19], the same person introduced the squirrel-cage rotor later. The induction motor became a workhorse everywhere in the industry, except for propulsion. However, in the late 1980's the induction motor had an renaissance in this area as a result of new technology in power electronics which led to a range of VSDs. This made the induction motor applicable in all industries[19] .

2.2 Physical Structure

The induction motor consists of two main parts; the stationary part, the stator, and the rotating part, the rotor.

The stator consists of a three-phase winding which is put in slots. The slots and the structure of the stator is composed of high-grade steel laminations. These thin laminations are insulated which helps reducing eddy currents[20]. The windings conduct the alternating currents which creates a rotating magnetic field.

The rotor is constructed by three main parts; an inner supporting structure, a laminated ferromagnetic material and the windings. The windings can be divided in

5

two types, the squirrel-cage winding (squirrel-cage rotor) and the wound-rotor winding (wound rotor)[21].

The squirrel-cage rotor consists of copper or aluminum bars short circuited and embedded in the rotor slots. This type of rotor is not designed for a specific amount of poles. This is a more economical, simpler and rugged machine compared to the wound-rotor, and thereby the most used rotor.

The wound-rotor windings looks more like the stator with windings distributed in slots, and a specific pole number. This type is often referred to as the slip-ring rotor because of the use of slip rings. The slip rings are connected to a external circuit which usually consist of variable resistances. These resistances can help decreasing the starting currents and regulate the speed of the motor. In later years, the use of slip rings to control the speed is for the most part replaced by VSDs.

2.3 Working Principles

In this section a two-pole three-phase motor is studied. The winding arrangements of the stator are distributed around the inner circumference and represented as aa', bb' and cc' as shown in Figure 1
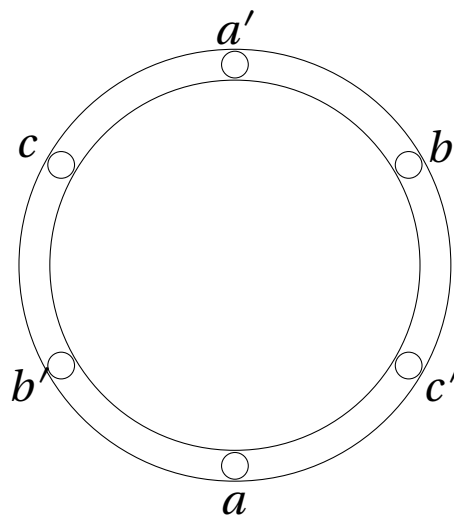
Figure 1: Winding distribution of a 2-pole induction motor

We can start by looking at the three-phase supplying currents which are

$$i_a = I_m \cos \omega_b t$$
$$i_b = I_m \cos(\omega_b t - \frac{2\pi}{3})$$
$$i_c = I_m \cos(\omega_b t + \frac{2\pi}{3})$$

(2.1)

where I_m is the amplitude and $\omega_b = 2\pi f$, where f is the frequency. Equation 2.1 is shown in Figure 2
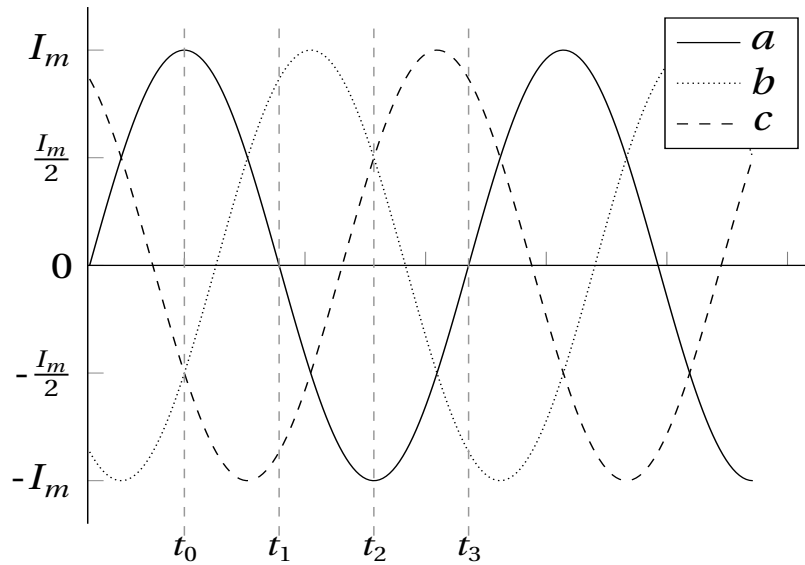
Figure 2: Three-phase current sine wave separated by $\frac{2\pi}{3}$ radians. t_0, t_1, t_2 and t_3 are references to the text[20]

We will use the graphical method to understand how the currents in the stator produces a revolving magnetic field[20]. Let us consider several steps of $\frac{\pi}{2}$ on the x-axis and look at the resulting magnetomotive force (MMF). At $t = t_0$ from Figure 2 the magnitude of the currents are as follows

$$i_a = I_m \qquad i_b = -\frac{I_m}{2} \qquad i_c = -\frac{I_m}{2}$$

(2.2)

The MMF is proportional to the current which produces it, yielding a sinusoidally MMF as well. The direction of the MMF can be found by using the right-hand rule. The direction of the currents are noted by dots and crosses, where these indicates current going out and into the page, respectively. The MMF produced from phase

7

a will be at its maximum and is represented by a vector $F_a = F_{max}$ in the direction of the axis of phase a. The MMF produced by phase b and c will be half the maximum in the opposite direction along their respective axes $F_b = F_c = \frac{F_{max}}{2}$. Adding these three will result in a MMF $\boldsymbol{F} = \frac{3}{2}F_{max}$ as shown in Figure 3
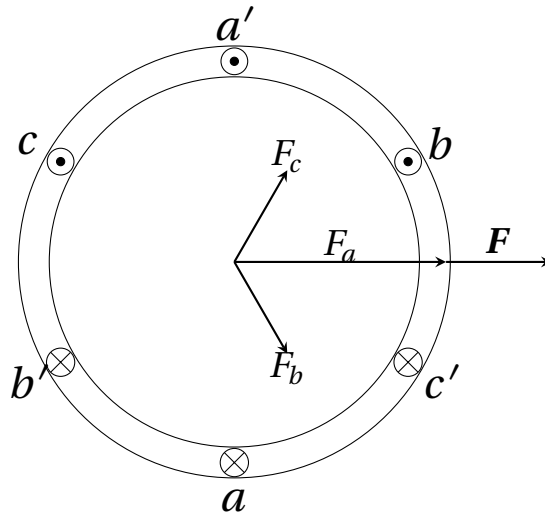
Figure 3: Resulting magnetomotive force at $t = 0$. Dots indicates current going into the page and crosses indicates current coming out from the page. MMF direction can be found by right-hand rule.

If we look at $t = t_1$ from Figure 2 the currents and MMFs are

$$i_a = 0 \qquad F_a = 0$$

$$i_b = \frac{\sqrt{3}}{2} I_m \qquad F_b = \frac{\sqrt{3}}{2} F_{max}$$

$$i_c = -\frac{\sqrt{3}}{2} I_m \qquad F_c = -\frac{\sqrt{3}}{2} F_{max}$$

this yields a MMF distribution as follows.
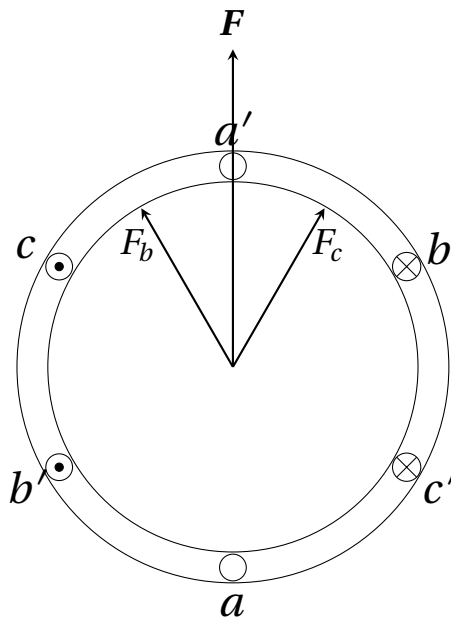
Figure 4: Resulting magnetomotive force at $t = t_1$. Dots indicates current going into the page and crosses indicates current coming out from the page. MMF direction can be found by right-hand rule.

The next two intervals $t = t_2$ and $t = t_3$ can be shown respectively as
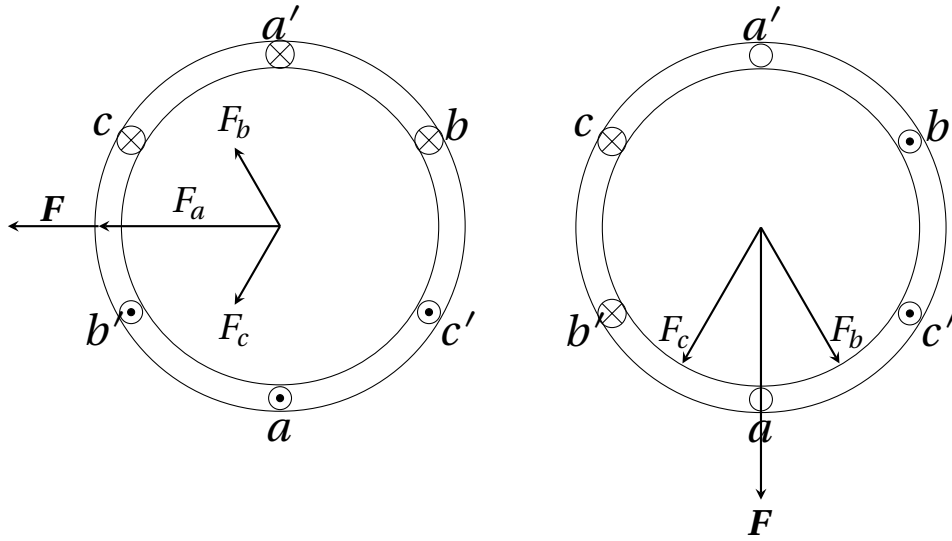
Figure 5: Resulting MMF at $t = t_2$ and $t = t_3$, respectively. Dots indicates current going into the page and crosses indicates current coming out from the page. MMF direction can be found by right-hand rule.

The resulting MMF will continue rotating with the currents. In a 2-pole machine as we studied, the MMF rotates one round per period. In a P-pair pole machine the speed in revolutions per minute (rpm) can be found as

$$n_s = \frac{2 \cdot 60 f}{P}$$

where f is the supply frequency and P is the pole pair. This speed is often referred to as synchronous speed. As earlier mentioned the induction motor is often referred to as the asynchronous motor, this is because the rotor does not rotate at the same speed as the MMF, but behind. The speed difference between the synchronous speed and the rotor speed is known as slip s and defined as

$$s = \frac{n_s - n_r}{n_s}$$

It is the amount of magnetic flux under each pole which determines the induced voltage and developed torque in the induction motor. The flux under per pole can

be determined by integrating the flux density distribution in the air-gap[22]

$$\Phi_{pole} = \int_{-\pi/2}^{\pi/2} \frac{B_{max}}{P} l\, r \cos(\theta) = \frac{2}{P} B_{max} l\, r \qquad (2.3)$$

where l is the axial length of the stator and r is the mean radius of the stator air-gap. The flux linkages will vary with the coils position and the flux density. The maximum flux linked will be $N\Phi_{pole}$ where N is the amount of turns in the coil. If we let the time when the coil's axis coincides with the maximum of flux B be zero, this yields a flux linkage as follows

$$\lambda(t) = N\Phi_{pole} \cos(\omega_b t) \qquad (2.4)$$

If we assume that the flux density distribution and flux per pole are constant(which it normally is under steady-state operation), the induced voltage can be obtained by Faraday's law as

$$e = -\frac{d\lambda(t)}{dt} = \omega_b N\Phi_{pole} \sin(\omega_b t) \qquad (2.5)$$

The induced voltage produces currents in either the rotor bars or the rotor windings. From the current a new MMF is produced, this MMF reacts with the stator MMF and produces a torque. The torque is only produced when there is a relative speed between the rotor and rotating MMF. This means that in motoring mode $s > 0$ as a result of losses in the motor.

The frequency of the current in the rotor is dependent on the rotor speed relative to the synchronous field. When starting at $0\, rpm$ the frequency in the rotor is the same as in the stator, but when the rotor speed increases the frequency decreases. The relationship between the current frequency in the rotor f_{sr} often referred to as slip frequency and stator is found as

$$f_{sr} = s f$$

where s is the slip and f is the supply frequency.

2.4 Induction Motor Speed Control

As mentioned, the induction motor became a workhorse everywhere in the industry except for propulsion, the reason for this is the difficulties controlling the speed and torque. The induction motor was more a fixed speed motor. When variable speeds were necessary, a direct-current(DC) motor was normally used. However, the DC-motor are more expensive, needs more maintenance and are not suitable in hazardous areas[20]. When the VSD came to the market the induction motor became applicable in all industries. By manipulating the voltage and frequency, the speed and torque could easily be controlled.

2.4.1 Variable Speed Drive

A VSD can be classified into different categories. The main categories are voltage source inverters(VSI) and current source inverters(CSI). The VSI drive is the more applicable of the two[23] and the one being further discussed. The VSI can also be divided into different categories on how it is run, but the focus in this study is on pulse-width-modulated(PWM) inverters. The goal with a PWM inverter in a motoring context is to create a desired frequency and voltage which will control the motor. The output of a PWM running at $50Hz$ with a DC voltage of $300V$ is showed in Figure 6.
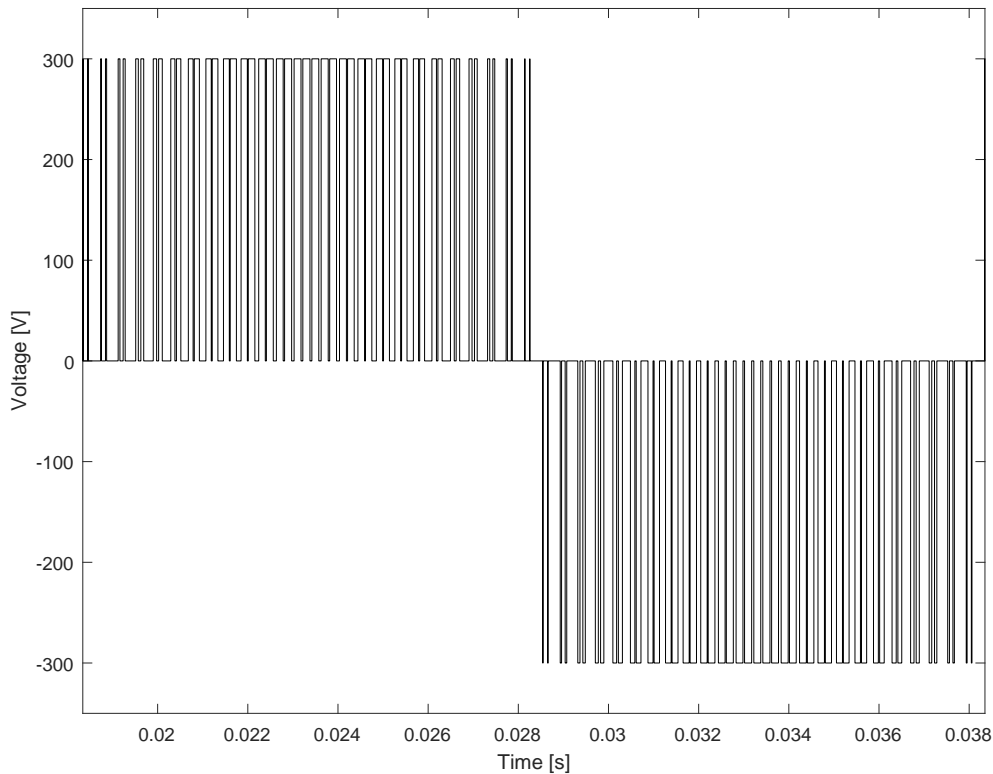
Figure 6: Simulated PWM ouput voltage with $300V$ DC value and $50Hz$ frequency. Illustrating how a output voltage can be from a VSD in steady state.

As shown in the figure, the output from a PWM inverter is a pulsating DC voltage. The variable voltages are acquired from some sort of switching mode, for example insulated-gate bipolar transistors(IGBT).

2.5   Condition monitoring

Condition monitoring is a process where the parameters of the subject are monitored. If any changes from regular operations occur, they can indicate present or future failures. This will give the observer an insight of the state of the subject, and a chance to do maintenance if necessary.

In the developed countries the average modern home contains 20-30 electric motors in the range of $0-1kW$. These are relatively small motors and are typically used in toys, kitchen equipment, clocks and so on. Also, these countries are heavily dependent on machines of bigger dimensions. Generators used in production

of electricity is often in MWs and can exceed $1000MW$. In the industry the motors used to drive pumps, compressors, or propulsion can range from $100kW$ to $100MW$[24].

Condition monitoring is not relevant for all the motors in existence, for many of the smaller motors their lifetime regularly expand the lifetime of the parent product. In the bigger motors and especially motors with higher consequences in failures, condition monitoring can be crucial. Machines with lower power than $20kW$ would likely not benefit from condition monitoring, unless the machine has a vital function[24].

2.5.1 Techniques

There are numerous on-line condition monitoring techniques of induction motors, both electrical and mechanical. The mechanical techniques can be, vibration monitoring, temperature monitoring, chemical and wear monitoring[24] etc. The electrical techniques are power monitoring, electrical discharge monitoring, MCSA and so on.

MCSA is the most preferred non-invasive technique for condition monitoring of induction motors[16]. This technique uses the frequency domain based on fast Fourier transform(FFT). By analyzing the spectrum acquired from the stator or supply current, different types of fault and developing faults can be detected. The FFT is further explained in section 2.6.

2.5.2 Different Types of Fault

There are four main types of faults in induction motors; rotor faults, eccentricity faults, bearing faults and stator faults. These four types account for more than 90% of all faults in induction motors[5].

Rotor Faults   Although the rotor in a induction motor is rugged, faults do occur. Rotor related faults accounted for at least 10% on utility-sized motors (>100hp)[25].

The biggest reason for this is due to the starting duties where the currents are as high as 9 times rated current[21] which result in high thermal stress. This stress will regularly not result in momentarily breakdown[5], but can instead over time result in broken rotor bars or end-rings. A squirrel cage rotor without the core can be seen in Figure 7, it is clear that when one of the rotors or end rings breaks or partially breaks, the stress will increase on the healthy ones. Other sources of failure are: magnetic stress caused by electromagnetic forces, residual stress due to manufacturing problems, mechanical stress due to loose laminations[16].
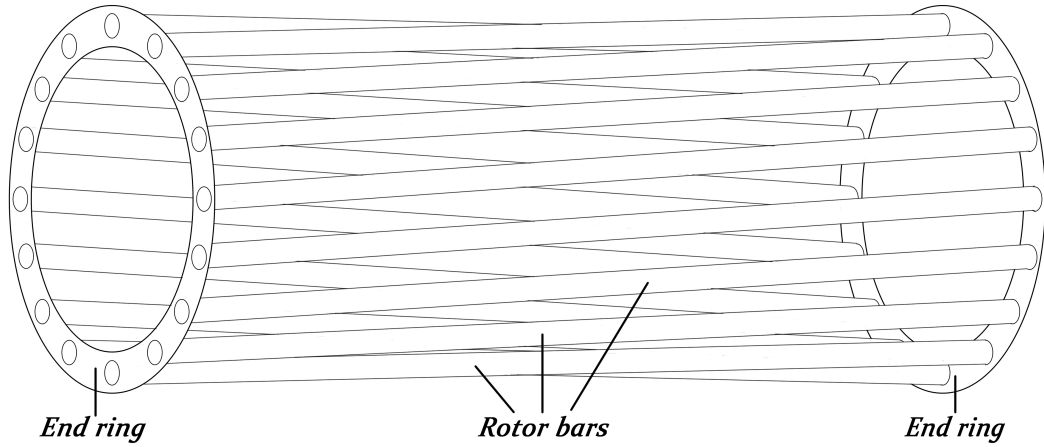
Figure 7: Squirrel cage rotor without a core and with skewed rotor bars. The rotor bars are short-circuited by the end rings, breaking or partially breaking will result in higher stress on undamaged bars or end rings.

The frequency components produced by broken rotor bars can be found as[16]

$$f_{BRB} = (1 \pm 2ns)f \tag{2.6}$$

where s is the slip, f is the supply frequency and $n = 1, 2, 3....$

Based on numerous case histories the amount of broken rotor bars under full load can be estimated from the FFT results as follows[26]

$$n = \frac{2R}{10^{\frac{N_{dB}}{20}} + P} \tag{2.7}$$

where R is the amount of rotor bars, N_{dB} is the mean difference between the two sidebands ($50 \pm 2s50$) and the supply frequency f and P is the pole-pair.

Eccentricity fault   An eccentricity fault is when a non-uniform distance in the air between rotor and stator occurs, this air is referred to as the air-gap. We can divide this type of fault in two categories, static- and dynamic eccentricity[16]. Static eccentricity is when the rotor is at constant offset from the center, the air-gap is constant, although not uniform as shown in the three bottom figures from Figure 8. From the stator perspective the air-gap looks constant. The reason for static eccentricity can be a ovality of the stator core or a tilt in stator, rotor or both. Dynamic eccentricity is when the non-uniform air-gap revolves with the rotor, from the rotors perspective it looks constant as shown at the top three figures from Figure 8. Dynamic eccentricity may be caused by bent rotor shaft, bearing wear, misalignment, etc.[16]. In reality both of these usually coexist in some degree.
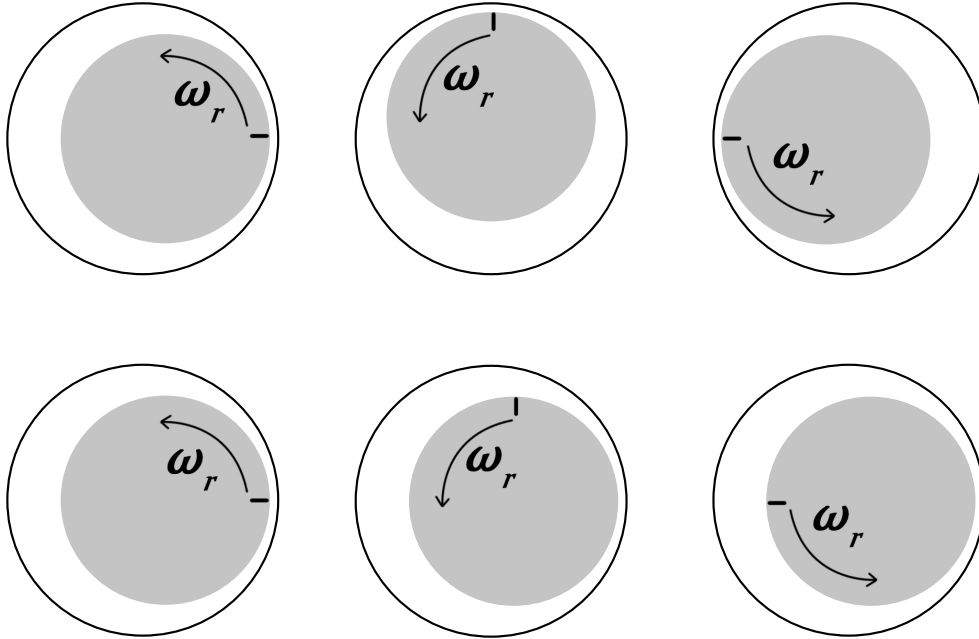
Figure 8: The different types of eccentricity. The top three are dynamic eccentricity, the bottom three are static eccentricity

The frequency components produced by the eccentricity fault can be obtained by

$$f_{ecc1} = f\left[(nR \pm n_d)\left(\frac{1-s}{P}\right) \pm h\right] \tag{2.8}$$

where f is the supply frequency, n is any integer, R is the number of rotor bars, n_d is the eccentricity order number, P is the number of pole pairs, s is the slip and h is the harmonic of the stator MMF time harmonics[27]. For a static eccentricity fault $n_d = 1, 2, 3$ and for dynamic eccentricity fault $n_d = 0$.

f_{ecc1} is at the higher frequencies. In the case of mixed eccentricity low frequency components is also produced. These are given by

$$f_{ecc2} = (f \pm n f_r) \tag{2.9}$$

where

$$f_r = \frac{1-s}{P} f \quad f, s, P \quad \text{and} \quad n \quad \text{is the same as in} \quad f_{ecc1}$$

Bearing fault Bearing faults accounts for more than 40% of all faults in electric motors[28]. Bearing faults can be a result of numerous non-ideal conditions like ambient mechanical vibration, misalignment, corrosion, wrong lubrication and so on[16]. Over time these minor impacts becomes significant and mechanical vibration occurs.

The main causes of vibration is divided by outer raceway defect, inner raceway defect, ball defect and cage defect. These mechanical vibrations cause a slight rotor displacement in the air gap, which is like an instant eccentricity. MCSA can be used to find these defects and the frequency components produced are[27]

$$f_{ob} = \frac{N}{2} f_r \left(1 - b_d \frac{\cos(\beta)}{p_d} \right) \qquad \text{outer bearing race defect}$$

$$f_{ib} = \frac{N}{2} f_r \left(1 + b_d \frac{\cos(\beta)}{p_d} \right) \qquad \text{inner bearing race defect}$$

$$f_b = \frac{p_d}{b_d} f_r \left(1 - \left(b_d \frac{\cos(\beta)}{p_d} \right)^2 \right) \qquad \text{ball race defect}$$

$$f_c = \frac{1}{2} f_r \left(1 - b_d \frac{\cos(\beta)}{p_d} \right) \qquad \text{cage defect}$$

where f_r is the mechanical rotational frequency $\left(f_r = \frac{2(1-s)}{P}f\right)$, N is the number of bearing balls, b_d is the ball diameter, p_d is the ball pitch diameter and β is the contact angle between the ball and the races. Figure 9 shows a typical bearing geometry[5]. In the frequency spectrum the vibration frequencies can be found as

$$f_{BF} = |f \pm n f_x|$$

where f is the fundamental frequency, $n = 1, 2, 3...$ and f_x is one of the frequencies components above.
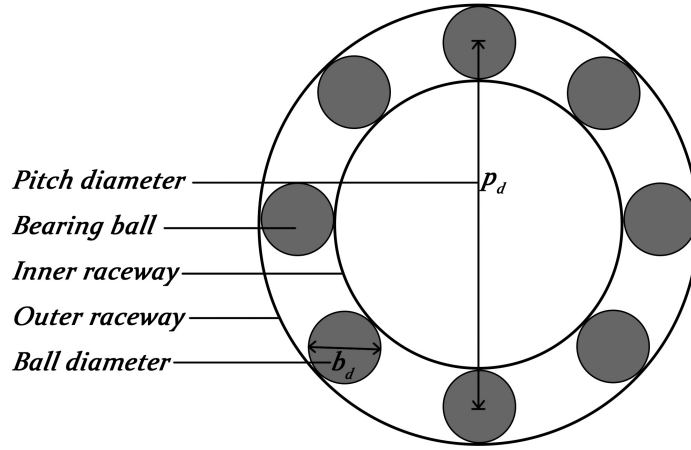
Figure 9: Typical geometry of a bearing with labels on relevant parameters

Stator faults   37% of all electric motor failures occurs as a result of stator faults[28]. This type of fault is often due to stator inter-turn winding fault caused by insulation breakdown and will result in an unbalanced stator[29]. The insulation breakdown can be caused by numerous reasons, such as; high stator core or winding temperature, short circuit or starting stress, partial discharges, etc.[16]. A key feature when monitoring for stator fault is a quick detection and response because of the high progress rate, often in the matter of seconds[5]. The stator inter-turn fault produces stator current harmonics such as[30]

$$f_{ss1} = \left(k \pm n\frac{1-s}{p}\right)f \tag{2.10}$$

where $k = 1,3,5...$, $n = 1,2,3...$, s is slip, P is pole pair and f is supply frequency. However, since this is the same frequency component as produced by mixed eccentricity it is not enough to determine stator fault alone.

One frequency component which can identify the stator fault is the odd harmonics[31].

$$f_{ss2} = 3kf \qquad (2.11)$$

where f is the supply frequency and $k = 1,3,5....$

2.6 Fast Fourier Transform

As mentioned earlier, a FFT will be used on the current to extract the frequency spectrum that is needed for the analysis. FFT is an algorithm which computes the discrete Fourier transform(DFT) in an efficient way. J.W. Cooley and J. Tukey are recognized as creators of the FFT when they published "An Algorithm for the Machine Calculation of Complex Fourier Series" in 1965 [32], although it may look like the German mathematician Carl Friedrich Gauss invented the same algorithm already in 1805[33]. To understand both FFT and DFT a short review of the Fourier transformation is appropriate.

2.6.1 Fourier Transform

The Fourier transform takes a signal from the time domain and describes it in the frequency domain. The inverse Fourier transform will do the opposite. The Fourier transform is defined as[34]

$$X(F) = \int_{-\infty}^{\infty} x(t)e^{-j2\pi F t}\, dt \qquad (2.12)$$

and its inverse

$$x(t) = \int_{-\infty}^{\infty} X(F)e^{j2\pi x t}\, dF \qquad (2.13)$$

where x is a function of time t, F is the frequency and $j = \sqrt{-1}$. Both these are continuous functions, and when going from analog to digital the signal can not be sampled continuously, instead there will be set of discrete values or bins. This is why the discrete Fourier transform is used when converting signal from time domain to frequency domain.

2.6.2 Discrete and Fast Fourier Transform

The discrete Fourier transform is defined as

$$X_k = \sum_{n=0}^{N-1} x_n e^{\frac{-j2\pi rk}{N}} \tag{2.14}$$

and its inverse

$$x_n = \frac{1}{N} \sum_{k=0}^{N-1} X_k e^{\frac{j2\pi nk}{N}} \tag{2.15}$$

where N is the number of samples, x_n denotes the nth sample, X_k is the kth coefficient of the DFT and $j = \sqrt{-1}$[35]. The integral operator is now exchanged with a summation operator, because of the signals discrete values.

The FFT is a technique which performs the DFT in a efficient way. For comparison the computations of DFT simply on the definition are N^2 where N is the number of samples. With the FFT algorithm the number of computations are $2N \log_2 N$[35]. For illustrative purposes if there are 1024 samples the number of computations will be 1 048 576 and 20 480 for direct DFT and FFT, respectively.

The FFT also has its limitations, one of these is when measuring a over a non-integer number of periods or non-periodic functions. This results in spectral leakage which gives a unrealistic view of the frequency spectrum. By using windowing on the raw data before the FFT, we can reduce the effects of spectral leakage, enhancing the FFT to extract spectral data, but windowing can also decrease resolution[36].

2.7 DQ model

The DQ model also known as the two-axis model, is used in many cases for dynamic analysis of electric machinery. The model transforms the variables to a common reference frame, which makes the flux independent from rotor position.

2.7.1 Background

There are several variable changes used in the analysis of induction machines. In 1929 R. H. Park published[37], which introduced a new approach of referring the variables related to the stator over to the reference frame of the rotor. This was derived for a synchronous machine where the rotor rotates at the same speed as the rotating MMF and is commonly referred as the Park's transformation.

In 1938 H. C. Stanley published[38], where he showed how to transform the variables from the rotor to the stator. This transformation is commonly referred to as the "stationary reference frame". In G. Kron's book[39], he introduced a change in variables which transformed the stator- and rotor variables to a synchronously rotating reference frame, which is commonly known as the "synchronous reference frame".

As mentioned, the Park's transformation was meant for the synchronously machine. In 1957 D. S. Brereton et al.[40] showed how to change the variables by transforming the stator variables to a reference frame fixed on the rotor. This is the Park's transformation equivalent for induction machines. Common for all of these approaches are the elimination of time-varying inductances. Which approach to use is determined by the particular application[41].

All of these different approaches were derived and treated separately until a general transformation was derived in 1965 by P. C. Krause and C. H. Thomas[3]. Now the variables associated with the stator and rotor can be referred to a frame of reference that may be stationary or rotate at any angular velocity, known as the "arbitrary reference frame". To obtain any of the known transformations simply assign the appropriate speed of rotation.

3 Modelling of Induction Motor

There are many advantages with modelling and simulation, such as reducing the needs for resources both in manpower and cost, avoiding health risking experiments, reducing time consumption and making it easier to monitor every aspect of the object. On the other hand, there are many assumptions to be made when deciding which model to use. A good model should be realistic, simple to understand and easy to manipulate, though these often are restricting requirements. Realistic models are seldom simple and simple models are rarely realistic[22]. In this chapter the induction motor model will be thoroughly explained both in a healthy and compromised condition.

3.1 Healthy Induction Motor Model

For a three-phase, two-pole, wye connected symmetrical machine the winding arrangement is shown in Figure 10 and the equivalent circuit in Figure 11[41].
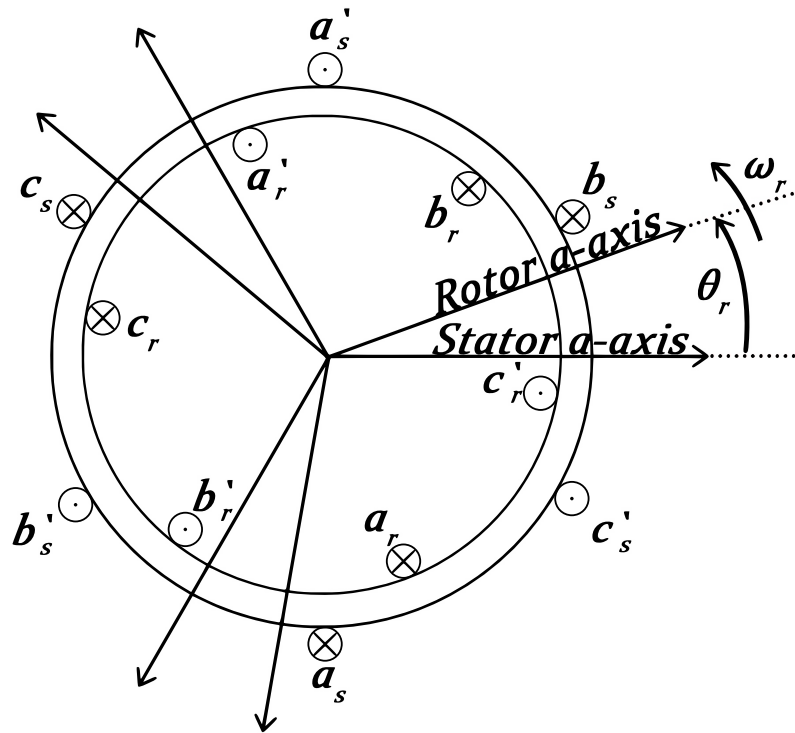
Figure 10: Two-pole, three-phase symmetrical induction machine. Lower case *s* and *r* indicates stator- and rotor variables, respectively. Dots indicates current coming out from page and cross indicates current going into page. ω_r is angular velocity of rotor and θ_r is rotor angle with stator a-axis as reference
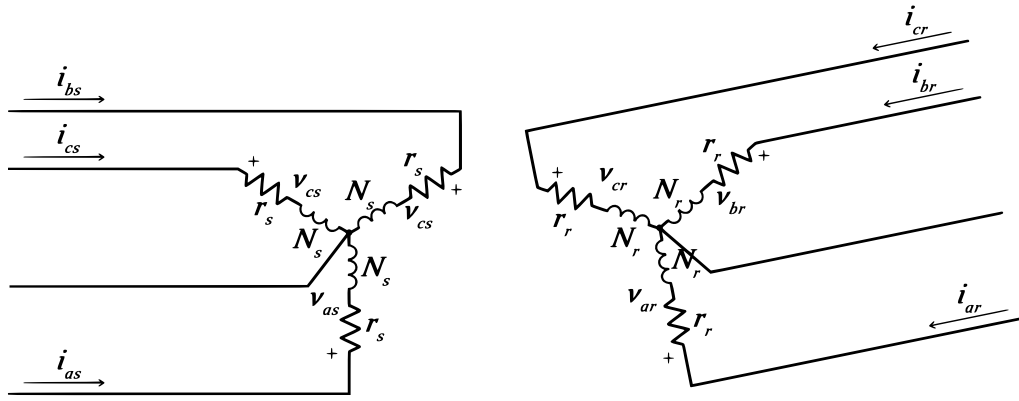
Figure 11: Equivalent circuit for a two-pole, three-phase symmetrical induction machine. The rotor circuit is tilted which indicates the speed difference from stator MMF speed and rotor speed.

Before looking at the equations of the machine, the assumptions made in the model will be declared. Normally in induction machines the rotor bars are skewed to reduce harmonic torques, this design is not featured in this model. Instead of saturation of the magnetic fields, there will be a linear relation. The change in resistance due to temperature and frequency variations will be neglected and also, the iron losses in both stator and rotor are neglected[3].

The model is of an ideal machine, accordingly the stator windings are identical and sinusoidally distributed 120° apart, with N_s equivalent turns. The rotor will also be considered as three identical windings sinusoidally distributed 120° apart with N_r equivalent turns[41], also for a squirrel-cage rotor. Both the stator resistance r_s and rotor resistance r_r will have the same phase values and the air-gap is uniform.

The voltage equations can be found by using coupled circuit approach and may be expressed in matrix notation for the stator and rotor respectively as[22]

$$
\begin{aligned}
\boldsymbol{v}_s^{abc} &= \boldsymbol{i}_s^{abc} \boldsymbol{r}_s + \frac{d\boldsymbol{\lambda}_s^{abc}}{dt} \\
\boldsymbol{v}_r^{abc} &= \boldsymbol{i}_r^{abc} \boldsymbol{r}_r + \frac{d\boldsymbol{\lambda}_r^{abc}}{dt}
\end{aligned}
\tag{3.1}
$$

where stator resistance $\boldsymbol{r}_s$ and rotor resistance $\boldsymbol{r}_r$ are diagonal matrices

$$\boldsymbol{r}_s = \begin{bmatrix} r_s & 0 & 0 \\ 0 & r_s & 0 \\ 0 & 0 & r_s \end{bmatrix} \qquad \boldsymbol{r}_r = \begin{bmatrix} r_r & 0 & 0 \\ 0 & r_r & 0 \\ 0 & 0 & r_r \end{bmatrix} \tag{3.2}$$

and

$$\boldsymbol{v}_s^{abc} = \begin{bmatrix} v_{as} \\ v_{bs} \\ v_{cs} \end{bmatrix} \quad \boldsymbol{v}_r^{abc} = \begin{bmatrix} v_{ar} \\ v_{br} \\ v_{cr} \end{bmatrix} \quad \boldsymbol{i}_s^{abc} = \begin{bmatrix} i_{as} \\ i_{bs} \\ i_{cs} \end{bmatrix} \quad \boldsymbol{i}_r^{abc} = \begin{bmatrix} i_{ar} \\ i_{br} \\ i_{cr} \end{bmatrix}$$

$$\boldsymbol{\lambda}_s^{abc} = \begin{bmatrix} \lambda_{as} \\ \lambda_{bs} \\ \lambda_{cs} \end{bmatrix} \quad \boldsymbol{\lambda}_r^{abc} = \begin{bmatrix} \lambda_{ar} \\ \lambda_{br} \\ \lambda_{cr} \end{bmatrix}$$

The flux linkage equations can be written as

$$\begin{bmatrix} \boldsymbol{\lambda}_s^{abc} \\ \boldsymbol{\lambda}_r^{abc} \end{bmatrix} = \begin{bmatrix} \boldsymbol{L}_{ss}^{abc} & \boldsymbol{L}_{sr}^{abc} \\ \boldsymbol{L}_{rs}^{abc} & \boldsymbol{L}_{rr}^{abc} \end{bmatrix} \begin{bmatrix} \boldsymbol{i}_s^{abc} \\ \boldsymbol{i}_r^{abc} \end{bmatrix} \tag{3.3}$$

$\boldsymbol{L}_{ss}^{abc}$ and $\boldsymbol{L}_{rr}^{abc}$ are symmetrical matrices of the self inductance of the stator and rotor windings where

$$\boldsymbol{L}_{ss}^{abc} = \begin{bmatrix} L_{ls} + L_{ss} & L_{sm} & L_{sm} \\ L_{sm} & L_{ls} + L_{ss} & L_{sm} \\ L_{sm} & L_{sm} & L_{ls} + L_{ss} \end{bmatrix} \tag{3.4}$$

$$\boldsymbol{L}_{rr}^{abc} = \begin{bmatrix} L_{lr} + L_{rr} & L_{rm} & L_{rm} \\ L_{rm} & L_{lr} + L_{rr} & L_{rm} \\ L_{rm} & L_{rm} & L_{lr} + L_{rr} \end{bmatrix} \tag{3.5}$$

The mutual inductance between the stator and rotor also known as the magnetizing

inductance is dependent on the rotor angle and may be expressed as

$$\boldsymbol{L}_{sr}^{abc} = \left[\boldsymbol{L}_{rs}^{abc}\right]^T = L_{sr} \begin{bmatrix} \cos\theta_r & \cos\left(\theta_r + \frac{2\pi}{3}\theta_r\right) & \cos\left(\theta_r - \frac{2\pi}{3}\theta_r\right) \\ \cos\left(\theta_r - \frac{2\pi}{3}\theta_r\right) & \cos\theta_r & \cos\left(\theta_r + \frac{2\pi}{3}\theta_r\right) \\ \cos\left(\theta_r + \frac{2\pi}{3}\theta_r\right) & \cos\left(\theta_r - \frac{2\pi}{3}\right) & \cos\theta_r \end{bmatrix} \quad (3.6)$$

L_{ls} is the per phase stator winding leakage inductance and correspondingly for the rotor L_{lr}. L_{ss} and L_{rr} are the self inductance of the stator winding and rotor winding, respectively. L_{sm} is the mutual inductance between the stator windings and L_{rm} is the mutual inductance between the rotor windings. L_{sr} is the amplitude of the stator-to-rotor mutual inductance[22]. Note that only the mutual inductance between the stator and rotor is dependent on the rotor angle θ_r.

3.2 Changing Reference Frame

As shown in Equation 3.6 the mutual inductances will vary with respect to the rotor angle θ_r. This variation is undesirable, but can be eliminated by a change of the variables, which can transform both the current and voltage from rotor and stator to a common reference frame[3].

3.2.1 Arbitrary Reference Frame

Before deciding which reference frame to use, the arbitrary reference frame will be derived. We will use the $q, d, 0$ variables. The rotation speed ω is rotating in the same direction as the rotor in an arbitrary speed. The geometrical relationship between traditional abc and arbitrary $qd0$ reference frame is illustrated in Figure 12.
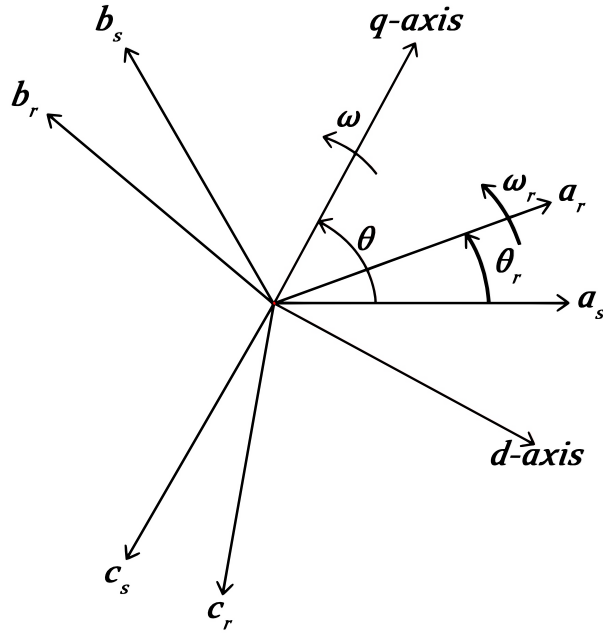
Figure 12: Geometrical relationship between abc and $qd0$ reference frame. ω is the arbitrary speed while ω_r is the rotor angular speed. The stator and rotor variables are noted with subscript s and r respectively.

To get from abc to arbitrary $qd0$ we'll use the arbitrary $qd0$ transformation which is given by

$$
\begin{bmatrix} f_q \\ f_d \\ f_0 \end{bmatrix} = \begin{bmatrix} \boldsymbol{T}_{qd0}(\theta) \end{bmatrix} \begin{bmatrix} f_a \\ f_b \\ f_c \end{bmatrix} \tag{3.7}
$$

where

$$
\begin{bmatrix} \boldsymbol{T}_{qd0}(\theta) \end{bmatrix} = \frac{2}{3} \begin{bmatrix} \cos(\theta) & \cos(\theta - \frac{2\pi}{3}) & \cos(\theta + \frac{2\pi}{3}) \\ \sin(\theta) & \sin(\theta - \frac{2\pi}{3}) & \sin(\theta + \frac{2\pi}{3}) \\ \frac{1}{2} & \frac{1}{2} & \frac{1}{2} \end{bmatrix} \tag{3.8}
$$

The variable f can be phase voltages, currents or flux linkages. The transformation angle $\theta(t)$ which is the angle between the a-axis of the stationary stator winding and the q-axis rotating at the arbitrary speed ω may be expressed as

$$
\theta(t) = \int_0^t \omega(t) dt + \theta(0)
$$

Also for the rotor angle θ_r which is the angle between the stator and rotor a-phases can be found for a rotor rotating at the speed $\omega_r(t)$ by

$$\theta_r(t) = \int_0^t \omega_r(t)dt + \theta_r(0) \tag{3.9}$$

$\theta(0)$ and $\theta_r(0)$ are the initial angles, when $t = 0$. The inverse arbitrary $qd0$ transform is given as

$$\left[\boldsymbol{T}_{qd0}(\theta)\right]^{-1} = \begin{bmatrix} \cos(\theta) & \sin(\theta) & 1 \\ \cos\left(\theta - \frac{2\pi}{3}\right) & \sin\left(\theta - \frac{2\pi}{3}\right) & 1 \\ \cos\left(\theta + \frac{2\pi}{3}\right) & \sin\left(\theta + \frac{2\pi}{3}\right) & 1 \end{bmatrix} \tag{3.10}$$

3.3 $qd0$ Equations

The abc equations are transformed to $qd0$ in this section, by using the transformation described in the last section.

3.3.1 $qd0$ Voltage Equations

The stator abc voltage from Equation 3.1 can be expressed as

$$\boldsymbol{v}_s^{abc} = p\boldsymbol{\lambda}_s^{abc} + \boldsymbol{r}_s^{abc}\boldsymbol{i}_s^{abc}$$

where p equals the operator $\frac{d}{dt}$. By applying $[\boldsymbol{T}_{qd0}(\theta)]$ to the voltage, flux linkage and current, the equation becomes

$$\boldsymbol{v}_s^{qd0} = [\boldsymbol{T}_{qd0}(\theta)]p[\boldsymbol{T}_{qd0}(\theta)]^{-1}\boldsymbol{\lambda}_s^{qd0} + [\boldsymbol{T}_{qd0}(\theta)]\boldsymbol{r}_s^{abc}[\boldsymbol{T}_{qd0}(\theta)]^{-1}\boldsymbol{i}_s^{qd0}$$

$$\boldsymbol{v}_s^{qd0} = \omega \begin{bmatrix} 0 & 1 & 0 \\ -1 & 0 & 0 \\ 0 & 0 & 0 \end{bmatrix} \boldsymbol{\lambda}_s^{qd0} + p\boldsymbol{\lambda}_s^{qd0} + \boldsymbol{r}_s^{qd0}\boldsymbol{i}_s^{qd0} \tag{3.11}$$

A similar approach is used when transforming the rotor voltages, except the transformation angle which is now $\theta - \theta_r$, yielding

$$\boldsymbol{v}_r^{qd0} = (\omega - \omega_r) \begin{bmatrix} 0 & 1 & 0 \\ -1 & 0 & 0 \\ 0 & 0 & 0 \end{bmatrix} \boldsymbol{\lambda}_r^{qd0} + p\boldsymbol{\lambda}_r^{qd0} + \boldsymbol{r}_r^{qd0} \boldsymbol{i}_r^{qd0} \qquad (3.12)$$

A more detailed deriving for both $\boldsymbol{v}_s^{qd0}$ and $\boldsymbol{v}_r^{qd0}$ can be found in appendix A.2.1 and A.2.2.

3.3.2 $qd0$ Flux Linkage Equations

To obtain the $qd0$ flux linkages for the stator and rotor, $[\boldsymbol{T}_{qd0}(\theta)]$ and $[\boldsymbol{T}_{qd0}(\theta - \theta_r)]$ are used[22]. For the stator from equation 3.3

$$\boldsymbol{\lambda}_s^{qd0} = [\boldsymbol{T}_{qd0}(\theta)](\boldsymbol{L}_{ss}^{abc} \boldsymbol{i}_s^{abc} + \boldsymbol{L}_{sr}^{abc} \boldsymbol{i}_r^{abc})$$

$$\boldsymbol{\lambda}_s^{qd0} = [\boldsymbol{T}_{qd0}(\theta)]\boldsymbol{L}_{ss}^{abc}[\boldsymbol{T}_{qd0}(\theta)]^{-1}\boldsymbol{i}_s^{qd0} + [\boldsymbol{T}_{qd0}(\theta)]\boldsymbol{L}_{sr}^{abc}[\boldsymbol{T}_{qd0}(\theta - \theta_r)]^{-1}\boldsymbol{i}_r^{qd0}$$

$$\boldsymbol{\lambda}_s^{qd0} = \begin{bmatrix} L_{ls} + \frac{3}{2}L_{ss} & 0 & 0 \\ 0 & L_{ls} + \frac{3}{2}L_{ss} & 0 \\ 0 & 0 & L_{ls} \end{bmatrix} \boldsymbol{i}_s^{qd0} + \begin{bmatrix} \frac{3}{2}L_{sr} & 0 & 0 \\ 0 & \frac{3}{2}L_{sr} & 0 \\ 0 & 0 & 0 \end{bmatrix} \boldsymbol{i}_r^{qd0}$$

The $qd0$ rotor flux linkages is given similarly

$$\boldsymbol{\lambda}_r^{qd0} = [\boldsymbol{T}_{qd0}(\theta - \theta_r)]\boldsymbol{L}_{rs}^{abc}[\boldsymbol{T}_{qd0}(\theta)]^{-1}\boldsymbol{i}_s^{qd0} + [\boldsymbol{T}_{qd0}(\theta - \theta_r)]\boldsymbol{L}_{rr}^{abc}[\boldsymbol{T}_{qd0}(\theta - \theta_r)]^{-1}\boldsymbol{i}_r^{qd0}$$

$$\boldsymbol{\lambda}_r^{qd0} = \begin{bmatrix} \frac{3}{2}L_{sr} & 0 & 0 \\ 0 & \frac{3}{2}L_{sr} & 0 \\ 0 & 0 & 0 \end{bmatrix} \boldsymbol{i}_s^{qd0} + \begin{bmatrix} L_{ls} + \frac{3}{2}L_{ss} & 0 & 0 \\ 0 & L_{ls} + \frac{3}{2}L_{ss} & 0 \\ 0 & 0 & L_{ls} \end{bmatrix} \boldsymbol{i}_r^{qd0}$$

A more detailed deriving of the four inductance matrices can be found in A.2.5, A.2.6, A.2.7 and A.2.8. By using these relationships $L_m = \frac{3}{2}L_{ss} = \frac{3}{2}\frac{N_s}{N_r}L_{sr} = \frac{3}{2}\frac{N_s}{N_r}L_{rr}$

we can compactly express the stator and rotor flux linkage relationship as follows

$$
\begin{bmatrix} \lambda_{qs} \\ \lambda_{ds} \\ \lambda_{0s} \\ \lambda'_{qr} \\ \lambda'_{dr} \\ \lambda'_{0r} \end{bmatrix} = \begin{bmatrix} L_{ls} + L_m & 0 & 0 & L_m & 0 & 0 \\ 0 & L_{ls} + L_m & 0 & 0 & L_m & 0 \\ 0 & 0 & L_{ls} & 0 & 0 & 0 \\ L_m & 0 & 0 & L'_{lr} + L_m & 0 & 0 \\ 0 & L_m & 0 & 0 & L'_{lr} + L_m & 0 \\ 0 & 0 & 0 & 0 & 0 & L'_{lr} \end{bmatrix} \begin{bmatrix} i_{qs} \\ i_{ds} \\ i_{0s} \\ i'_{qr} \\ i'_{dr} \\ i'_{0r} \end{bmatrix}
$$

$$(3.13)$$

The rotor quantities are primed to show that they have been referred to stator side. The relationship between primed rotor to stator quantities are as follows

$$
\lambda'_{qr} = \frac{N_s}{N_r} \lambda_{qr} \qquad \lambda'_{dr} = \frac{N_s}{N_r} \lambda_{dr} \quad i'_{qr} = \frac{N_r}{N_s} i_{qr} \quad i'_{dr} = \frac{N_r}{N_s} i_{dr}
$$

$$
L'_{lr} = \left(\frac{Ns}{Nr} \right)^2 L_{lr}
$$

By substituting Equation 3.13 into Equation 3.11 and Equation 3.12 we can obtain the equivalent circuits for the arbitrary reference frame shown in Figure 13.
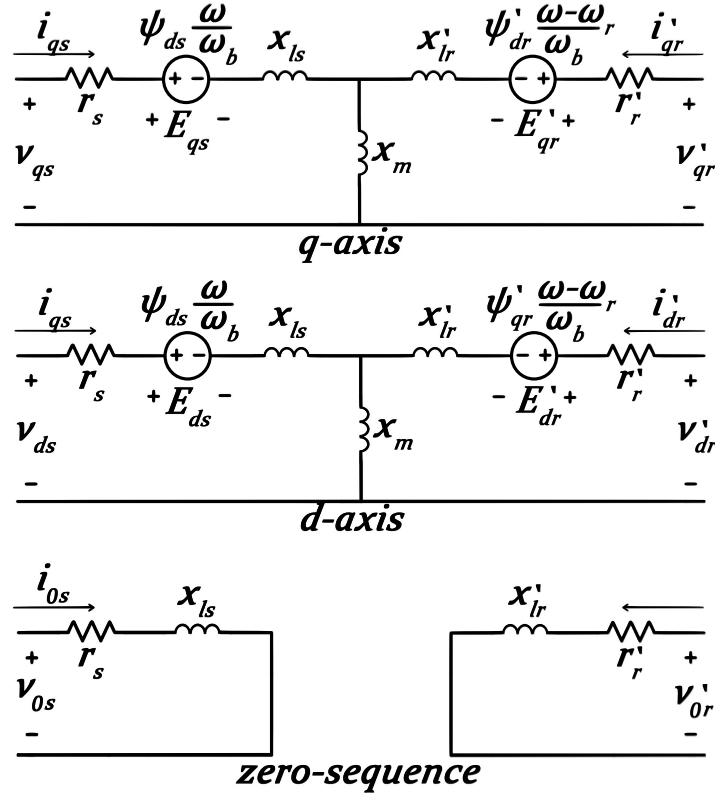
Figure 13: Equivalent circuits for q-axis, d-axis and $zero$-sequence

3.3.3 $qd0$ Torque Equations

The instantaneous input power for the stator is a follows

$$p_{ins} = v_{as} i_{as} + v_{bs} i_{bs} + v_{cs} i_{cs} \tag{3.14}$$

and for the rotor

$$p_{inr} = v'_{ar} i'_{ar} + v'_{br} i'_{br} + v'_{cr} i'_{cr} \tag{3.15}$$

The sum of instantanious power is

$$p_{in} = p_{ins} + p_{inr} \tag{3.16}$$

31

and changing abc into $qd0$ variables gives

$$p_{in} = \frac{3}{2}\left(v_{qs}iqs + v_{ds}i_{ds} + 2v_{0s}i_{os} + v'_{qr}i'_{qr} + v'_{dr}i'_{dr} + 2v'_{0r}i'_{0r}\right)$$ (3.17)

By substituting equation 3.11 and 3.12 for the voltages in equation 3.17 we get

$$T_{em} = \frac{3}{2}\frac{P}{2\omega_r}\left[\omega\left(\lambda_{ds}i_{qs} - \lambda_{qs}i_{ds}\right) + (\omega - \omega_r)\left(\lambda'_{dr}i'_{qr} - \lambda'_{qr}i'_{dr}\right)\right]$$ (3.18)

By using equation 3.13 we can show that

$$\lambda_{ds}i_{qs} - \lambda_{qs}i_{ds} = -\left(\lambda'_{dr}i'_{qr} - \lambda'_{qr}i'_{dr}\right) = L_m\left(i_{dr}i_{qs} - i_{qr}i_{ds}\right)$$ (3.19)

We can also show express equation 3.18 as[22]

$$
\begin{aligned}
T_{em} &= \frac{3}{2}\frac{P}{2}\left(\lambda'_{qr}i'_{dr} - \lambda'_{dr}i'_{qr}\right) \\
T_{em} &= \frac{3}{2}\frac{P}{2}\left(\lambda_{ds}i_{qs} - \lambda_{qs} - i_{ds}\right) \\
T_{em} &= \frac{3}{2}\frac{P}{2}L_m\left(i'_{dr}i_{qs} - i'_{qr}i_{ds}\right)
\end{aligned}
$$ (3.20)

3.3.4 Summary of $qd0$ Equations in Arbitrary Reference Frame

Stator voltage $qd0$ equations

$$
\begin{aligned}
v_{qs} &= p\lambda_{qs} + \omega\lambda_{ds} + r_s i_{qs} \\
v_{ds} &= p\lambda_{ds} + \omega\lambda_{qs} + r_s i_{ds} \\
v_{0s} &= p\lambda_{0s} + r_s i_{0s}
\end{aligned}
$$ (3.21)

Rotor voltage $qd0$ equations

$$
\begin{aligned}
v'_{qr} &= p\lambda'_{qr} + \omega\lambda'_{dr} + r'_r i'_{qr} \\
v'_{dr} &= p\lambda'_{dr} + \omega\lambda'_{qr} + r'_r i'_{dr} \\
v'_{0r} &= p\lambda'_{0r} + r'_r i'_{0r}
\end{aligned}
$$ (3.22)

where

$$
\begin{bmatrix} \lambda_{qs} \\ \lambda_{ds} \\ \lambda_{0s} \\ \lambda'_{qr} \\ \lambda'_{dr} \\ \lambda'_{0r} \end{bmatrix} = \begin{bmatrix} L_{ls}+L_m & 0 & 0 & L_m & 0 & 0 \\ 0 & L_{ls}+L_m & 0 & 0 & L_m & 0 \\ 0 & 0 & L_{ls} & 0 & 0 & 0 \\ L_m & 0 & 0 & L'_{lr}+L_m & 0 & 0 \\ 0 & L_m & 0 & 0 & L'_{lr}+L_m & 0 \\ 0 & 0 & 0 & 0 & 0 & L'_{lr} \end{bmatrix} \begin{bmatrix} i_{qs} \\ i_{dq} \\ i_{0s} \\ i'_{qr} \\ i'_{dr} \\ i'_{0r} \end{bmatrix}
$$

(3.23)

Torque $qd0$ equations

$$
\begin{aligned}
T_{em} &= \frac{3}{2}\frac{P}{2\omega_r}\left[\omega\left(\lambda_{ds}i_{qs}-\lambda_{qs}-i_{ds}\right)+(\omega-\omega_r)\left(\lambda'_{dr}i'_{qr}-\lambda'_{qr}i'_{dr}\right)\right] \\
T_{em} &= \frac{3}{2}\frac{P}{2}L_m\left(\lambda'_{qr}i'_{dr}-\lambda'_{dr}i'_{qr}\right) \\
T_{em} &= \frac{3}{2}\frac{P}{2}L_m\left(\lambda_{ds}i_{qs}-\lambda_{qs}i_{ds}\right) \\
T_{em} &= \frac{3}{2}\frac{P}{2}L_m\left(i'_{dr}i_{qs}-i'_{qr}i_{ds}\right)
\end{aligned}
$$

Machine parameters are often given as ohms or per unit of base impedance, this is why it is often more convenient to express the voltage and flux linkage equations in terms of reactances x instead of inductances. The flux linkages are now flux linkages per second ψ and has the unit of volts[41][22]. The relationship between ψ and λ, and x and L is given as

$$
\psi = \omega_b\lambda \quad \text{and} \quad x = \omega_b L \tag{3.24}
$$

Summarizing the equations in terms of x and ψ yields

Stator $qd0$ equations in terms of ψ's and x's

$$
\begin{aligned}
v_{qs} &= \frac{p}{\omega_b}\psi_{qs}+\frac{\omega}{\omega_b}\psi_{ds}+r_s i_{qs} \\
v_{ds} &= \frac{p}{\omega_b}\psi_{ds}+\frac{\omega}{\omega_b}\psi_{qs}+r_s i_{ds} \\
v_{0s} &= \frac{p}{\omega_b}\psi_{0s}+r_s i_{0s}
\end{aligned}
$$

(3.25)

Rotor $qd0$ equations in terms of ψ's and x's

$$v'_{qr} = \frac{p}{\omega_b}\psi'_{qr} + \left(\frac{\omega - \omega_r}{\omega_b}\right)\psi'_{dr} + r'_r i'_{qr}$$

$$v'_{dr} = \frac{p}{\omega_b}\psi'_{dr} - \left(\frac{\omega - \omega_r}{\omega_b}\right)\psi'_{qr} + r'_r i'_{dr} \tag{3.26}$$

$$v'_{0r} = \frac{p}{\omega_b}\psi'_{0r} + r'_r i'0r$$

where

$$
\begin{bmatrix} \psi_{qs} \\ \psi_{ds} \\ \psi_{0s} \\ \psi'_{qr} \\ \psi'_{dr} \\ \psi'_{0r} \end{bmatrix}
=
\begin{bmatrix}
x_{ls} + x_m & 0 & 0 & x_m & 0 & 0 \\
0 & x_{ls} + x_m & 0 & 0 & x_m & 0 \\
0 & 0 & x_{ls} & 0 & 0 & 0 \\
x_m & 0 & 0 & x'_{lr} + x_m & 0 & 0 \\
0 & x_m & 0 & 0 & x'_{lr} + x_m & 0 \\
0 & 0 & 0 & 0 & 0 & x'_{lr}
\end{bmatrix}
\begin{bmatrix} i_{qs} \\ i_{ds} \\ i_{0s} \\ i'_{qr} \\ i'_{dr} \\ i'_{0r} \end{bmatrix}
\tag{3.27}
$$

**Torque $qd0$ equations in terms of ψ's and x's**

$$T_{em} = \frac{3}{2}\frac{P}{2\omega_r}\left[\frac{\omega}{\omega_b}\left(\psi_{ds}i_{qs} - \psi_{qs}i_{ds}\right) + \frac{\omega - \omega_r}{\omega_b}\left(\psi'_{dr}i'qr - \psi'_{qr}i'dr\right)\right]$$

$$T_{em} = \frac{3}{2}\frac{P}{2\omega_b}\left(\psi'_{qr}i'_{dr} - \psi'_{dr}i'_{qr}\right)$$

$$T_{em} = \frac{3}{2}\frac{P}{2\omega_b}\left(\psi_{ds}i_{qs} - \psi_{qs}i'_{ds}\right) \tag{3.28}$$

$$T_{em} = \frac{3}{2}\frac{P}{2\omega_b}x_m\left(i'_{dr}i_{qs} - i'_{qr}i_{ds}\right)$$

3.4   Implementing Model in Matlab/Simulink

The objective of this chapter is to show how to use the derived equations for the induction motor and implement these in Matlab/Simulink. This simulation will only be for a single fed SCIM, the voltages v'_{qr} and v'_{dr} will accordingly be zero[3].

3.4.1 Conversion of Input Voltages

The input voltages v_{ag}, v_{bg} and v_{cg} are three of the four inputs to the model, the fourth being mechanical load to the motor. The stator voltages v_{as}, v_{bs} and v_{cs} can be found as[22]

$$
\begin{aligned}
v_{as} &= v_{ag} - v_{sg} \\
v_{bs} &= v_{bg} - v_{sg} \\
v_{cs} &= v_{cg} - v_{sg}
\end{aligned}
\tag{3.29}
$$

In this case, the point s and g are solidly connected, then $v_{sg} = 0$ which yields

$$
\begin{aligned}
v_{as} &= v_{ag} \\
v_{bs} &= v_{bg} \\
v_{cs} &= v_{cg}
\end{aligned}
\tag{3.30}
$$

These are now the input voltages to the model. The voltages are still in abc reference frame and needs to be converted to the $qd0$ reference frame wanted. In this model the stationary reference frame will be used, accordingly θ is set to 0 in Equation 3.7 which gives

$$
\begin{bmatrix} v_q \\ v_d \\ v_0 \end{bmatrix} = [\boldsymbol{T}_{qd0}(0)] \begin{bmatrix} v_a \\ v_b \\ v_c \end{bmatrix} = \frac{2}{3} \begin{bmatrix} 1 & -\frac{1}{2} & -\frac{1}{2} \\ 0 & -\frac{\sqrt{3}}{2} & \frac{\sqrt{3}}{2} \\ \frac{1}{2} & \frac{1}{2} & \frac{1}{2} \end{bmatrix} \begin{bmatrix} v_a \\ v_b \\ v_c \end{bmatrix}
$$

The Simulink block for this transformation is showed in Figure 14
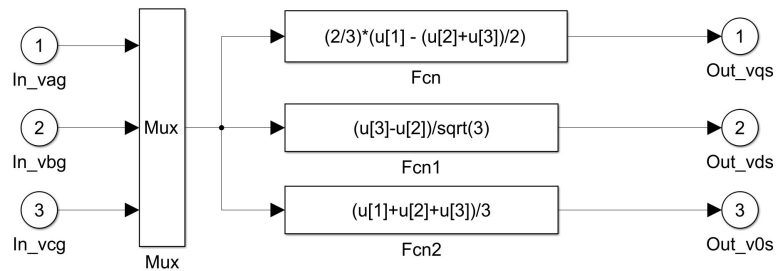
Figure 14: Simulink subsystem which converts the input abc voltages to stationary $qd0$ voltages

3.4.2 Flux Linkages per Second

Some signals will have discontinuities and can also include ripples, this is why derivatives should be avoided and replaced by integrals[42]. To calculate the flux linkages per second the Equation 3.25 and Equation 3.26 are rearranged as the following

$$
\boldsymbol{\psi}_s^{qd0} = wb \int \left\{ \boldsymbol{v}_s^{qd0} - \boldsymbol{r}_s^{qd0} \boldsymbol{i}_s^{qd0} \right\} dt
$$

$$
\boldsymbol{\psi}_r^{qdo} = wb \int \left\{ \boldsymbol{v}_r^{qd0} + \frac{\omega_r}{\omega_b} \begin{bmatrix} 0 & 1 & 0 \\ -1 & 0 & 0 \\ 0 & 0 & 0 \end{bmatrix} \boldsymbol{\psi}_r^{qd0} - \boldsymbol{r}_r^{qd0} \boldsymbol{i}_r^{qd0} \right\} dt
$$

(3.31)

The current equations are extracted from Equation 3.27 as

$$
i_{qs} = \frac{\psi_{qs} - i'_{qr} x_m}{x_{ls} + xm} \qquad i'_{qr} = \frac{\psi_{qr} - i_{qs} x_m}{x'_{lr} + xm}
$$

$$
i_{ds} = \frac{\psi_{ds} - i'_{dr} x_m}{x_{ls} + xm} \qquad i'_{dr} = \frac{\psi_{dr} - i_{ds} x_m}{x'_{lr} + xm}
$$

$$
i_{0s} = \frac{\psi_{0s}}{x_{ls}} \qquad\qquad i'_{0r} = \frac{\psi'_{0r}}{x'_{lr}}
$$

These equations are divided into subsystems of q-axis, d-axis and $zero$-sequence which are shown in Figure 15,Figure 16 and Figure 17.
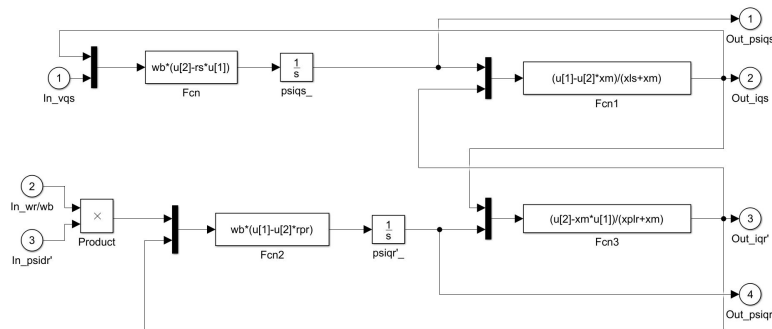
Figure 15: Simulink q-axis subsystem

36
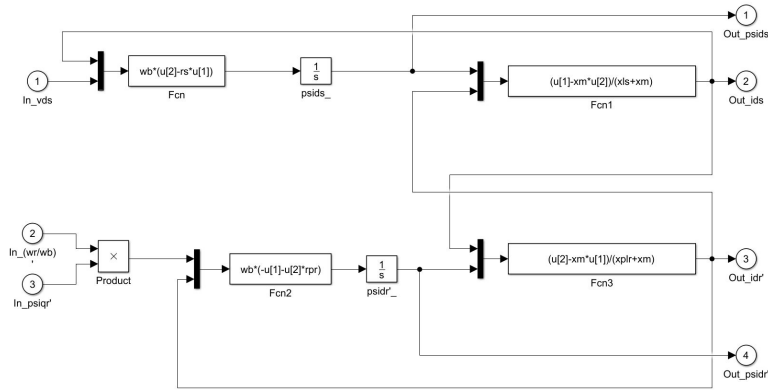
Figure 16: Simulink d-axis subsystem
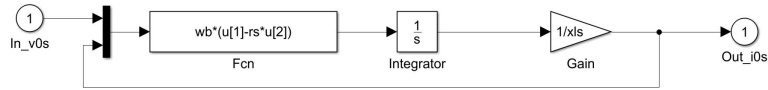
Figure 17: Simulink $zero$-sequence subsystem

3.4.3 Torque Calculation

Equations from 3.31 uses the per unit speed ($\frac{\omega_r}{\omega_b}$) to calculate the flux linkages per second, this can be found by integrating

$$2H\frac{d(\omega_r/\omega_b)}{dt} = T_{em} + T_{mech} - T_{damp} \tag{3.32}$$

where H is the inertia constant, defined as

$$H = \frac{J\omega_b^2}{2S_b} \tag{3.33}$$

J is the moment of inertia of the rotor in $kg\,m^2$ and S_b is the rated power of the machine in VA. T_{em} is the developed electromechanical torque, T_{damp} is the damping factor in opposing direction of the rotor and T_{mech} is the external applied torque, in direction of the rotor. This must be negative in motoring mode. This yields

$$\frac{\omega_r}{\omega_b} = \int \left\{ \frac{T_{em} + T_{mech} - T_{damp}}{2H} \right\} dt \tag{3.34}$$

which can be implemented in a subsystem in Simulink, illustrated in Figure 18.

37
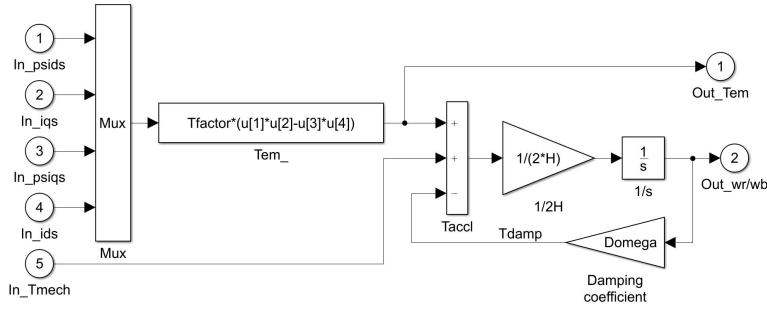
Figure 18: Simulink torque block subsystem which calculates the per unit speed and where the load input is implemented

3.4.4 Conversion of Output Currents

The rotor and stator currents are often transformed back to abc reference to be used in other parts of the simulation, in this case for the MCSA. This is done by using the inverse $qd0$ transformation and setting $\theta = 0$, which yields

$$
\begin{bmatrix} i_a \\ i_b \\ i_c \end{bmatrix} = \left[\boldsymbol{T}_{qd0}(0) \right]^{-1} \begin{bmatrix} i_q \\ i_d \\ i_0 \end{bmatrix} = \begin{bmatrix} 1 & 0 & 1 \\ -\frac{1}{2} & -\frac{\sqrt{3}}{2} & 1 \\ -\frac{1}{2} & \frac{\sqrt{3}}{2} & 1 \end{bmatrix} \begin{bmatrix} i_q \\ i_d \\ i_0 \end{bmatrix} \tag{3.35}
$$

This is implemented in the subsystem shown in Figure 19
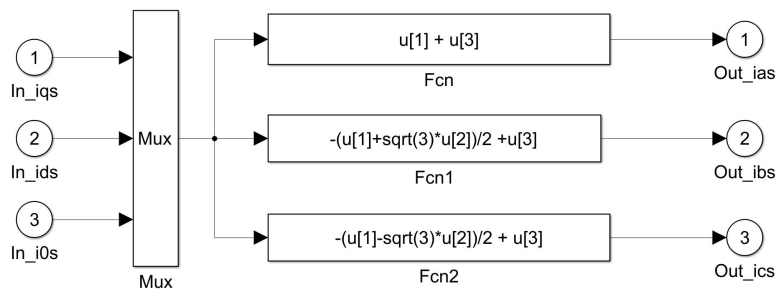
Figure 19: Simulink subsystem which converts from $qd0$ to abc

3.4.5 Overview and Evalution of the Model

The entire model which is much based on [22] and simplified as [9] is shown in Figure 20. There are two "To Workspace" blocks in the program which takes the

38

values into Matlab. The "X" is for plotting current, voltage, speed and torque. The "z1" is for the MCSA and does a FFT on the i_{as} current.
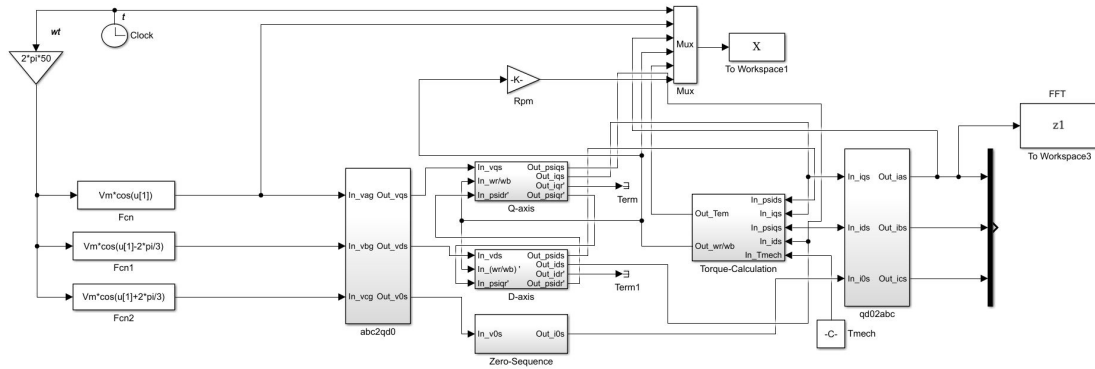
Figure 20: Showing the entire model of a symmetric healthy induction motor

A two seconds simulation of a free acceleration (no load) is showed in Figure 21. Stator voltage is a $50Hz$ sine wave. As shown in the figure the starting current is much larger in the beginnning and decreases as the rotor speed reaches steady-state, which is as mentioned one of the sources for rotor failure.
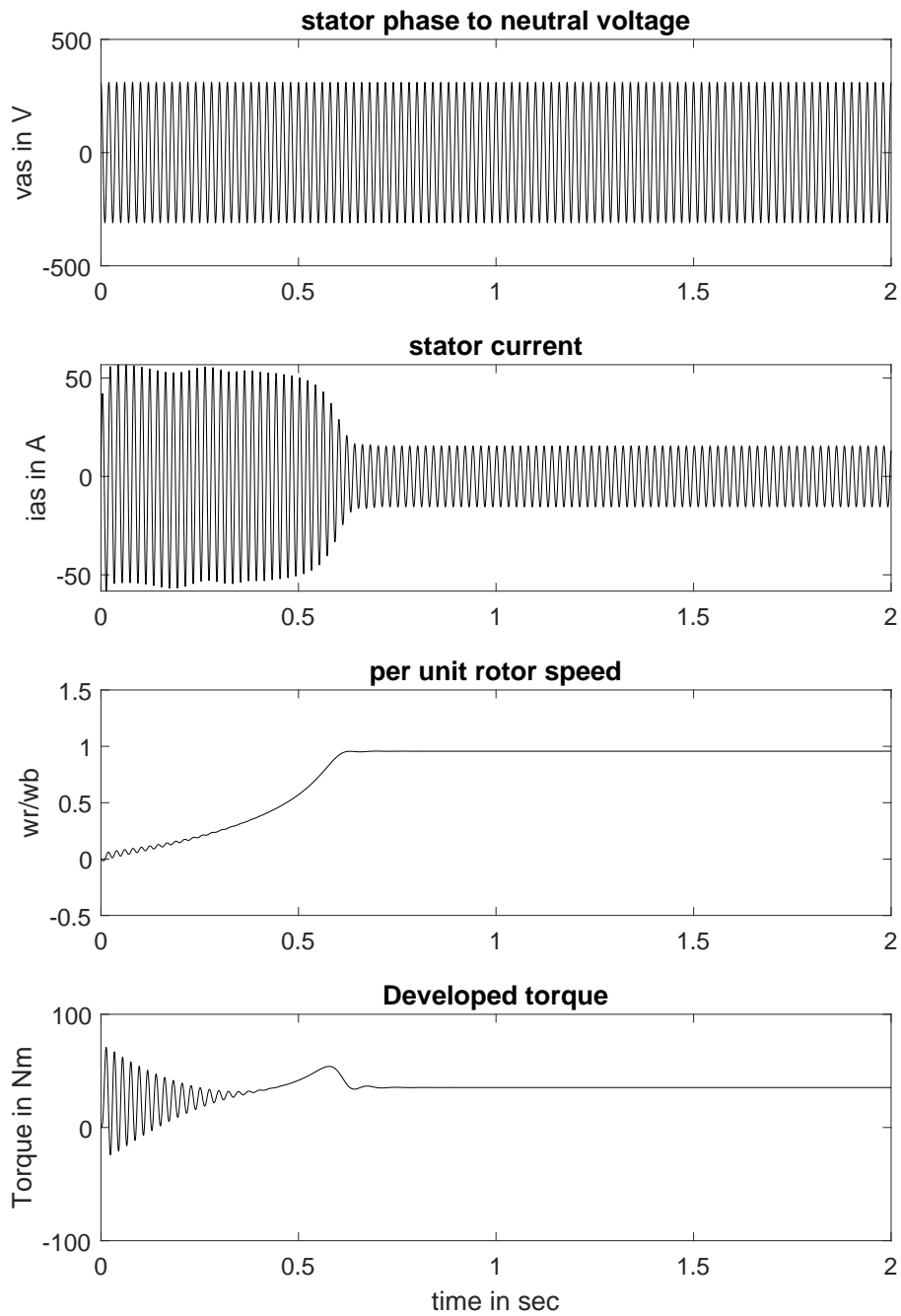
Figure 21: 2 seconds simulation of free acceleration with stator voltage, stator current, per unit rotor speed and developed torque.

3.5 Modelling of Broken Rotor Bars

Now that the healthy induction motor model is established, the focus can be redirected to the defected models, starting with broken rotor bars(BRB). Firstly we need to see how BRB affect the motor. Breaking or cracking a bar will decrease the conductivity thus increasing the resistance. This will give a non-symmetrical current in the rotor, increasing the current in the adjacent bar and decreasing the current in the present bar. For simplicity we will ignore the magnetizing current, leaving the inductance matrices the same and neglecting the end ring resistance. From the rotor voltage Equation 3.1 the resistance r_r is a diagonal matrix

$$\boldsymbol{r}_r^{abc} = \begin{bmatrix} r_r & 0 & 0 \\ 0 & r_r & 0 \\ 0 & 0 & r_r \end{bmatrix}$$

the new rotor resistance matrix $\boldsymbol{r}_r^*$ with BRB will have an increase for the relevant phase, yielding[11]

$$\boldsymbol{r}_r^{*abc} = \begin{bmatrix} (r_r + \Delta r_a) & 0 & 0 \\ 0 & (r_r + \Delta r_b) & 0 \\ 0 & 0 & (r_r + \Delta r_c) \end{bmatrix}$$

The change in resistance Δr can be found by calculating the phase resistance of both a healthy and a BRB case. In both cases the end ring resistance and magnetizing current are neglected, also the assumptions that the broken rotor bar is continuous is made. For the healthy rotor this yields[11, 43]

$$r_r = \frac{(2N_s)^2}{N/3} r_b$$

where N is the total amount rotor bars, N_s is the equivalent stator winding turns and r_b is the rotor bar resistance. In the case with BRB the rotor resistance can be found as

$$r_r^* = \frac{(2N_s)^2}{N/3 - n} r_b \tag{3.36}$$

where n is the amount of broken bars. The change in resistance can now be found as

$$\Delta r = r_r^* - r_r = \frac{3n}{N-3n} r_r$$

and is expressed with respect to the rotor resistance. Derivation of the equation is found in appendix A.1. To convert the change of resistance from abc to $qd0$ the same transformation is done as earlier $\Delta r_r^{*qd0} = \left[T_{qd0}(\theta - \theta_r) \right] \Delta r_r^{abc} \left[T_{qd0}(\theta - \theta_r) \right]^{-1}$, this yields

$$\Delta r_r^{*qd0} = \begin{bmatrix} r_{r11} & r_{r12} & r_{r13} \\ r_{r21} & r_{r22} & r_{r23} \\ r_{r31} & r_{r32} & r_{r33} \end{bmatrix}$$

where

$$r_{r11} = \frac{1}{3}(\Delta r_a + \Delta r_b + \Delta r_c) + \frac{1}{3}\cos(2\theta_r)\left(\Delta r_a - \frac{\Delta r_b}{2} - \frac{\Delta r_c}{2}\right) + \frac{\sqrt{3}}{6}\sin(2\theta_r)(\Delta r_c - \Delta r_b)$$

$$r_{r12} = \frac{1}{3}\sin(2\theta_r)\left(\Delta r_a - \frac{\Delta r_b}{2} - \frac{\Delta r_c}{2}\right) + \frac{\sqrt{3}}{6}\cos(2\theta_r)(\Delta r_b - \Delta r_c)$$

$$r_{r13} = \frac{1}{3}\cos\theta_r(2\Delta r_a - \Delta r_b - \Delta r_c) + \frac{\sqrt{3}}{3}\sin\theta_r(\Delta r_b - \Delta r_c)$$

$$r_{r21} = \frac{1}{3}\sin(2\theta_r)\left(\Delta r_a - \frac{\Delta r_b}{2} - \frac{\Delta r_c}{2}\right) + \frac{\sqrt{3}}{6}\cos(2\theta_r)(\Delta r_b - \Delta r_c)$$

$$r_{r22} = \frac{1}{3}(\Delta r_a + \Delta r_b + \Delta r_c) + \frac{1}{3}\cos(2\theta_r)\left(\frac{\Delta r_b}{2} + \frac{\Delta r_c}{2} - \Delta r_a\right) + \frac{\sqrt{3}}{6}\sin(2\theta_r)(\Delta r_b - \Delta r_c)$$

$$r_{r23} = \frac{2}{3}\sin\theta_r\left(\Delta r_a - \frac{\Delta r_b}{2} - \frac{\Delta r_c}{2}\right) + \frac{\sqrt{3}}{3}\cos\theta_r(\Delta r_c - \Delta r_b)$$

$$r_{r31} = \frac{1}{3}\cos\theta_r\left(\Delta r_a - \frac{\Delta r_b}{2} - \frac{\Delta r_c}{2}\right) + \frac{\sqrt{3}}{6}\sin\theta_r(\Delta r_b - \Delta r_c)$$

$$r_{r32} = \frac{1}{3}\sin\theta_r\left(\Delta r_a - \frac{\Delta r_b}{2} - \frac{\Delta r_c}{2}\right) + \frac{\sqrt{3}}{6}\cos\theta_r(\Delta r_c - \Delta r_b)$$

$$r_{r33} = \frac{1}{3}(\Delta r_a + \Delta r_b + \Delta r_c)$$

(3.37)

The total rotor resistance $\boldsymbol{r}_{rBRB}$ can now be found by adding the normal $\boldsymbol{r}_r^{qd0}$ with the change $\Delta\boldsymbol{r}_r^{*qd0}$ which equals

$$\boldsymbol{r}_{rBRB}^{qd0} = \begin{bmatrix} r_r + r_{11} & r_{12} & r_{13} \\ r_{21} & r_r + r_{22} & r_{23} \\ r_{31} & r_{32} & r_r + r_{33} \end{bmatrix} \tag{3.38}$$

Equation 3.37 is dependent on the rotor angle θ_r. In Figure 18 we can see the output from this block is the per unit speed, from this we can find the angle by multiplying the per unit speed with ω_b and using Equation 3.9. The rotor angle block is illustrated in Figure 22. Its also worth mentioning that increasing the resistance in all three phases will result in a symmetrical rotor.
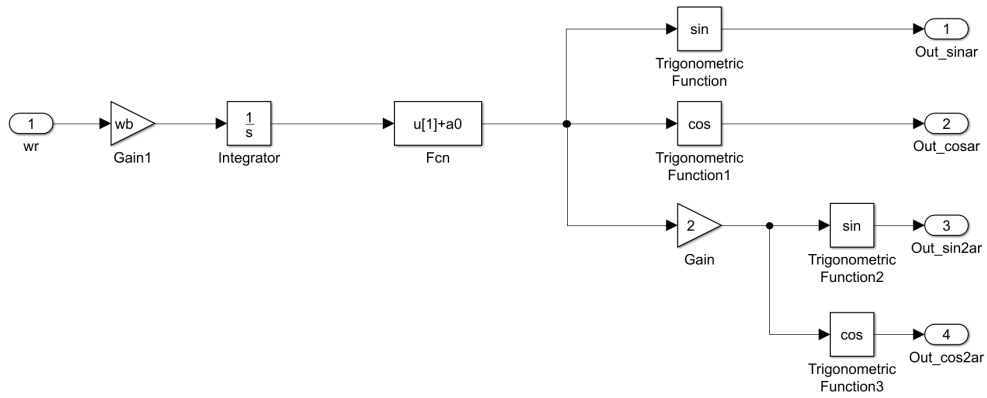
Figure 22: Subsystem from Simulink which uses the input per unit speed and sends out rotor angle calculations

Since the new resistance Equation 3.38 is no longer a diagonal matrix, there will be changes in the d-axis, q-axis and $zero$-sequence. We can find these changes by looking at the last element in Equation 3.31 which now looks like

$$\boldsymbol{\psi}_{BRBr}^{'qd0} = \omega_b \int \left\{ v_r^{'qd0} + \frac{\omega_r}{\omega_b} \begin{bmatrix} 0 & 1 & 0 \\ -1 & 0 & 0 \\ 0 & 0 & 0 \end{bmatrix} \boldsymbol{\psi}_r^{'qd0} - \boldsymbol{r}_{rBRB}^{'qd0} \boldsymbol{i}_r^{'qd0} \right\} dt \tag{3.39}$$

For the q-axis this yields

$$\psi'_{BRBqr} = \omega_b \int \left\{ v'_{qr} + \frac{\omega_r}{\omega_b}\psi'_{dr} - \left(i'_{qr}(r_r + r_{r11}) + i'_{dr}r_{r12} + i'_{0r}r_{r13} \right) \right\} dt \quad (3.40)$$

The new q-axis subsystem from Simulink is showed in Figure 23
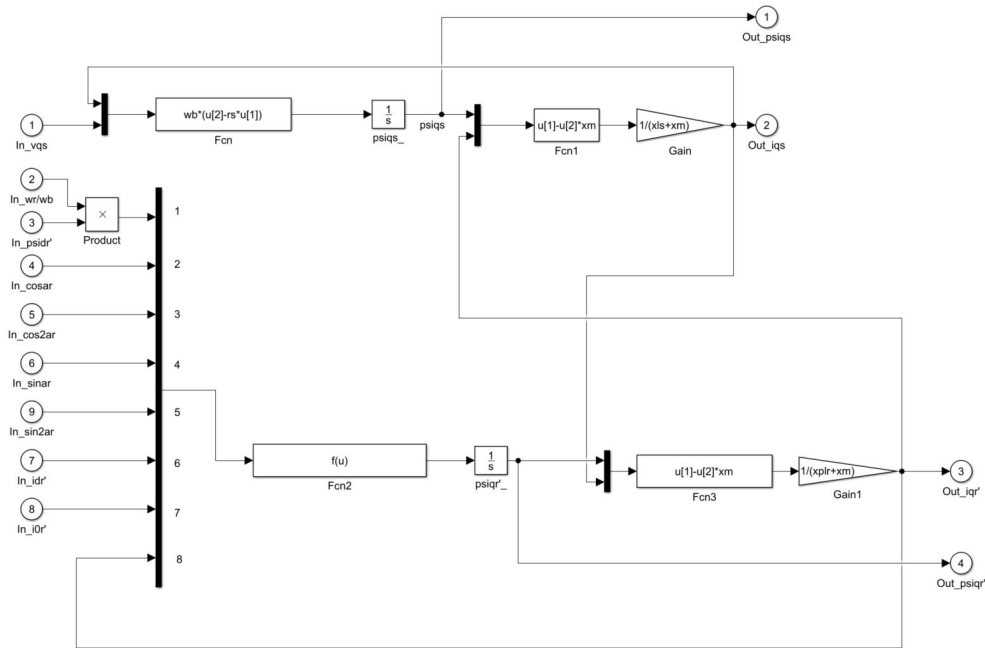
Figure 23: Subsystem of the q-axis in Simulink with BRB.

In Figure 24 we can see the frequency spectrum of the current i_{as} from a simulation of a SCIM running in rated operations. The machine is simulated with 1 BRB in phase a. The parameters of the motor can be found in Appendix B.1
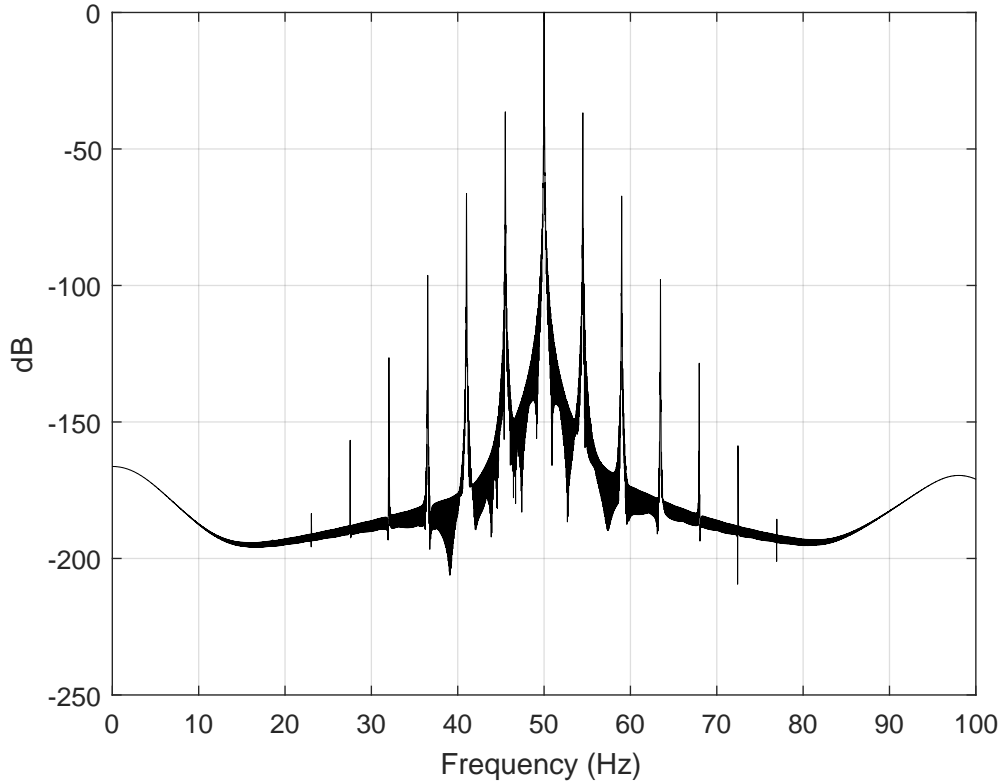
Figure 24: Frequency spectrum of current i_{as} with one BRB running at rated operations. The parameters of the motor can be found in Appendix B.1

3.6 Modelling of Eccentricity faults

As mentioned earlier in practice only mixed eccentricity occur. Isolated dynamic- or static eccentricity can only be modelled. In this chapter a general model to simulate mixed eccentricity fault is developed.

3.6.1 Inductance Calculation

In a healthy condition $\boldsymbol{L}_{ss}$ and $\boldsymbol{L}_{rr}$ from Equation 3.3 are constants. In a mixed eccentricity condition the air-gap will vary, thus the inductance in both stator and rotor will also vary. This means that all the inductances ($\boldsymbol{L}_{ss}$, $\boldsymbol{L}_{sr}$, $\boldsymbol{L}_{rs}$ and $\boldsymbol{L}_{rr}$) are dependent on the rotor angle θ_r[44]. To simulate the new model the inductance can be calculated for different angles and stored in tables, or directly calculated continuously in simulation with rotor angle feedback.

In a non-symmetric condition, the stator inductance in abc reference, earlier expressed in Equation 3.4 can now be expressed as

$$\boldsymbol{L}_{ss}^{abc} = \begin{bmatrix} L_{asas}(\theta_r) & L_{asbs}(\theta_r) & L_{ascs}(\theta_r) \\ L_{bsas}(\theta_r) & L_{bsbs}(\theta_r) & L_{bscs}(\theta_r) \\ L_{csas}(\theta_r) & L_{csbs}(\theta_r) & L_{cscs}(\theta_r) \end{bmatrix} \tag{3.41}$$

where each inductance is dependent on the rotor angle θ_r. The mutual inductance between two windings for example a and b, can be found by using the modified winding function approach (MWFA) and can be expressed as[5]

$$L_{ba} = \frac{\lambda_{ba}}{i_a} = \mu_0 r l \int_0^{2\pi} n_b(\phi, \theta_r) M_a(\phi, \theta_r) g^{-1}(\phi, \theta_r) d\phi \tag{3.42}$$

θ_r is the rotor angle and ϕ is an arbitrary point at the inner surface of the stator. The magnetizing inductance of winding a can be found the same way

$$L_{aa} = \mu_0 r l \int_0^{2\pi} n_a(\phi, \theta_r) M_a(\phi, \theta_r) g^{-1}(\phi, \theta_r) d\phi \tag{3.43}$$

where μ_0 is the vacuum permeability, r is the stator inner radius, l is the length of the axial stack, $n(\phi, \theta_r)$ is the turn function of the winding, $M(\phi, \theta_r)$ is the modified winding function and $g^{-1}(\phi, \theta_r)$ is the inverse air-gap function.

By using MWFA it has been proven that even for non-uniform air-gap[44]

$$L_{ab} = L_{ba} \tag{3.44}$$

as long as the magnetic circuit is linear. With this in mind the stator inductance matrix will have some equal elements as shown

$$\boldsymbol{L}_{ss}^{abc} = \begin{bmatrix} L_{asas}(\theta_r) & L_{asbs}(\theta_r) & L_{ascs}(\theta_r) \\ L_{asbs}(\theta_r) & L_{bsbs}(\theta_r) & L_{bscs}(\theta_r) \\ L_{ascs}(\theta_r) & L_{bscs}(\theta_r) & L_{cscs}(\theta_r) \end{bmatrix} \tag{3.45}$$

This seems to be a good representation of eccentricity conditions, but it is a complex model and not best suited for the DQ-transformation. Instead a more man-

ageable model is developed.

3.6.2 Simplified Eccentricity Model

As in the broken rotor model there are simplifications that can be made when simulating eccentricity faults. One way to do this is by only varying the mutual inductance L_m between stator and rotor winding. Or the mutual reactance x_m which is related to the inductance by $x_m = \omega_b L_m$.

By using the healthy motor model, the reactance can be modified accordingly

$$x_m(\theta_m) = x_m \left(\frac{l_g}{l_g(\theta_m)} \right) \tag{3.46}$$

where $l_g(\theta_m)$ is the air-gap distance due to the eccentricity and l_g is the air-gap distance in a symmetric condition. The static- and dynamic eccentricity are modelled by two different equations which are found by basic geometry.

For static eccentricity the rotor gap is at a constant offset as shown in figure Figure 25 and modelled as[12]

$$l_g(\theta_m) = R - \sqrt{\left((e + r\cos(\theta_m))^2 + (r\sin(\theta_m))^2\right)} \qquad (3.47)$$

where R is the radius of the stator bore, e is the rotor offset from stator center, r is the rotor radius and θ_m is the mechanical rotor angle.
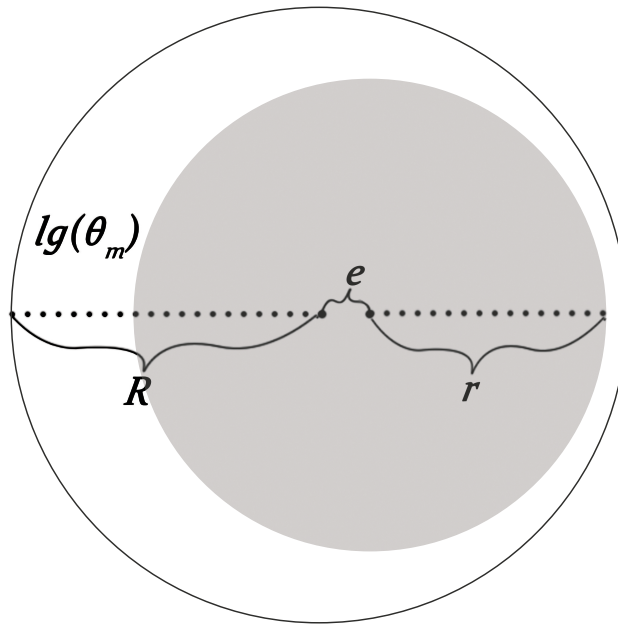
Figure 25: Geometry of static eccentricity. Outer circle is the stator, inner(grey) circle is the rotor. R is stator radius, r is rotor radius, e is offset from stator center and $lg(\theta_m)$ is the distance from stator to rotor.

The dynamic eccentricity is modelled as small deviations in the rotor profile, the rotor is simulated as an ellipse[12] as

$$l_g(\theta_m) = R - \frac{ab}{\sqrt{b^2\cos(\theta_m)^2 + a^2\sin(\theta_m)^2}} \qquad (3.48)$$

where a and b are the length of the major and minor axes, respectively. The ellipse rotor shape is illustrated in Figure 26.
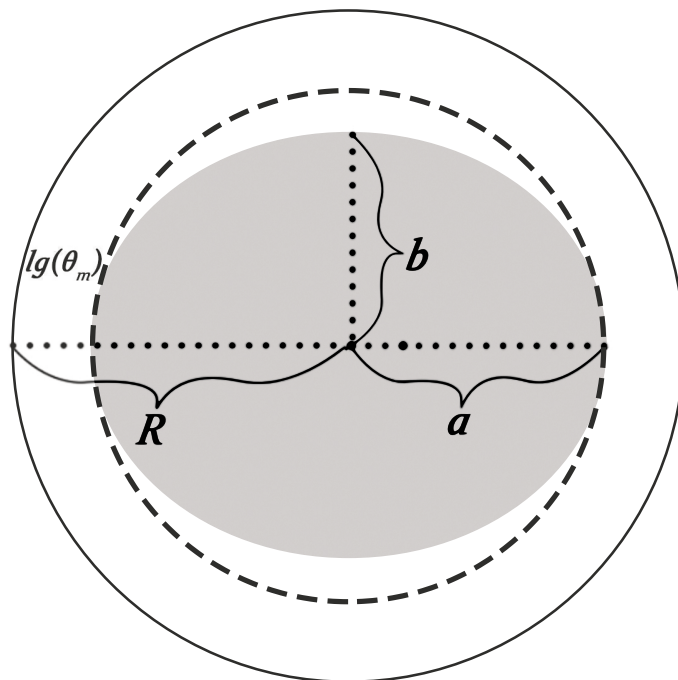
Figure 26: Geometry of dynamic eccentricity. Outer circle is the stator, inner(grey) circle is the rotor. R is stator radius, a and b are the major and minor axes of the ellipse, respectively and $lg(\theta_m)$ is the distance from stator to rotor.

49

To simulate mixed eccentricity the ellipse model is used, but shifted as illustrated in Figure 27 and modelled as

$$l_g(\theta_m) = R - \frac{2b^2 e \cos(\theta_m) + \sqrt{(2b^2 e \cos(\theta_m))^2 + 4(b^2 \cos(\theta_m) + a^2 \sin(\theta_m))(e^2 b^2 - a^2 b^2)}}{2(b^2 \cos(\theta_m) + a^2 \sin(\theta_m))}$$
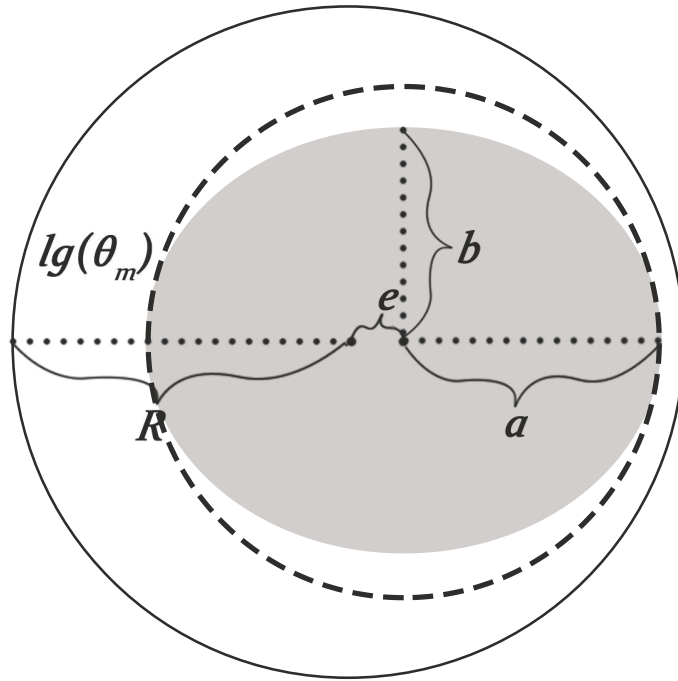
Figure 27: Geometry of mixed eccentricity. Outer circle is the stator, inner(grey) circle is the rotor. R is stator radius, a and b are the major and minor axes of the ellipse, respectively, e is offset from stator center and $lg(\theta_m)$ is the distance from stator to rotor.

The modulation is implemented in the q- and d-axis in Simulink, and is only dependent on one variable, rotor angle θ_m. It is worth mentioning that θ_m is the mechanical angle, which means the pole number needs to be taken into account. The q-axis subsystem with eccentricity is showed in Figure 28, the "Static" and "Dynamic" gain blocks is used to control the eccentricity. If both is activated at the same time, the mixed eccentricity will be activated. The "UniformField" blocks gets activated when disabling eccentricity. The frequency spectrum of mixed eccentricity is shown in Figure 29.
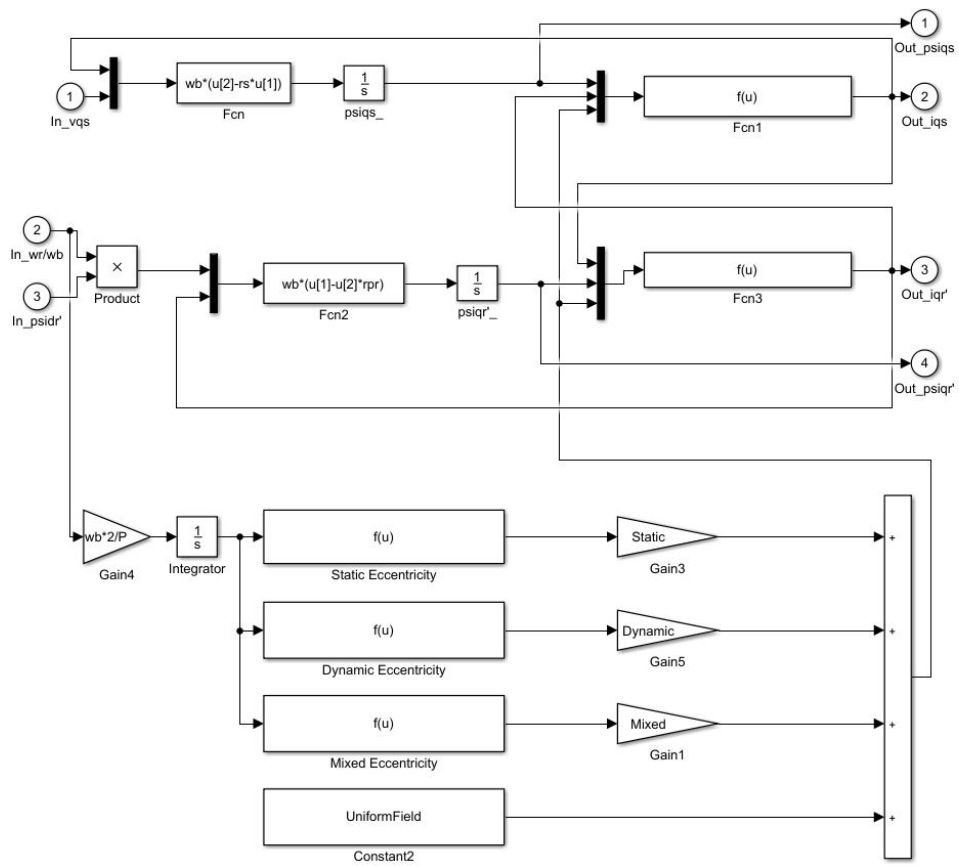
Figure 28: Subsystem in q-axis from Simulink showing how the eccentricity is manipulated
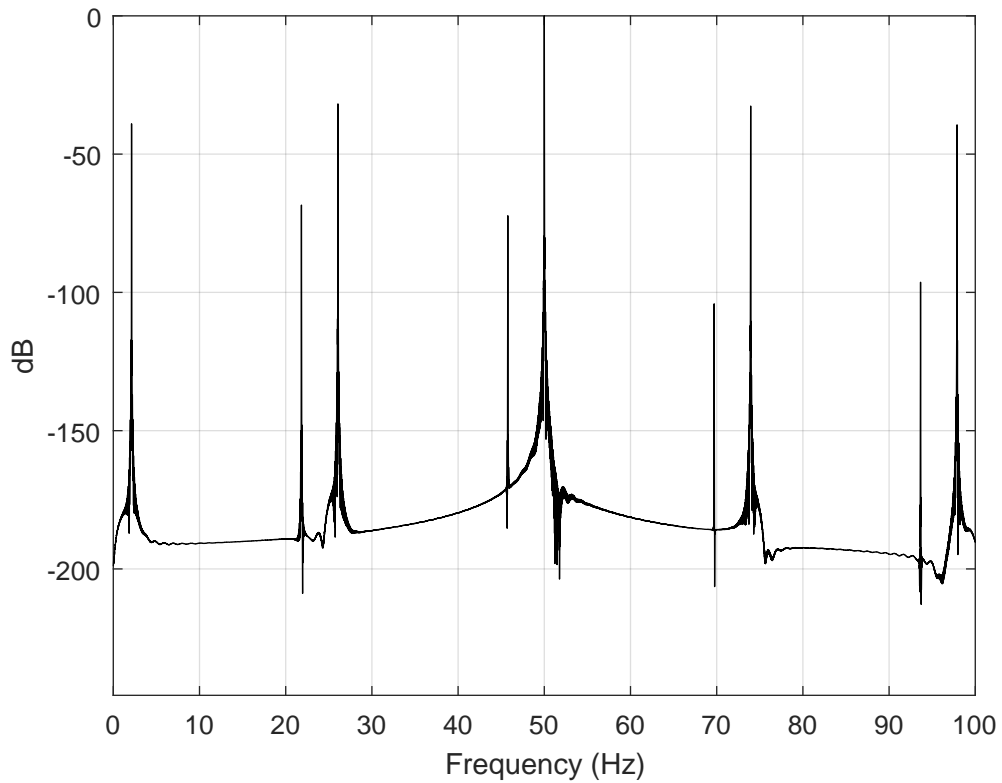
Figure 29: Simulated frequency spectrum of stator current i_a with mixed eccentricity, running at rated operations. The parameters of the motor can be found in Appendix B.1

3.7 Modelling Bearing Fault

As mentioned earlier bearing fault is like an instant eccentricity, and as the eccentricity fault it can be modelled by calculating the inductance under bearing fault using MWFA. This is much the same as the technique described when modelling eccentricity, but this will also give a complex solution in the DQ-reference frame. Instead we can look at how the bearing fault is developed and derive a expression which we can insert in the torque calculations, to use as torque modulation.

3.7.1 A Simplified Bearing Fault Model

Bearing fault are as previously mentioned classified as inner raceway defect, outer raceway defect, ball defect and cage defect. These defects can be found by looking at Figure 30.
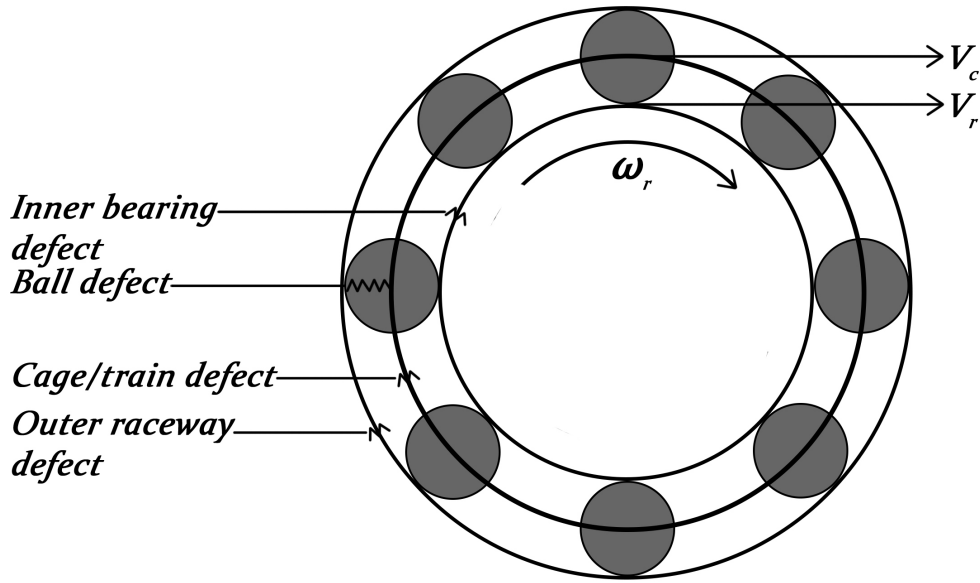
Figure 30: A bearing showing the four different bearing fault categories. Also the different speed parameters used when deriving fault occurrences

The next step is to derive an expression which determines how often the instant eccentricity occurs. If there is a defect on the outer raceway an instant eccentricity will occur when a bearing ball passes and gets influenced, this will be the same for the inner raceway. If there is an bearing ball defect the instant eccentricity will happen twice the spin rotation since its connected to both the inner and outer raceway[45]. For a cage defect bearing balls can slide instead of rolling, this defect is not dependent on the amount of bearing balls, only on the speed of the cage.

The linear velocity of the cage V_c from Figure 30 equals $\frac{V_r}{2}$, where V_r is the linear velocity of the rotor[46]. Angular velocity is defined as $\omega = \frac{V}{r}$, we can write the angular velocity of the cage as

$$\omega_c = \frac{V_c}{r_c} = \frac{\frac{V_r}{2}}{\frac{P_d}{2}} = \frac{V_r}{P_d}$$

where r_c is the cage radius and P_d is the pitch diameter. In this context its more convenient to express the angular cage velocity in terms of angular velocity of the rotor ω_r. $V_r = \omega_r r_r$ where r_r is the rotor radius which can be expressed as $\left(\frac{P_d}{2} - \frac{B_d \cos(\beta)}{2} \right)$, where B_d is ball diameter and β is the contact angle. Angular cage velocity can now

be expressed as

$$\omega_c = \frac{\omega_r \left(\frac{P_d}{2} - \frac{B_d \cos(\beta)}{2} \right)}{P_d} = \frac{1}{2} \omega_r \left(1 - \frac{B_d \cos(\beta)}{P_d} \right)$$

To find the frequencies of inner raceway defect we can look at the difference in angular velocities $\Delta\omega = \omega_r - \omega_c$ and multiply it with the number of bearing balls. We now end up with the same expression mentioned in section 2.5.2.

$$f_{ib} = \frac{N_b}{2} f_r \left(1 + \frac{B_d \cos(\beta)}{P_d} \right) \tag{3.49}$$

where $f_r = \frac{\omega_r}{\pi P}$ the mechanical rotational frequency. This is also true for the other bearing faults which yields

$$
\begin{aligned}
f_{ob} &= \frac{N}{2} f_r \left(1 - b_d \frac{\cos(\beta)}{d_p} \right) && \text{outer bearing race defect} \\
f_b &= \frac{d_p}{d_b} f_r \left(1 - \left(b_d \frac{\cos(\beta)}{d_p} \right)^2 \right) && \text{ball race defect} \\
f_t &= \frac{1}{2} f_r \left(1 - b_d \frac{\cos(\beta)}{d_p} \right) && \text{train defect}
\end{aligned}
\tag{3.50}
$$

3.7.2 Implementing Simplified Model in Simulink

As mentioned earlier the expressions derived can be implemented in the torque subsystem as load modulation[13]. Bearing fault is a mechanic fault that will make instant eccentricities, but also a variying load pattern. For example when a bearing ball goes into a little crack on one of the raceways, this will counteract on the developed torque. We assume that this works as a sine wave, working against developed torque on half the period and along with the torque on the other half period, this is a simplification.

In Figure 31 the torque subsystem is showed. There will be an extra input for the time. The speed of the rotor in revolutions per minute is calculated by the "RPM" block. Different calculations of the fault frequencies are named accordingly. And the different sine waves are calculated in the "GeneratingSineWave" blocks. The

last step is to decrease the amplitude of the sine wave to make it more realistic of a bearing faults. All the different fault categories are added together so they can all be simulated simultaneously. The frequency spectrum of a outer bearing defect is showed in Figure 32
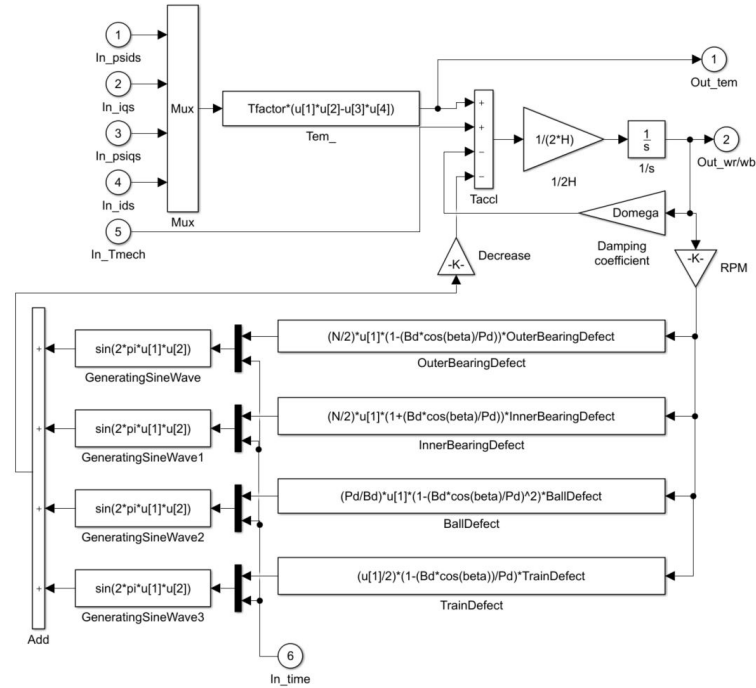
Figure 31: Torque subsystem with load modulation. The 4 different "GeneratingSineWave" functions generates a sine wave in the frequency given by the equations from Equation 3.49 and Equation 3.50
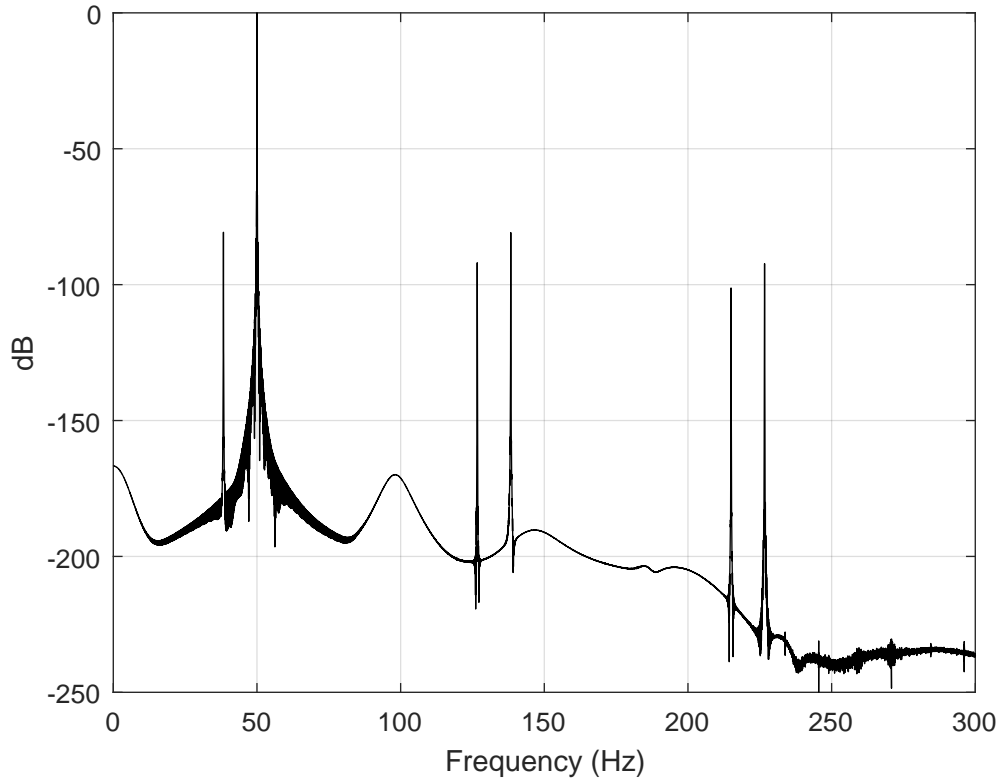
Figure 32: Simulated frequency spectrum of stator current i_a with outer raceway defect

3.8 Modelling of Stator Fault

The stator fault model derived in this section is developed to simulate cases with stator unbalance, such as inter-turn short circuits[8, 9]. If a short circuit in a winding occurs, the amount of effective turns in the winding will decrease. This affect both the resistance and the inductance.

3.8.1 Defining Model

We define p^*_{sca}, p^*_{scb} and p^*_{scc} as the percentage of short circuit in the stator phases a, b and c, respectively[8]. The coefficient for how healthy the phases are will be

defined as

$$p_{sca} \overset{\Delta}{=} 1 - p^*_{sca}$$

$$p_{scb} \overset{\Delta}{=} 1 - p^*_{scb}$$

$$p_{scc} \overset{\Delta}{=} 1 - p^*_{scc}$$

If there is no short circuits $p_{sca} = p_{scb} = p_{scc} = 1$. The stator resistance, stator inductance and mutual inductance are the affected parts of an unbalanced stator.

The stator resistance matrix r_s can be modified accordingly

$$r_s^{*abc} = \begin{bmatrix} p_{sca}r_s & 0 & 0 \\ 0 & p_{scb}r_s & 0 \\ 0 & 0 & p_{scc}r_s \end{bmatrix} \tag{3.51}$$

and needs to be transformed to $qd0$ reference by

$$r_s^{*qd0} = \left[T_{qd0}(\theta) \right] r_s^{*abc} \left[T_{qd0}(\theta) \right]^{-1} \tag{3.52}$$

where $\theta = 0$, this yields

$$r_s^{*qd0} = \frac{2}{3} \begin{bmatrix} 1 & -\frac{1}{2} & -\frac{1}{2} \\ 0 & -\frac{\sqrt{3}}{2} & \frac{\sqrt{3}}{2} \\ \frac{1}{2} & \frac{1}{2} & \frac{1}{2} \end{bmatrix} \begin{bmatrix} p_{sca}r_s & 0 & 0 \\ 0 & p_{scb}r_s & 0 \\ 0 & 0 & p_{scc}r_s \end{bmatrix} \begin{bmatrix} 1 & 0 & 1 \\ -\frac{1}{2} & -\frac{\sqrt{3}}{2} & 1 \\ -\frac{1}{2} & \frac{\sqrt{3}}{2} & 1 \end{bmatrix}$$

$$r_s^{*qd0} = \begin{bmatrix} \frac{1}{6}r_s\left(4p_{sca}+p_{scb}+p_{scc}\right) & \frac{1}{2\sqrt{3}}r_s\left(p_{scb}-p_{scc}\right) & \frac{1}{3}r_s\left(2p_{sca}-p_{scb}-p_{scc}\right) \\ \frac{1}{2\sqrt{3}}r_s\left(p_{scb}-p_{scc}\right) & \frac{1}{2}r_s\left(p_{scb}+p_{scc}\right) & \frac{1}{\sqrt{3}}r_s\left(p_{scc}-p_{scb}\right) \\ \frac{1}{6}r_s\left(2p_{sca}-p_{scb}-p_{scc}\right) & \frac{1}{2\sqrt{3}}r_s\left(p_{scb}-p_{scc}\right) & \frac{1}{3}r_s\left(p_{sca}+p_{scb}+p_{scc}\right) \end{bmatrix}$$

The inductance matrix of the stator can be modified accordingly

$$L_{ss}^{*abc} = \begin{bmatrix} p_{sca}^2\left(L_{ls}+L_{ss}\right) & p_{sca}p_{scb}L_{sm} & p_{sca}p_{scc}L_{sm} \\ p_{sca}p_{scb}L_{sm} & p_{scb}^2\left(L_{ls}+L_m\right) & p_{scb}p_{scc}L_{sm} \\ p_{sca}p_{scc}L_{sm} & p_{scb}p_{scc}L_{sm} & p_{scc}^2\left(L_{ls}+L_{sm}\right) \end{bmatrix} \tag{3.53}$$

and transformed to $qd0$ coordinates as

$$[\boldsymbol{T}_{qd0}(\theta)]\boldsymbol{L}_{ss}^{*abc}[\boldsymbol{T}_{qd0}(\theta)]^{-1}$$

yielding

$$\boldsymbol{L}_{ss}^{*qd0} = \begin{bmatrix} L_{ss11} & L_{ss12} & L_{ss13} \\ L_{ss21} & L_{ss22} & L_{ss23} \\ L_{ss31} & L_{ss32} & L_{ss33} \end{bmatrix}$$

where

$$L_{ss11} = \frac{1}{6}L_{ls}\left(4p_{sca}^2 + p_{scb}^2 + p_{scc}^2\right) + \frac{1}{9}L_m\left(4p_{sca}^2 + p_{scb}^2 + p_{scc}^2 + 2p_{sca}p_{scb} + 2p_{sca}p_{scc} - p_{scb}p_{scc}\right)$$

$$L_{ss12} = \frac{1}{2\sqrt{3}}L_{ls}\left(p_{scb}^2 - p_{scc}^2\right) + \frac{1}{3\sqrt{3}}L_m\left(p_{scb}^2 - p_{scc}^2\right)$$

$$L_{ss13} = \frac{1}{3}L_{ls}\left(2p_{sca}^2 - p_{scb}^2 - p_{scc}^2\right) + \frac{1}{9}L_m\left(4p_{sca}^2 - 2p_{scb}^2 - 2p_{scc}^2 + 2p_{scb}p_{scc} - p_{sca}p_{scb} - p_{sca}p_{scc}\right)$$

$$L_{ss21} = \frac{1}{2\sqrt{3}}L_{ls}\left(p_{scb}^2 - p_{scc}^2\right) + \frac{1}{3\sqrt{3}}L_m\left(p_{scb}^2 - p_{scc}^2\right)$$

$$L_{ss22} = \frac{1}{2}L_{ls}\left(p_{scb}^2 + p_{scc}^2\right) + \frac{1}{3}L_m\left(p_{scb}^2 + p_{scc}^2 + p_{scb}p_{scc}\right)$$

$$L_{ss23} = \frac{1}{\sqrt{3}}L_{ls}\left(p_{scc}^2 - p_{scb}^2\right) + \frac{1}{3\sqrt{3}}L_m\left(p_{sca}p_{scb} - p_{sca}p_{scc} + 2p_{scc}^2 - 2p_{scb}^2\right)$$

$$L_{ss31} = \frac{1}{6}L_{ls}\left(2p_{sca}^2 - p_{scb}^2 - p_{scc}^2\right) + \frac{1}{18}L_m\left(4p_{sca}^2 - 2p_{scb}^2 - 2p_{scc}^2 - p_{sca}p_{scb} - p_{sca}p_{scc} + 2p_{scb}p_{scc}\right)$$

$$L_{ss32} = \frac{1}{2\sqrt{3}}L_{ls}\left(p_{scb}^2 - p_{scc}^2\right) + \frac{1}{6\sqrt{3}}L_m\left(2p_{scc}^2 - 2p_{scb}^2 + p_{sca}p_{scb} - p_{sca}p_{scc}\right)$$

$$L_{ss33} = \frac{1}{3}L_{ls}\left(p_{sca}^2 + p_{scb}^2 + p_{scc}^2\right) + \frac{2}{9}L_m\left(p_{sca}^2 + p_{scb}^2 + p_{scc}^2 - p_{sca}p_{scb} - p_{sca}p_{scc} - p_{scb}p_{scc}\right)$$

The mutual inductance $\boldsymbol{L}_{sr}$ can be modified as

$$\boldsymbol{L}_{sr}^{*abc} = L_{sr}\begin{bmatrix} p_{sca}\cos(\theta_r) & p_{sca}\cos\left(\theta_r + \frac{2\pi}{3}\right) & p_{sca}\cos\left(\theta_r - \frac{2\pi}{3}\right) \\ p_{scb}\cos\left(\theta_r - \frac{2\pi}{3}\right) & p_{scb}\cos(\theta_r) & p_{scb}\cos\left(\theta_r + \frac{2\pi}{3}\right) \\ p_{scc}\cos\left(\theta_r + \frac{2\pi}{3}\right) & p_{scc}\cos\left(\theta_r - \frac{2\pi}{3}\right) & p_{scc}\cos(\theta_r) \end{bmatrix}$$

and transformed by $\left[\boldsymbol{T}_{qd0}(\theta)\right]\boldsymbol{L}_{sr}^{abc}\left[\boldsymbol{T}_{qd0}(\theta-\theta_r)\right]^{-1}$ yielding

$$\boldsymbol{L}_{sr}^{*qd0} = \begin{bmatrix} L_{sr11} & L_{sr12} & L_{sr13} \\ L_{sr21} & L_{sr22} & L_{sr23} \\ L_{sr31} & L_{sr32} & L_{sr33} \end{bmatrix}$$

where

$$L_{sr11} = \frac{1}{6}L_m\left(4p_{sca}+p_{scb}+p_{scc}\right)$$

$$L_{sr12} = \frac{\sqrt{3}}{6}L_m\left(p_{scb}-p_{scc}\right)$$

$$L_{sr13} = 0$$

$$L_{sr21} = \frac{\sqrt{3}}{6}L_m\left(p_{scb}-p_{scc}\right)$$

$$L_{sr22} = \frac{1}{2}L_m\left(p_{scb}+p_{scc}\right)$$

$$L_{sr23} = 0$$

$$L_{sr31} = \frac{1}{6}L_m\left(2p_{sca}-p_{scb}-p_{scc}\right)$$

$$L_{sr32} = \frac{\sqrt{3}}{6}L_m\left(p_{scc}-p_{scb}\right)$$

$$L_{sr33} = 0$$

The last affected inductance $\boldsymbol{L}_{rs}^{abc} = \left[\boldsymbol{L}_{sr}^{abc}\right]^T$ is transformed by $\left[\boldsymbol{T}_{qd0}(\theta-\theta_r)\right]\boldsymbol{L}_{sr}^{abc}\left[\boldsymbol{T}_{qd0}(\theta_r)\right]^{-1}$ yielding

$$\boldsymbol{L}_{rs}^{*qd0} = \begin{bmatrix} L_{rs11} & L_{rs12} & L_{rs13} \\ L_{rs21} & L_{rs22} & L_{rs23} \\ L_{rs31} & L_{rs32} & L_{rs33} \end{bmatrix}$$

where

$$L_{rs11} = \frac{1}{6}L_m\left(4p_{sca} + p_{scb} + p_{scc}\right)$$

$$L_{rs12} = \frac{\sqrt{3}}{6}L_m\left(p_{scb} - p_{scc}\right)$$

$$L_{rs13} = \frac{1}{3}L_m\left(2p_{sca} - p_{scb} - p_{scc}\right)$$

$$L_{rs21} = \frac{\sqrt{3}}{6}L_m\left(p_{scb} - p_{scc}\right)$$

$$L_{rs22} = \frac{1}{2}L_m\left(p_{scb} + p_{scc}\right)$$

$$L_{rs23} = \frac{\sqrt{3}}{6}L_m\left(p_{scc} - p_{scb}\right)$$

$$L_{rs31} = L_{rs32} = L_{rs33} = 0$$

All these new inductances and the new resistance are used in Equation 3.31. The modification of the model will be done in the q,d and $zero$ subsystem. The q-axis is shown in Figure 33. In Figure 34 the frequency spectrum of phase a with 1% shorted stator is showed.
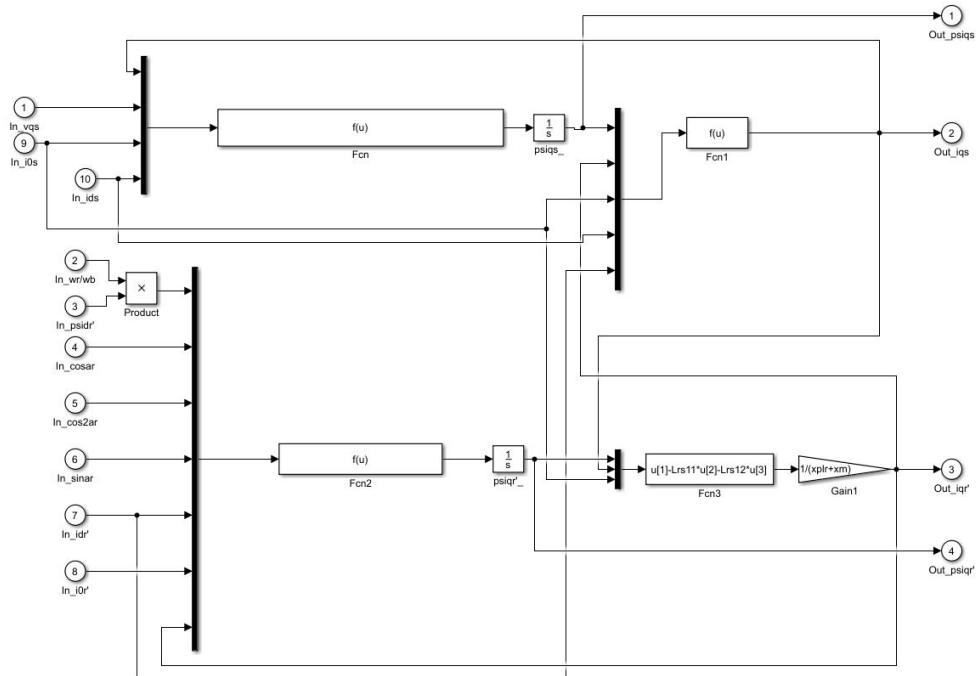
Figure 33: q-axis subsystem from Simulink with stator fault
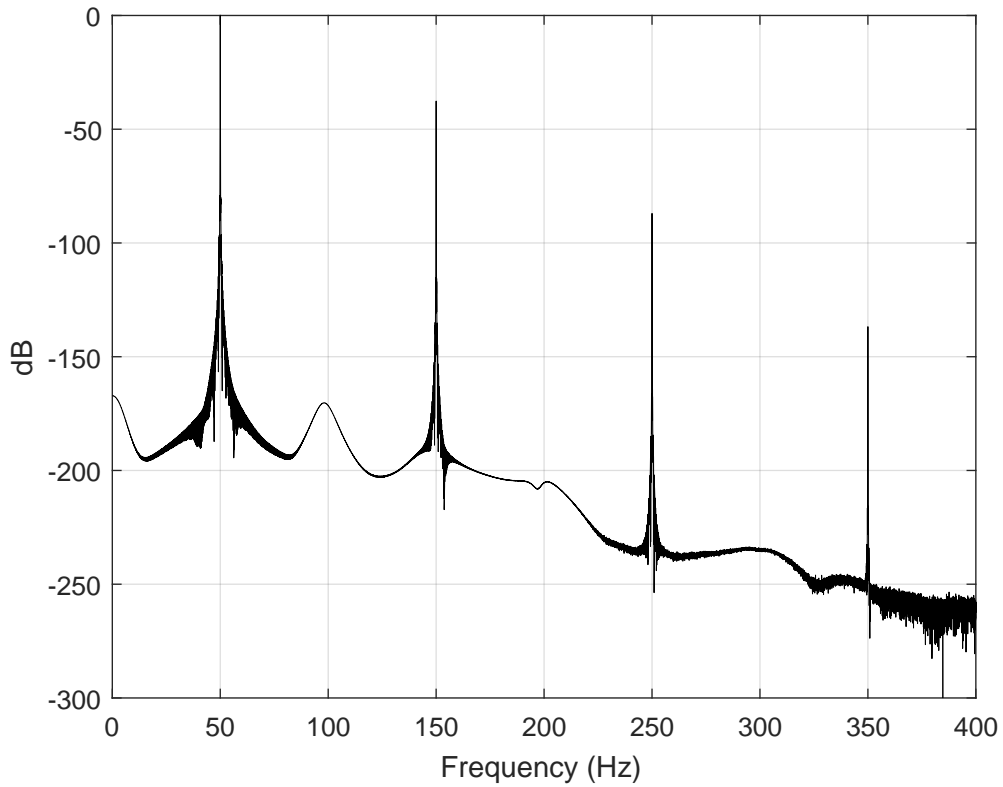
Figure 34: Simulated frequency spectrum of stator current i_a with 1% shorted in phase a

3.9   Damping Factor

A damping factor is used in the torque subsystem from Figure 18. This factor accounts for all the losses which are not included in the simulation model. It needs to be correct if an operator wants to compare many of the values in the simulation against practical experiments. To find the damping factor we need to have a look at the power flow in an induction motor. This is shown in Figure 35. P_{in} is the power delivered to the motor. P_{ag} is the air-gap power, which is the input power minus stator core loss P_{fe} and stator resistance loss P_{cu1}. P_{mech} is the mechanical power after losses in rotor resistance P_{cu2} and rotor core losses P_{fe2}. The rotor core loss is normally negligible since its amplitude is dependent on the frequency in the rotor f_2, which in normal operations are very low. The power transferred to the rotor P_{out} is the mechanical power minus friction, windage and ventilation.
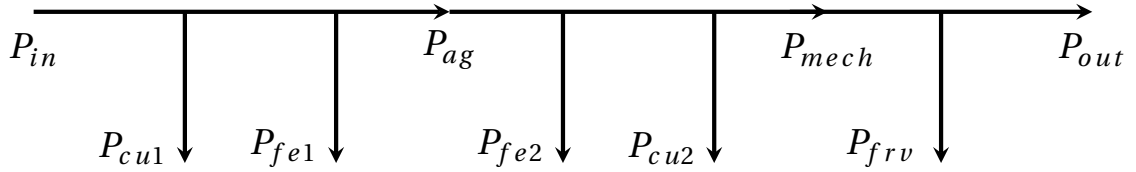
Figure 35: Power flow in an induction motor

In the model developed, stator and rotor core losses are neglected as well as friction, ventilation and windage, we define these neglected losses as P_{neg}. If the operator does not have any of these at hand, they can be easy calculated as follows

$$P_{neg} = P_{in} - P_{cu1} - P_{cu2} - P_{out} \tag{3.54}$$

which gives a damping factor as

$$T_{damp} = \frac{P_{neg}}{\omega_N} \tag{3.55}$$

where ω_N is the mechanical angular rated velocity.

3.10   Generic Model

The object of this chapter is to integrate all the previous developed models to a generic model. The BRB and bearing fault models does not interfere with each other or the other models, these are straight forward and easy to integrate. On the other hand, eccentricity and stator fault does interfere. The mutual reactance which is modulated in the eccentricity fault is used in all the new inductance calculations in the stator fault. In Figure 36 the q-axis subsystem is shown, the d-axis and $zero$-sequence subsystems have similar modifications. The rotor subsystem is the same as with the bearing faults.
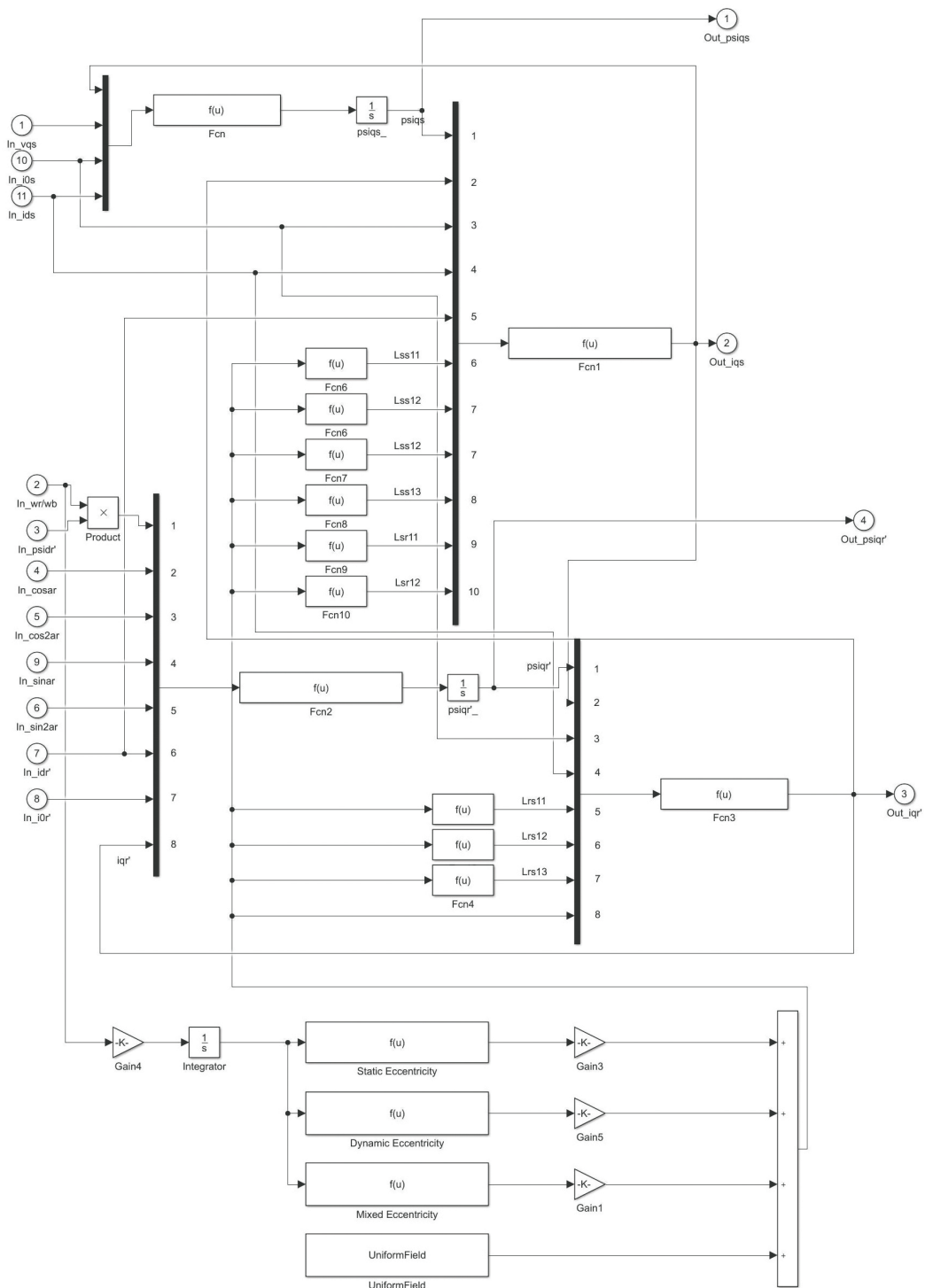
Figure 36: q-axis subsystem in the generic model. All the previous faulty models are integrated, creating a generic model.

63

3.11 Subsea Model

As mentioned earlier, some oil and gas resources can be reached with only sub-sea equipment. Some of the components on the seabed can be driven by SCIMs, for example pumps and compressors. This subsea connection is also modelled in Simulink. Normally the motor is run by a VSD which often uses PWM to get the acquired voltage and frequency. Since the simulation only needs steady state operations, a PWM is used at a set frequency. The PWM is connected to a step-up transformer from Simulink library which increases the voltage and decreases the losses in the cable. The step-up transformer is connected to a cable model from Simulink library. A step-down transformer can be used after the cable, but this depends on overall cost and motor specifications[6]. A principal sketch of the central components is shown in Figure 37.
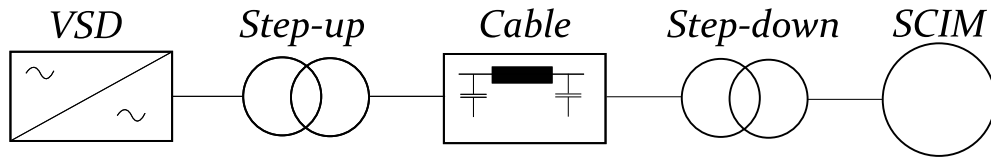
Figure 37: One-line diagram of the central components from the VSD to the SCIM[6].

The parameters used when testing the model for subsea operations are found from previous studies on modelling and testing converter-fed motor drives[6, 14]. The parameters for cable and motor can be found in Appendix B.2. The voltage after the cable is modelled as ideal, this means it will not get influenced by the motor when running. This also means that the current running in the cable model will also not get influenced, and thereby is not usable in an analyzing context. Instead the current extracted from the model needs to be sent back through to the model from ideal current sources. This current is influenced by the motor and should give a realistic view of the condition of the motor. FFT is applied on the values extracted from the "z1" block as shown in Figure 38.
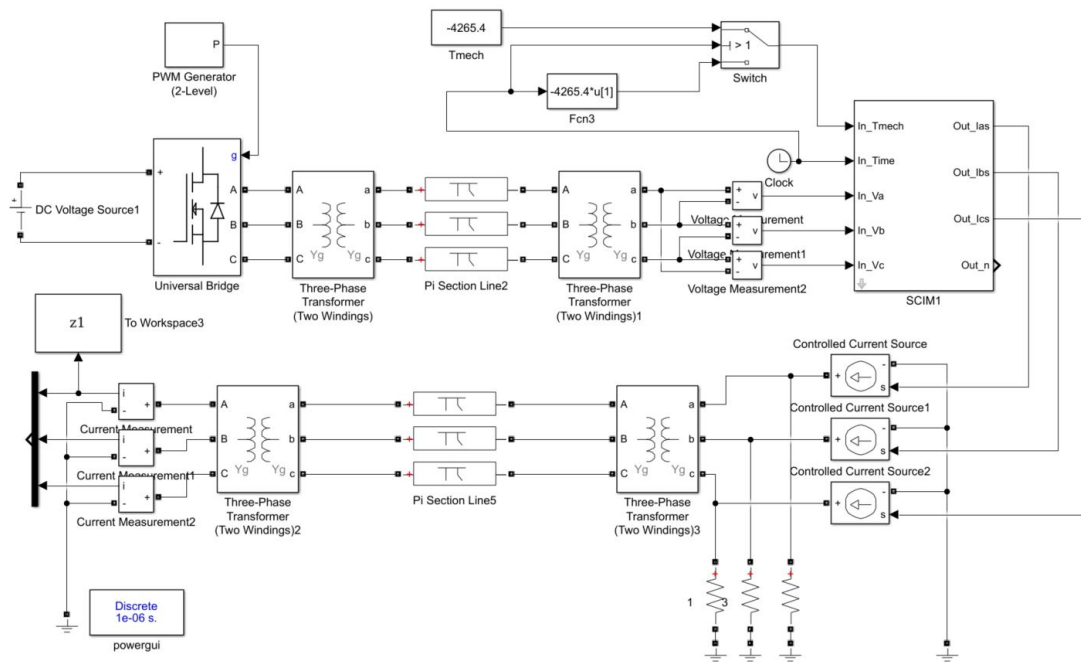
Figure 38: Figure of Simulink program with PWM and cable model. The voltage after cable model works as ideal voltage source, the currents are extracted and run through the cable model, produced by ideal current sources. The FFT analysis is extracted from the "to workspace" block "z1"

3.12 Graphical User Interface

A graphical user interface (GUI) is implemented to make the generic model easier to operate. The user do not need to declare variables in Matlab as earlier[22]. The input to the model are voltages, time and load, the output are currents and speed. The speed can be used if the load is dependent on it, as it usually is. The parameter settings are showed in Figure 39 and BRB settings are showed in Figure 40. The other fault options are similar to BRB, by first activating the fault and then setting the details.
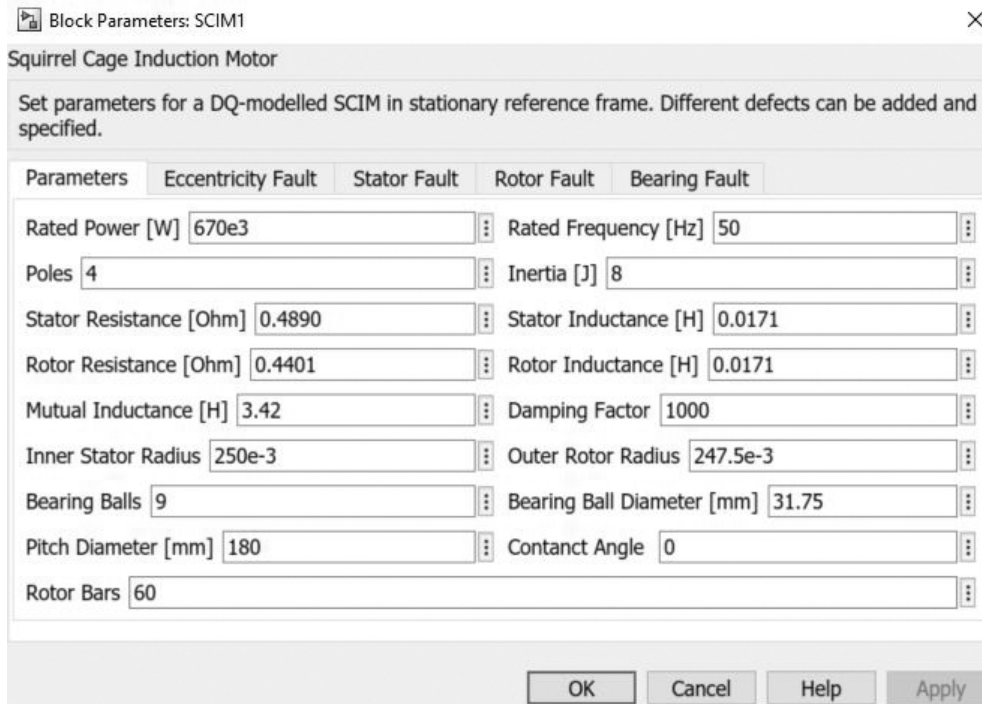
Figure 39: Graphical user interface of SCIM model, parameters. The operator can easily change parameters of the motor
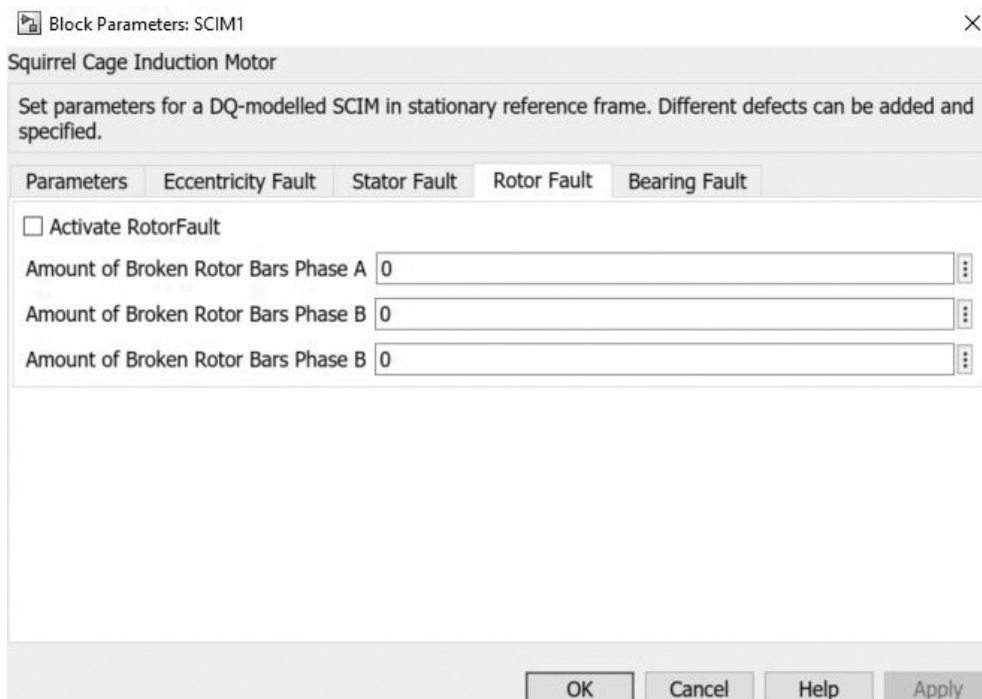
Figure 40: Graphical user interface of SCIM model, . The operator can easily initialize faults in the motor. From this figure the rotor fault options are open. The fault must first be activated, then the amount of broken bar in the desired phase can be initiated

3.13   Expected Frequencies

The frequency components which can be expected are presented in Table 1. These are calculated from section 2.4.2, in rated operations. The parameters used for the motor can be found in Appendix B.1.

Table 1: Expected frequencies in rated operations, $k = 1, 2, 3$ except in f_{eccd} and f_{eccs} where $k = v = 1$, negative frequencies are neglected

	Equation	Frequency component $[Hz]$
Eccentricity	$f_{ecc1} = f \pm k f_r$	2.17, 26.08, 73.92, 97.83, 121.75
Eccentricity	$f_{eccd} = f\left((kR \pm n_d)\left(\frac{1-s}{P}\right) \pm v\right)$	595.75, 643.58, 695.75, 743.58
Eccentricity	$f_{eccs} = f\left(kR\left(\frac{1-s}{P}\right) \pm v\right)$	619.67, 719.67
Bearing	$f_{ob} = \mid f \pm k f_{ob} \mid$	38.33, 126.66, 138.33, 214.99, 226.66, 314.99
Bearing	$f_{ib} = \mid f \pm k f_{ib} \mid$	76.92, 176.92, 203.84, 303.84, 330.76, 430.76
Bearing	$f_b = \mid f \pm k f_b \mid$	79.11, 179.11, 208.23, 308.23, 337.34, 437.34
Bearing	$f_t = \mid f \pm k f_t \mid$	20.56, 30.37, 40.19, 59.71, 69.61, 79.44
Rotor	$f_{BRB1} = f(1 \pm 2ks)$	37.00, 41.33, 45.67, 54.33, 58.67, 63.00
Rotor	$f_{BRB2} = f(3 \pm 2ks)$	137.00, 141.33, 145.67, 154.33, 158.67, 163.00
Rotor	$f_{BRB3} = f(5 \pm 2ks)$	237.00, 241.33, 245.67, 254.33, 258.67, 263.00
Stator	$f_{ss1} = f\left(k \pm n\frac{1-s}{p}\right)$	26.08, 73.92, 76.08, 123.92, 126.08, 173.92
Stator	$f_{ss2} = 3f$	150.00

4 Results

All the simulation results are presented in this section. All tests were done in rated operations with the generic model, parameters can be found in Appendix B.1. The simulation time is 60 seconds with a maximum step size of $0.0001s$ at variable step with ode45 solver. As a result of the defects the rotor speed drops and oscillates below rated speed, the mean speed is used when calculating slip in these cases. When a mean speed is used the estimated result is presented with *. All frequency plots are normalized with respect to the $50Hz$ component and presented in the dB scale. To decrease the spectral leakage hann window (sometimes referred to as hanning window) is applied[47]. The script used for the FFT can be found in Appendix C.

4.1 Healthy

A healthy simulation of the motor is presented in Figure 41.
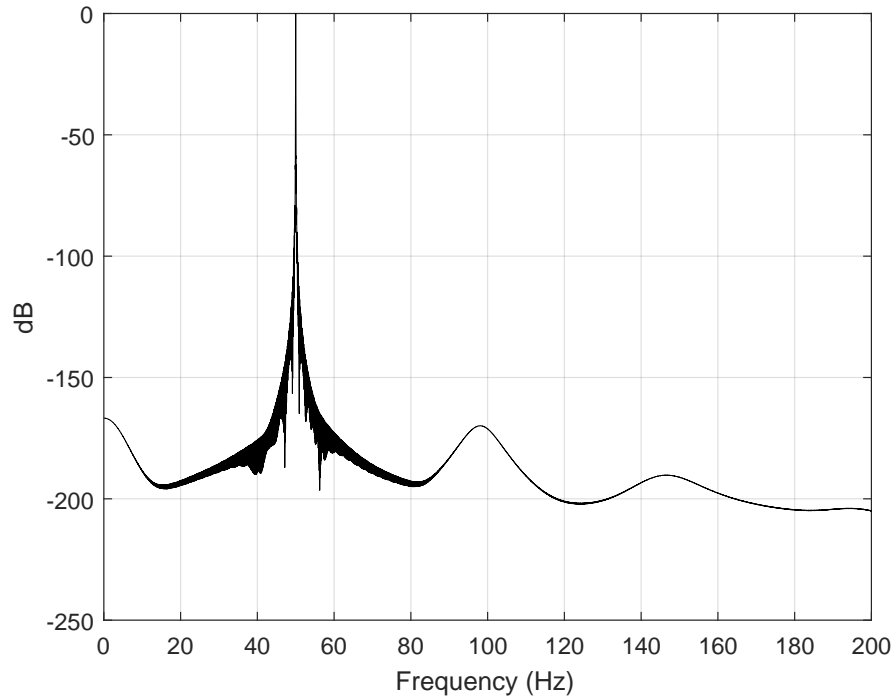
Figure 41: Simulated frequency spectrum from stator current in a healthy motor. Simulation time is 60 seconds with maximum step size of $0.0001s$ in variable steps with ode45 solver. The motor is running in rated operations.

4.2 Broken Rotor Bars

The simulations with 1 and 3 broken rotor bars in phase a are presented in Figure 42 and Figure 43 with detailed information in Table 2 and Table 3. With one broken rotor bar the mean rotor speed was 1432.6 rpm and for three broken rotors bars the mean rotor speed was 1427 rpm.
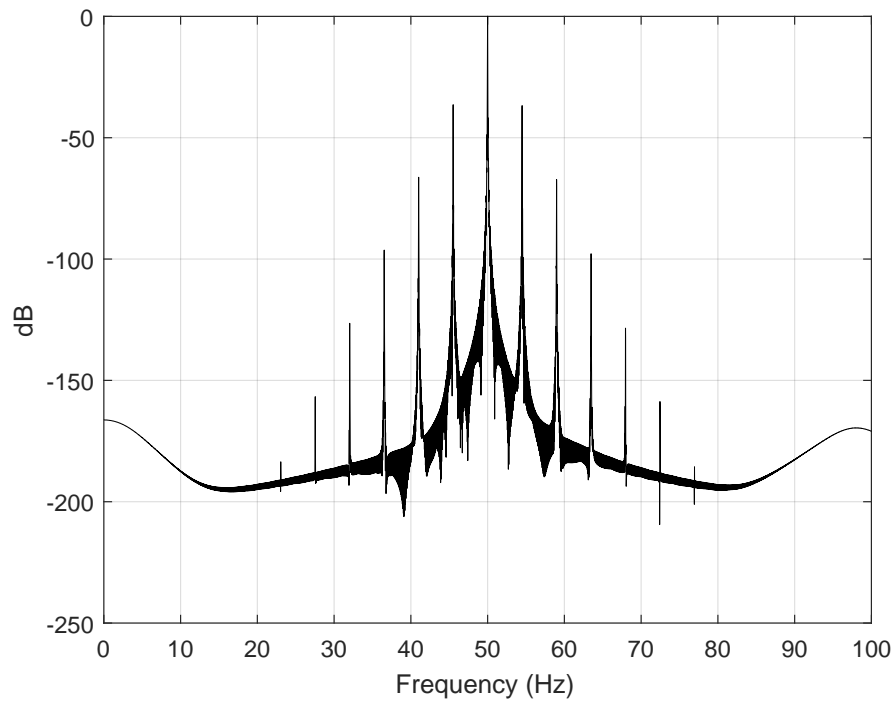
Figure 42: Simulated frequency spectrum from stator current with one broken rotor bar. Simulation time is 60 seconds with maximum step size of $0.0001s$ in variable steps with ode45 solver. The motor is running in rated operations.

Table 2: Results from simulation with one broken rotor bar

	Rated*	Sim[Hz]	Sim[dB]
$f(1+2s)$	54.49	54.49	−36.76
$f(1+4s)$	58.99	58.99	−67.25
$f(1+6s)$	63.48	63.48	−97.82
$f(1-2s)$	45.51	45.51	−36.39
$f(1-4s)$	41.01	41.01	−66.29
$f(1-6s)$	36.52	36.53	−96.30

When using Equation 2.7 to determine how many broken rotor bar there are, it equals $n = 0.81$.

Figure 43: Simulated frequency spectrum from stator current with three broken rotor bars. Simulation time is 60 seconds with maximum step size of $0.0001s$ in variable steps with ode45 solver. The motor is running in rated operations.

Table 3: Results from simulation with three broken rotor bars

	Rated*	Sim[Hz]	Sim[dB]
$f(1+2s)$	54.87	54.87	-26.61
$f(1+4s)$	59.73	59.73	-46.76
$f(1+6s)$	64.60	63.60	-66.82
$f(1-2s)$	45.13	45.14	-26.24
$f(1-4s)$	40.27	40.27	-45.84
$f(1-6s)$	35.40	35.41	-65.40

When using Equation 2.7 to determine how many broken rotor bar there are, it equals $n = 2.44$.

4.3 Eccentricity Fault

Since the frequency components from Equation 2.8 uses parameters which is not included in the model with eccentricity fault, these will not be inspected. The mixed eccentricity components from Equation 2.9 with $k = 1, 2, 3, 4, 5$ will be inspected instead. Also, there are no formula for the frequency components around the fundamental with static or dynamic individually, the results are presented anyhow. The mean rotor speed for this simulation in rpm were; 1435, 1437.7 and 1430.3 for static, dynamic and mixed, respectively. The offset is set at $0.1mm$ for static, the major and minor axes are set as $47.7mm$ and $47.5mm$ for dynamic, respectively.
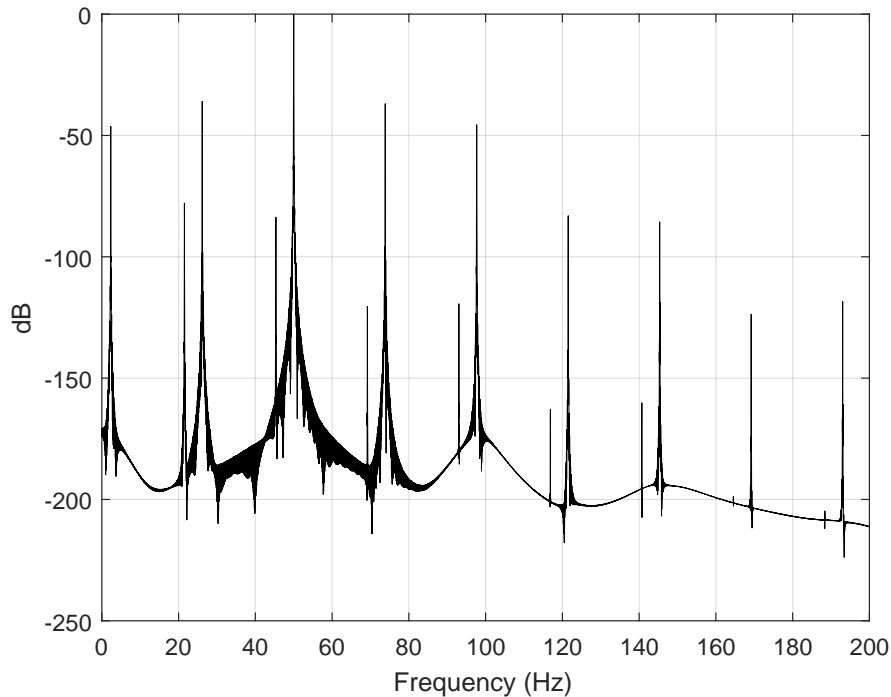
Figure 44: Simulated frequency spectrum from stator current with mixed eccentricity. The center offset is $0.1mm$, major axes $47.7mm$ and minor axes $47.5mm$. Simulation time is 60 seconds with sampling frequency of 0.0001 in variable steps with ode45 solver. The motor is running in rated operations.

Table 4: Results from simulation with mixed eccentricity fault

	Rated*	Sim[Hz]	Sim[dB]
$|f+1f_r|$	73.83	73.84	−36.92
$|f+2f_r|$	97.68	97.68	−45.60
$|f+3f_r|$	121.52	121.52	−83.08
$|f+4f_r|$	145.35	145.36	−85.63
$|f+5f_r|$	169.19	169.19	−123.62
$|f-1f_r|$	26.16	26.16	−35.89
$|f-2f_r|$	2.32	2.33	−46.22
$|f-3f_r|$	21.52	21.52	−77.87
$|f-4f_r|$	45.35	45.35	−83.76
$|f-5f_r|$	69.19	69.19	−120.42

The static- and dynamic eccentricity individually are presented in Figure 45 and Figure 46.
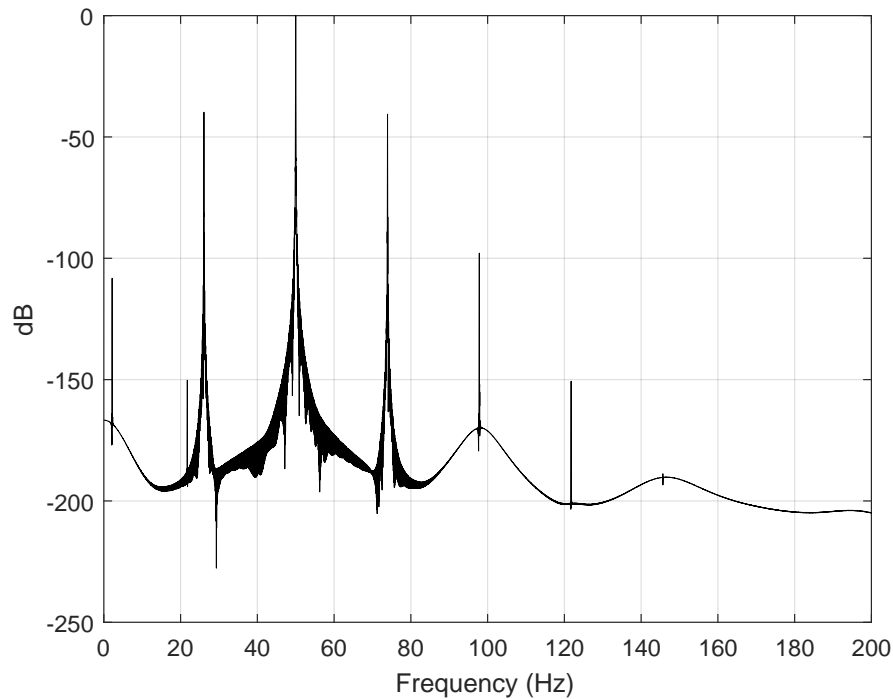
Figure 45: Simulated frequency spectrum from stator current with static eccentricity. The center offset is $0.1mm$. Simulation time is 60 seconds with maximum step size of $0.0001s$ in variable steps with ode45 solver. The motor is running in rated operations.
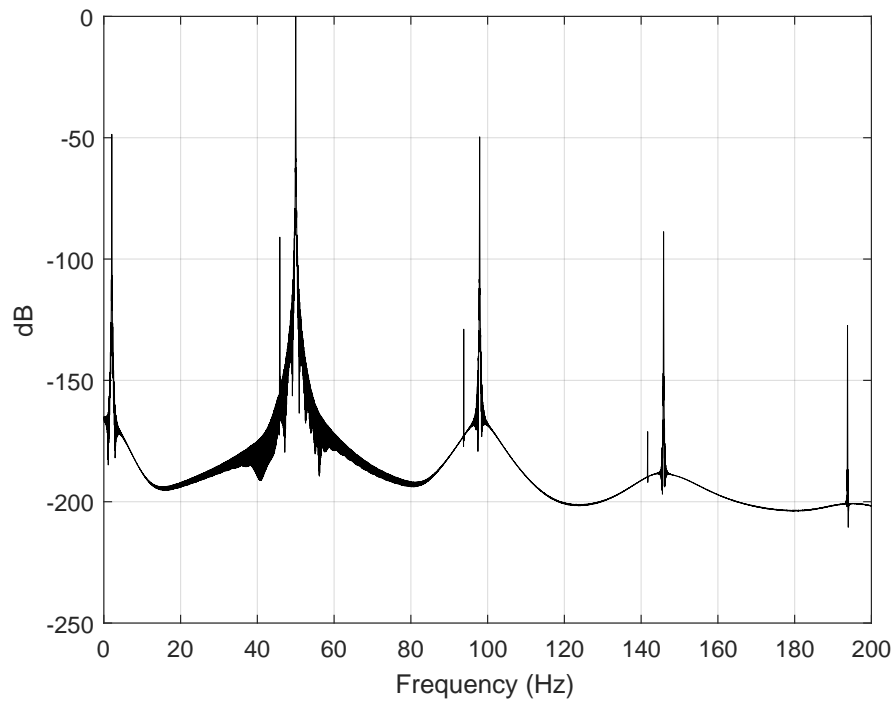
Figure 46: Simulated frequency spectrum from stator current with dynamic eccentricity. The major axes is $47.7mm$ and minor axes is $47.5mm$. Simulation time is 60 seconds with maximum step size of $0.0001s$ in variable steps with ode45 solver. The motor is running in rated operations.

4.4 Bearing Fault

The four different categories of bearing faults are simulated independently. The rotor speed is at rated values. Outer raceway defect is showed in Figure 47 with details in Table 5.
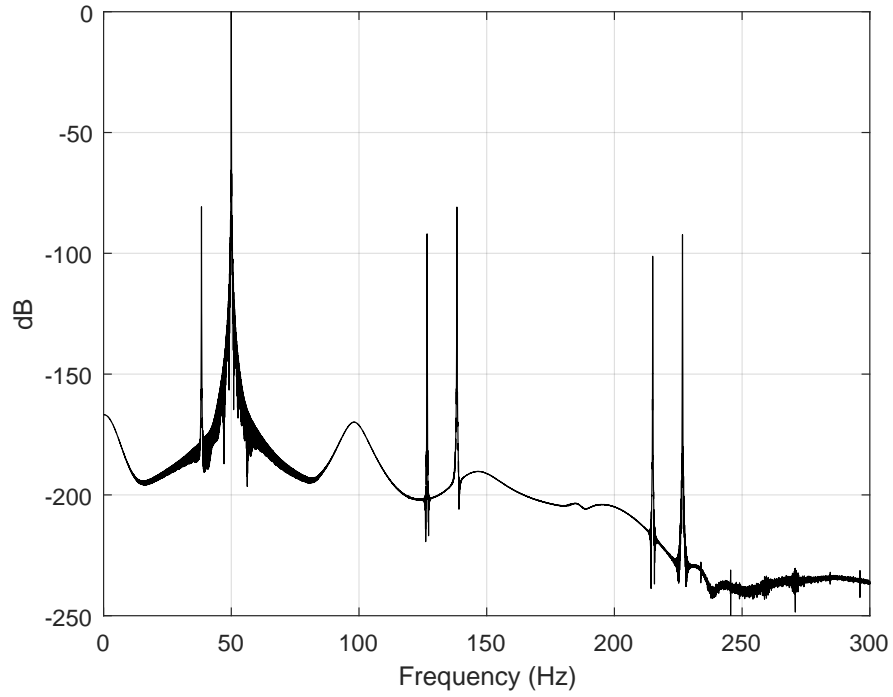
Figure 47: Simulated frequency spectrum from stator current with outer race-way defect. Simulation time is 60 seconds with maximum step size of $0.0001s$ in variable steps with ode45 solver. The motor is running in rated operations.

Table 5: Results from simulation with outer raceway defect

	Rated	Sim[Hz]	Sim[dB]
$\lvert f + 1f_{ob} \rvert$	138.33	138.33	-95.44
$\lvert f + 2f_{ob} \rvert$	226.66	226.66	-112.32
$\lvert f - 1f_{ob} \rvert$	38.33	38.33	-95.97
$\lvert f - 2f_{ob} \rvert$	126.66	126.66	-112.32
$\lvert f - 3f_{ob} \rvert$	215	215	-133.70

Simulation of inner raceway defect is showed in Figure 48, details can be found in Table 6.
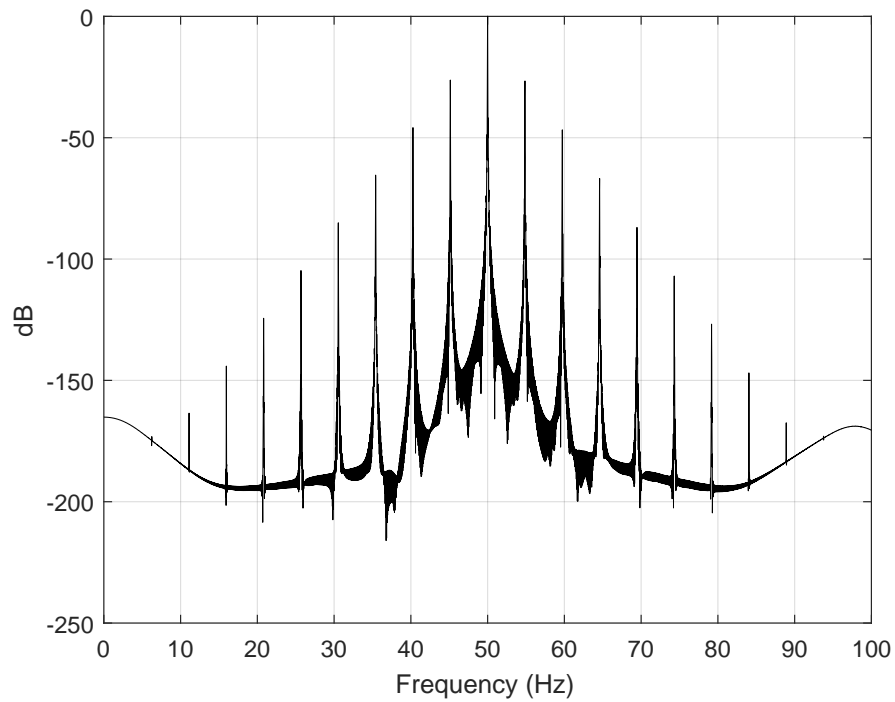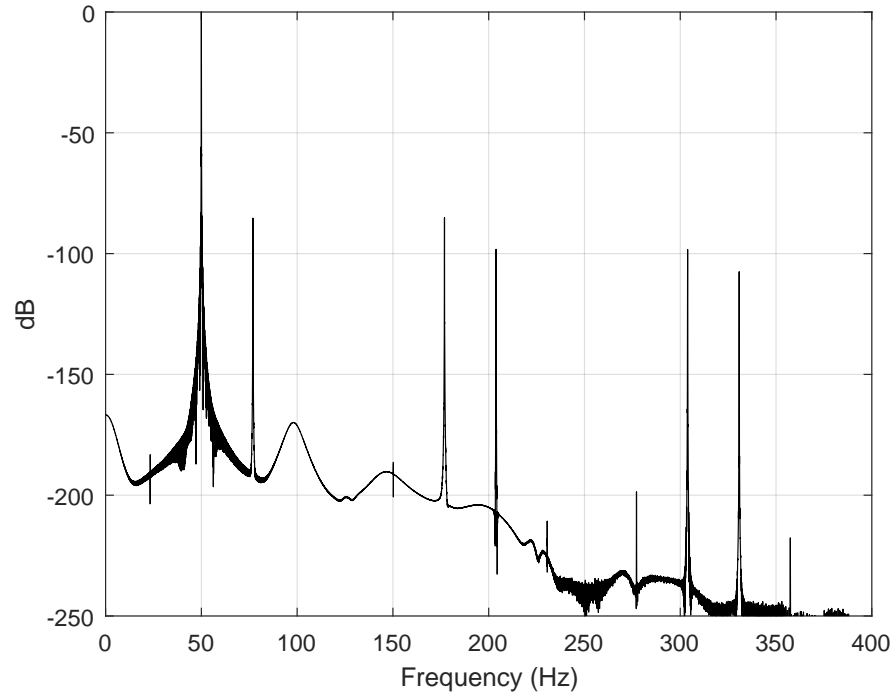

Figure 48: Simulated frequency spectrum from stator current with inner raceway defect. Simulation time is 60 seconds with maximum step size of $0.0001s$ in variable steps with ode45 solver. The motor is running in rated operations.

Table 6: Results from simulation with inner raceway defect

	Rated	Sim[Hz]	Sim[dB]
$\lvert f+1f_{ib} \rvert$	176.92	176.93	-93.15
$\lvert f+2f_{ib} \rvert$	303.84	303.85	-114.89
$\lvert f-1f_{ib} \rvert$	76.92	76.92	-92.75
$\lvert f-2f_{ib} \rvert$	203.84	203.85	-114.48
$\lvert f-3f_{ib} \rvert$	330.76	330.77	-134.34

Simulation of ball defect is showed in Figure 49, details can be found in Table 7.
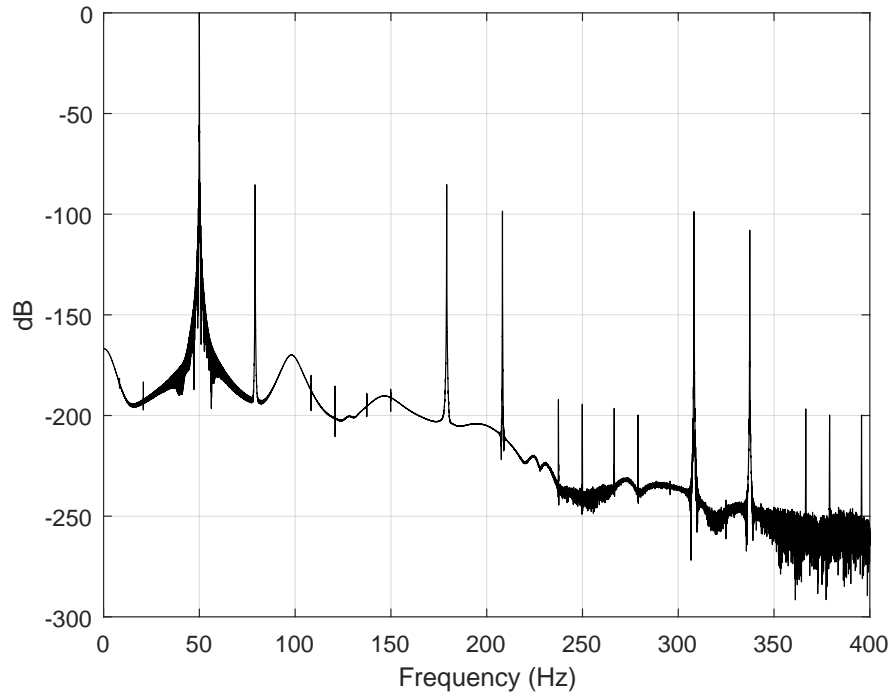
Figure 49: Simulated frequency spectrum from stator current with ball defect. Simulation time is 60 seconds with maximum step size of $0.0001s$ in variable steps with ode45 solver. The motor is running in rated operations.

Table 7: Results from simulation with ball defect

	Rated	Sim$[Hz]$	Sim$[dB]$
$\|f+1f_b\|$	179.11	179.11	-93.26
$\|f+2f_b\|$	308.23	308.22	-114.80
$\|f-1f_b\|$	79.11	79.12	-92.80
$\|f-2f_b\|$	208.22	208.24	-114.87
$\|f-3f_b\|$	337.33	337.35	-133.87

Simulation of cage defect is showed in Figure 50, details can be found in Table 8.

Figure 50: Simulated frequency spectrum from stator current with cage defect. Simulation time is 60 seconds with maximum step size of $0.0001s$ in variable steps with ode45 solver. The motor is running in rated operations.

Table 8: Results from simulation with cage defect

	Rated	Sim[Hz]	Sim[dB]
$\lvert f+1f_t \rvert$	59.81	59.82	-100.76
$\lvert f+2f_t \rvert$	69.63	69.63	-156.02
$\lvert f-1f_t \rvert$	40.19	40.19	-96.83
$\lvert f-2f_t \rvert$	30.37	30.38	-153.15

4.5 Stator Fault

The simulation of the stator fault with 1% shorted a phase is showed in Figure 51 and details in Table 9.
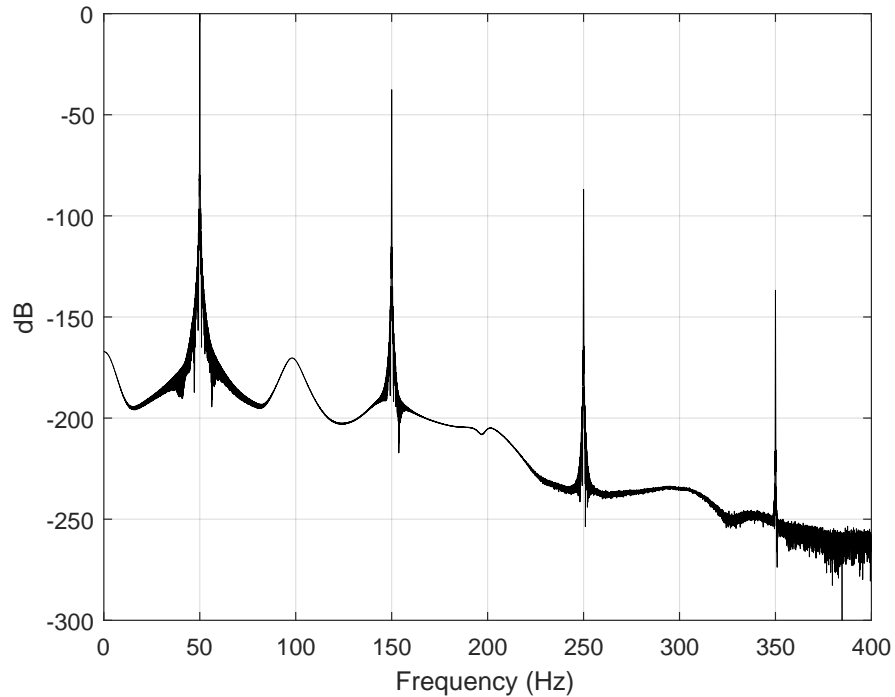
Figure 51: Simulated frequency spectrum from stator current with 1% shorted windings in phase a. Simulation time is 60 seconds with maximum step size of $0.0001s$ in variable steps with ode45 solver. The motor is running in rated operations.

Table 9: Results from simulation with 1% shorted stator winding

	Rated	Sim[Hz]	Sim[dB]
$3f$	150.00	150.00	-37.90
$5f$	250.00	250.00	-87.01
$7f$	350.00	350.00	-136.80

79

Simulation of stator fault with 3% shorted a phase is showed Figure 52 with details in Table 10.
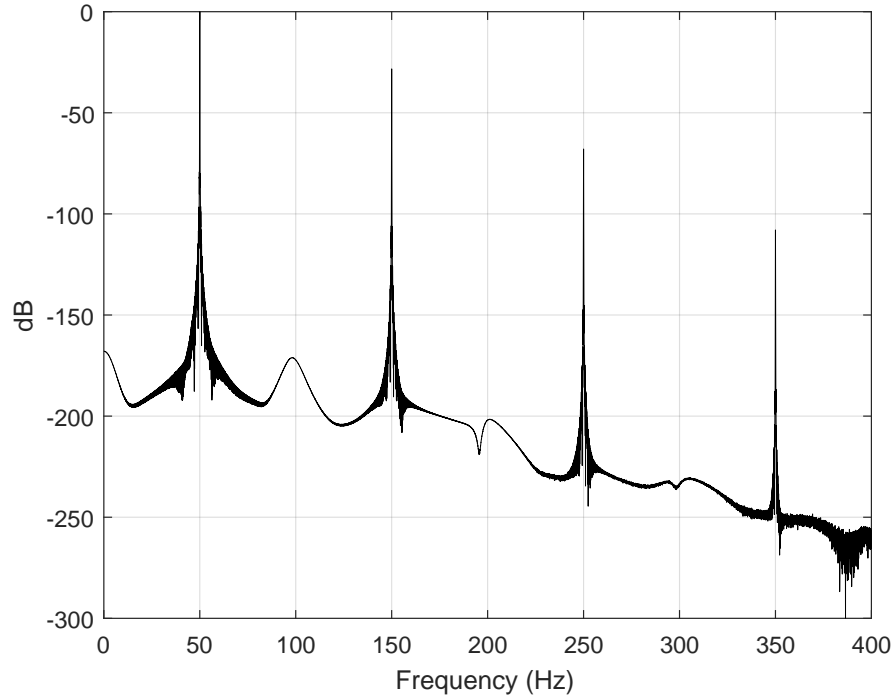
Figure 52: Simulated frequency spectrum from stator current with 3% shorted windings in phase a. Simulation time is 60 seconds with maximum step size of $0.0001s$ in variable steps with ode45 solver. The motor is running in rated operations.

Table 10: Results from simulation with 3% shorted stator winding

	Rated	Sim[Hz]	Sim[dB]
$3f$	150.00	150.00	-28.31
$5f$	250.00	250.00	-67.91
$7f$	350.00	350.00	-107.96

4.6 Subsea SCIM

The solver is set at discrete with a sample time of $1e-6s$, the simulation time is 60 seconds. The high sampling frequency results in a better performance of the PWM. From Figure 53 we can see how the sampling frequency affects the rotor speed. In figure a the sampling time is set at $1e-5s$ and the speed varies from 1431 to 1540.

When the sampling time is decreased to $1e-7s$ as in figure c, the speed varies from 1486 to 1494, but as a result of limited computer power the sampling is set at $1e-6s$ in the rest of the results. Some parameters from the subsea SCIM are estimated or taken from similar sized motors as they were not included in the source[4, 48]. To show if the faulted induction motor model is compatible in a subsea context, all four fault categories are simulated. The sampling frequency for the stator current is set at $10kHz$. The switching frequency of the PWM is $5kHz$
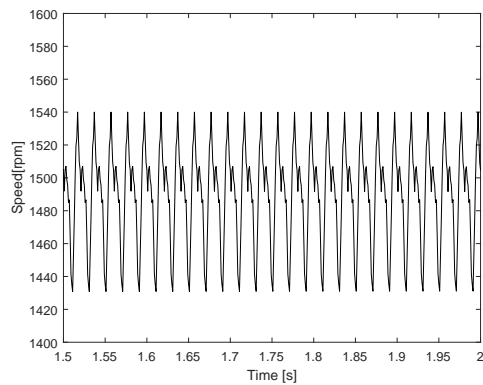
(a) Sample time set at $1e-5s$
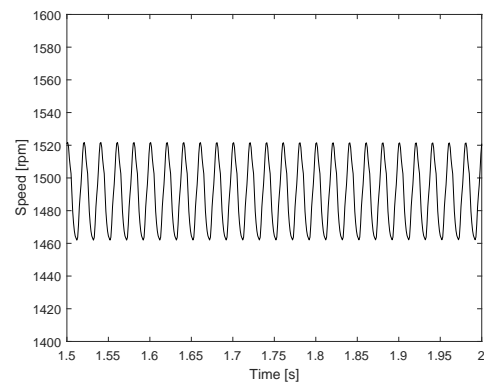
(b) Sample time set at $1e-6s$
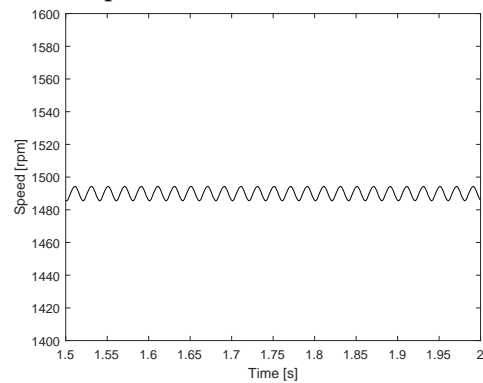
(c) Sample time set at $1e-7s$

Figure 53: Speed disparity related to sampling frequency. Sampling time is 60 seconds with a healthy motor in rated operations.

Three simulations with different sampling times are run in 10 seconds to test how the different sampling times affect the frequency spectra. The cable model are removed in this simulation. As can be seen in Figure 54, the harmonics are decreasing with increasing sampling frequency.
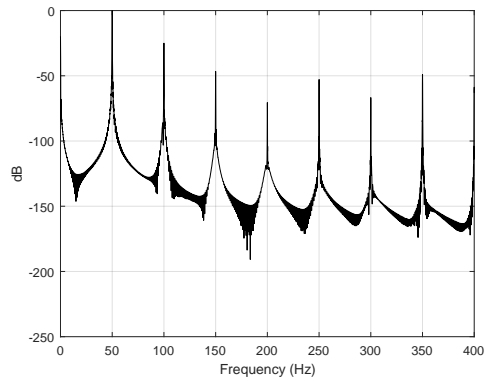
(a) Sample time set at $1e-5s$
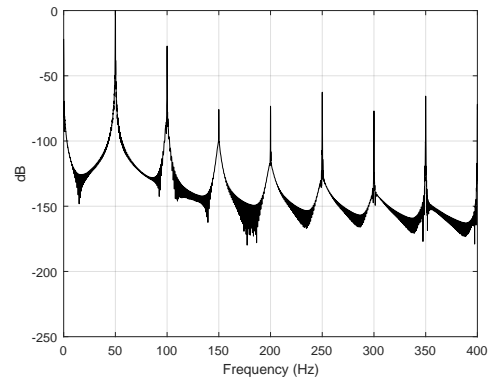
(b) Sample time set at $1e-6s$
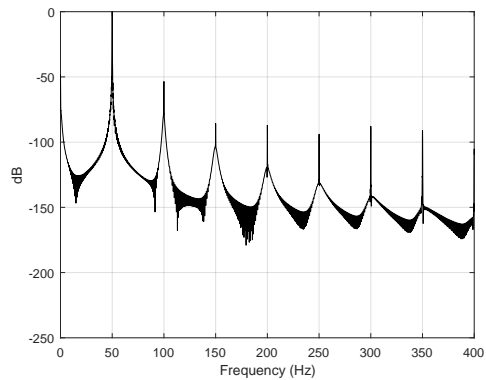
(c) Sample time set at $1e-7s$

Figure 54: Amplitude disparity related to sampling frequency. Sampling time is 10 seconds with a healthy motor in rated operations.

**Healthy Motor** A healthy simulation is showed in Figure 55. The frequencies and amplitudes of the harmonics are presented in Table 11.

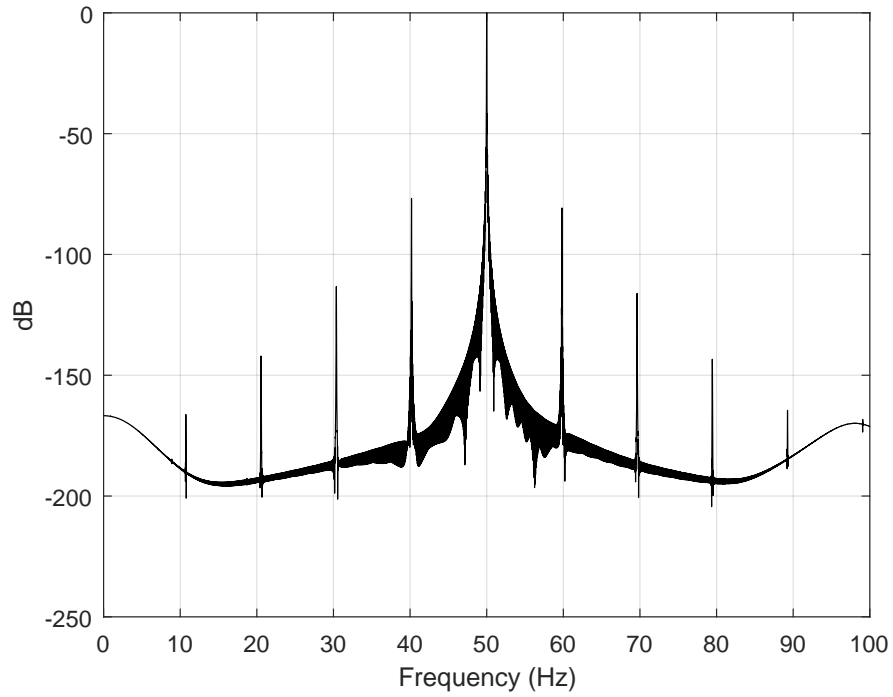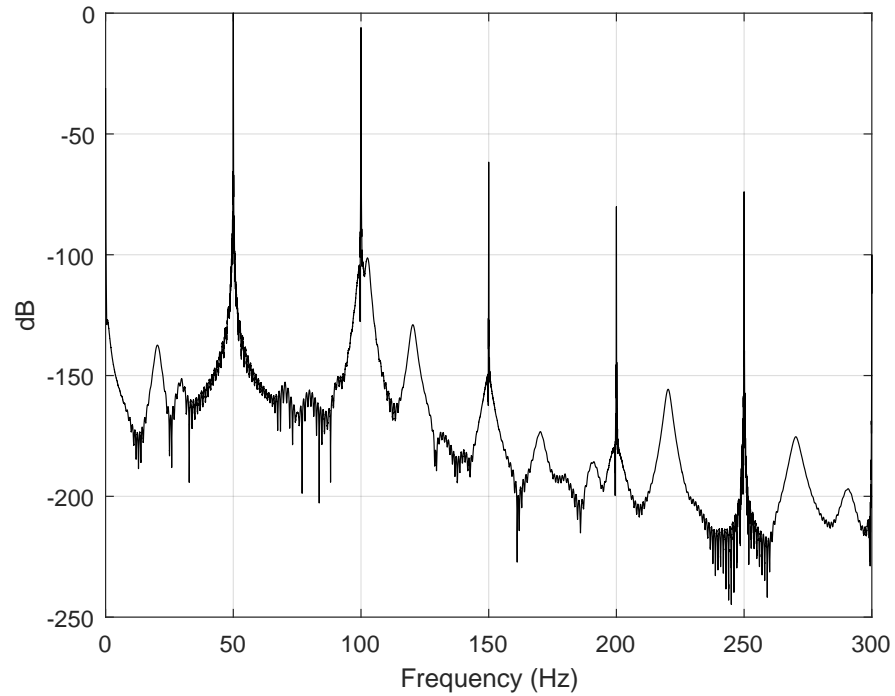
Figure 55: Simulated frequency spectrum from stator current with healthy motor. Simulation time is 60 seconds with step size $1e-6$ in discrete steps.

Table 11: Results from simulation with three broken rotor bars, PWM, transformers and subsea cable. Mean rotor speed is 1489.rpm

	Sim[Hz]	Sim[dB]
$2f$	100.00	-5.99
$3f$	150.00	-61.68
$4f$	200.00	-80.16
$5f$	250.00	-73.95

Broken rotor bars   A simulation with 3 broken rotor bars is showed in Figure 56, with details in Table 12. The mean rotor speed was 1489.1 rpm.

(a) $40-110Hz$

(b) $40-60Hz$
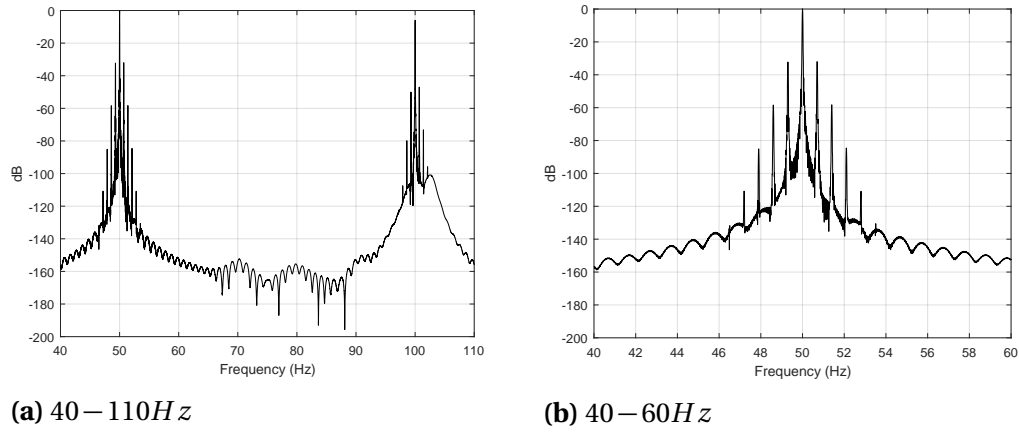
Figure 56: Simulated frequency spectrum from stator current with three broken rotor bars. Simulation time is 60 seconds with step size $1e-6$ in discrete steps. Mean rotor speed was 1489.1rpm.

Table 12: Results from simulation with three broken rotor bars, PWM, transformers and subsea cable. Mean rotor speed is 1489.1rpm.

	Rated*	Sim[Hz]	Sim[dB]
$f(1+2s)$	50.67	50.70	−31.99
$f(1+4s)$	51.35	51.40	−58.26
$f(1+6s)$	52.02	52.10	−84.55
$f(1-2s)$	49.33	49.30	−32.24
$f(1-4s)$	48.65	48.60	−58.40
$f(1-6s)$	47.98	47.90	−85.08

When using Equation 2.7 for estimating the amount of rotor bars, it yields 2.84.

Eccentricity   A simulation of mixed eccentricity with $1mm$ offset, $245mm$ as minor axes and $247.5mm$ as major axes is showed in Figure 57, with details in Table 13. The mean rotor speed in the simulation was $1490.0rpm$.
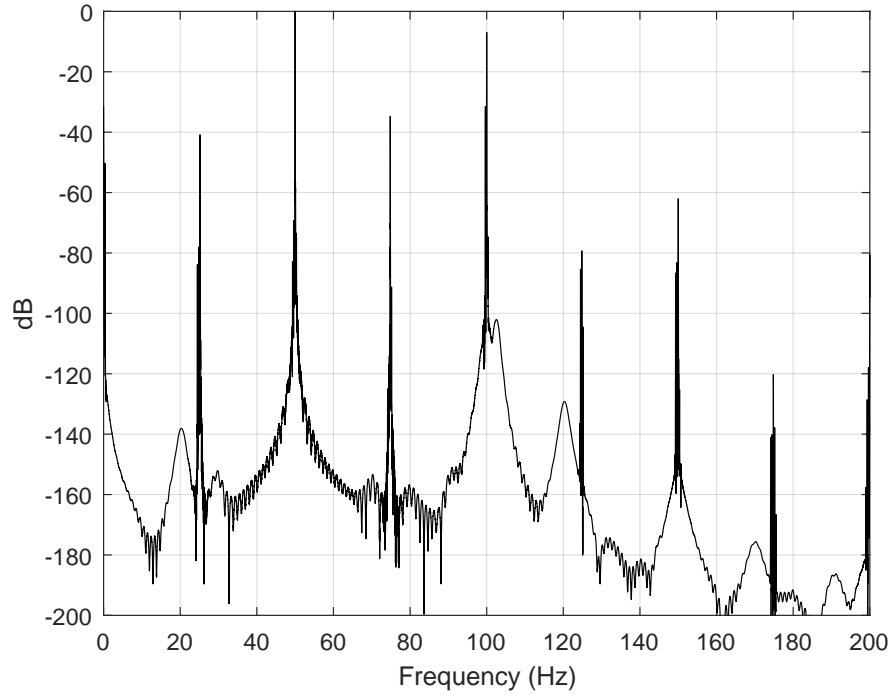
Figure 57: Simulated frequency spectrum from stator current with mixed eccentricity. Simulation time is 60 seconds with step size $1e-6$ in discrete steps. Mean rotor speed was 1490.0rpm.

Table 13: Results from simulation with mixed eccentricity, PWM, transformers and subsea cable. Mean rotor speed is 1490.0rpm

	Rated*	Sim[Hz]	Sim[dB]
$\lvert f+1f_r\rvert$	74.83	74.83	-34.76
$\lvert f+2f_r\rvert$	99.67	99.66	-31.48
$\lvert f+3f_r\rvert$	124.50	124.48	-85.36
$\lvert f+4f_r\rvert$	149.33	149.32	-86.63
$\lvert f+5f_r\rvert$	174.17	174.14	-141.06
$\lvert f-1f_r\rvert$	25.17	25.17	-40.87
$\lvert f-2f_r\rvert$	0.33	0.34	-50.25
$\lvert f-3f_r\rvert$	24.50	24.48	-83.85
$\lvert f-4f_r\rvert$	49.33	49.31	-82.80
$\lvert f-5f_r\rvert$	74.17	74.14	-125.01

Bearing Fault   A simulation of cage defect is showed in Figure 58, with details in Table 14. Only the two sideband frequencies from the fundamental harmonic can be found in the FFT, but there are also frequency peaks around the other harmonics as well, given as $f_{BFC} = | kf \pm nf_x |$ where f is the supply frequency, $k = 1, 2, 3..$, $n = 1, 2, 3..$ and f_x is f_c from Equation 3.49. The mean speed of the simulation was 1490.3 rpm.
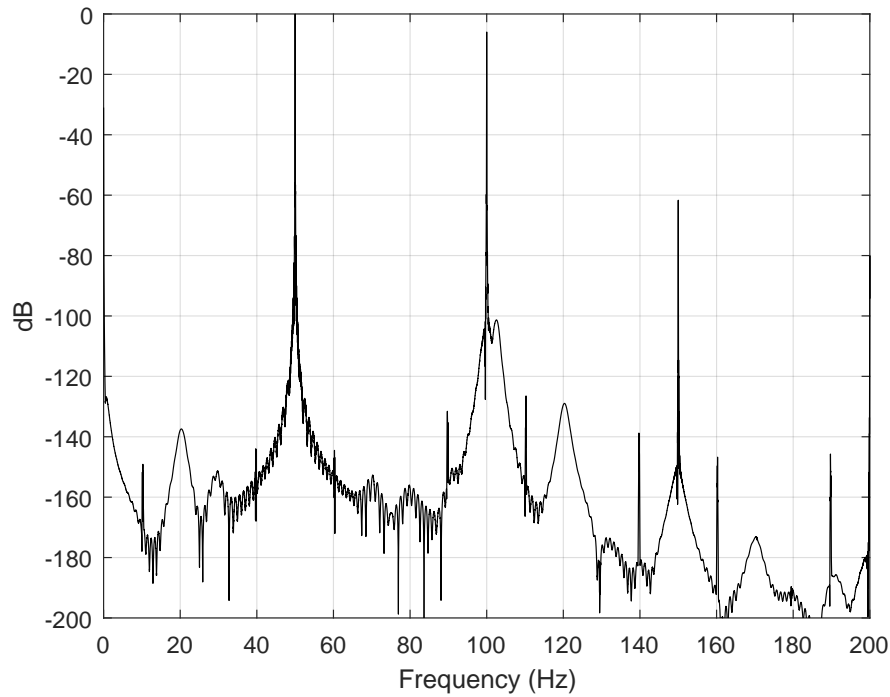
Figure 58: Simulated frequency spectrum from stator current with cage defect. Simulation time is 60 seconds with step size $1e-6$ in discrete steps. Mean rotor speed is 1490.3rpm.

Table 14: Results from simulation with cage defect, PWM, transformers and subsea cable. Mean rotor speed is 1490.3rpm. *The $| f - 1f_t |$ component is spread in three pikes from $39.65Hz$ to $39-87Hz$.

	Rated	Sim[Hz]	Sim[dB]
$| f + 1f_t |$	60.23	60.26	-144.51
$| f - 1f_t |$	39.77	$39.65-39.87*$	-144.02

Stator Fault A simulation of stator fault with 1% shorted *a* phase is showed inFigure 59 with details in Table 15.
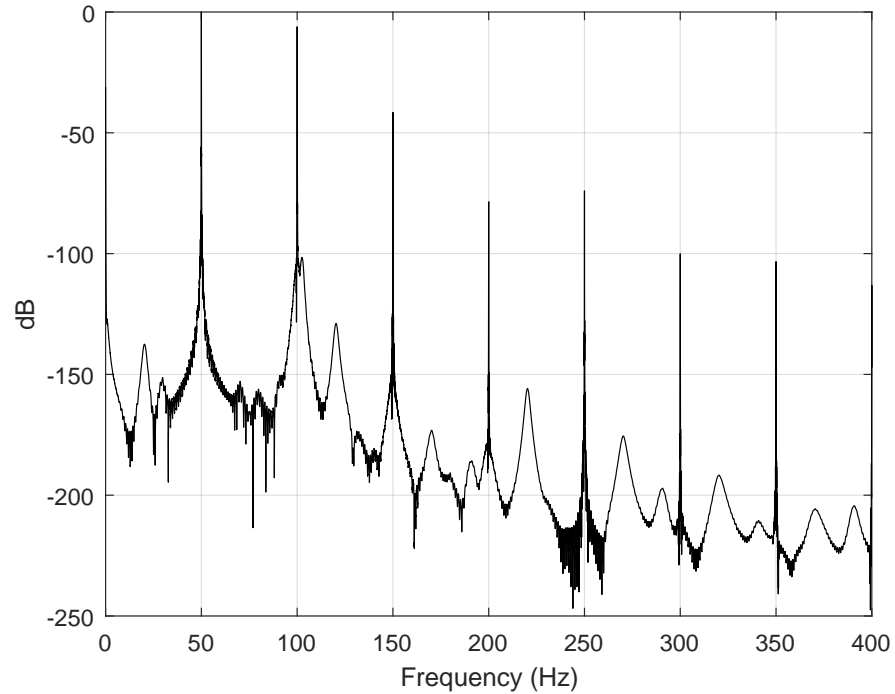
Figure 59: Simulated frequency spectrum from stator current with stator fault. Simulation time is 60 seconds with step size $1e-6$ in discrete steps.

Table 15: Results from simulation with stator fault PWM, transformers and subsea cable. Mean rotor speed is 1490.0rpm

	Rated	Sim[Hz]	Sim[dB]
$3f$	150.00	150.00	-41.55
$5f$	250.00	250.00	-74.04
$7f$	350.00	350.00	-103.32

5 Discussion

This section is divided into the different faults, discussing results with expected results and theory. It is worth mentioning that the FFT analysis is very sensitive to both sampling frequency and length. Holding sampling frequency constant and increasing length will give a higher resolution in the frequency spectra, which can affect the amplitude. This especially affects the process when determining the extent of the observed defect. In the results 60 seconds simulation are run which in the case of 3 broken rotor bars gives a mean amplitude of the first two side-bands at $-26.41dB$. When simulating the same case and only adjusting the simulation time to 300 seconds, gives a mean amplitude of $-25.83dB$ at the same frequencies. All of the expected frequencies can be found in the spectra, but there are minor deviations. Also, keep in mind that the y-axis is not linear, but in decibel dB. In the results for 1 BRB the mean amplitude for the first side-band components are $-36.58dB$, this yields a magnitude of $10^{\frac{-36.58}{20}}$ or 1.48% relative to the fundamental frequency.

The advantages with the DQ model are the simplicity, this results in shorter computation time. All the inductances are now time independent. The DQ model is also very practical when making a controller of the motor. If the synchronously rotating reference frame is used, the controller only needs to handle DC values, which means that a proportional-integral-derivative(PID) controller can be used.

The disadvantages are the assumptions that the motor is symmetrical. This works fine in a healthy case, but the assumption is no longer valid when simulation faults. The regular neat equations will now become messy and the diagonal matrices will be replaced by full 3x3 matrices. This is of course manageable as showed in this study.

5.1 Healthy Model

The healthy model is working satisfactory, although it does not include magnetic saturation or losses related to iron, friction, windage and ventilation. However, these losses are easy to include in the damping factor. If the saturation effect has

a vital role in the simulation this can be included as shown in[22]. This is a well documented model to simulate a symmetrical induction motor.

5.2   Broken Rotor Bar Model

The BRB model does not include end ring resistance and assumes symmetry in the rotor related inductance L_{rr}, L_{sr} and L_{rs}. This simplification gives a good response in the frequency domain where the side-band frequencies are as expected from Equation 2.6 with minor exceptions both in the $f(1-6s)$ frequency, this could be a resolution limitation. When increasing the amount of broken bars the amplitude of the side-band frequencies also increases, as expected. When using Equation 2.7 to determine how many broken bars there are, it falls short with a factor of 1.23 with both 1 and 3 BRB. Increasing the simulation time as previously mentioned decreases the deviation from the formula to a factor of 1.15. However, the formula for determining should only be used as an indication[49], and in practical cases it may be corrected by a known factor.

5.3   Eccentricity Model

In the case of mixed eccentricity all of the produced frequencies are as expected with minor deviations. The amplitude of the harmonics is also dependent on the amount of eccentricity, which it should. This is a simplification which did not include varying other than mutual inductance, but it gives satisfactory results around the fundamental frequency. The model does not include any of the higher frequencies found in Equation 2.8, this is an apparent drawback. If the operator wants a more realistic simulation of eccentricity fault, MWFA can be used to calculate the inductances under these conditions. How to use MWFA is described in section 3.6.1, but it also needs to be transformed to the DQ reference frame. This makes the MWFA inconvenient in the DQ model.

5.4 Bearing Fault Model

The bearing faults are developed from load modulation, the response in the frequency domain are as expected. This model does not include any varying of the inductance, but gives satisfactory performance anyhow. The magnitude of the load modulation is not calculated from any sources which may give an unrealistic response, this is however easy to fix in the "gain" block. Also, the load modulation is a sine wave, in a real case this may not be so, but can easily be changed through for example a "Matlab Function" block.

5.5 Stator Fault Model

The stator fault model does not include frequencies from Equation 2.10 which it should. The odd harmonic frequencies from Equation 2.11 are clearly visible.

5.6 Subsea Model

It is clear when simulating the subsea model in a healthy condition that the sampling frequency affects the performance of the motor. Both Figure 53 and Figure 54 indicates that higher sampling frequency results in a better performance. Although knowing this, the sampling step time is limited at $1e-6$. The subsea model uses a 6-pulse PWM as source, it is well known that PWM introduces harmonics[23]. Both even and odd harmonics can be found in Figure 54 , this can also be found in practical studies with VSD and SCIM[50]. One way of reducing the harmonics is as mentioned to increase sampling frequency in simulation and switching frequency of the PWM. Filters are used in practical cases to decrease harmonics[51].

Similar in all subsea simulation cases are the new frequency components around the harmonics. As for example with BRB, the frequency components to be expected are $f_{BRB} = (1 \pm 2ns)f$. In the subsea model these components are not only produced around the fundamental frequency, but also around the harmonics, as $f_{BRB2} = (l \pm 2ns)f$ where l is 1,2,3.. This also happens in the other simulations related to the subsea model.

The frequency components are in all cases where they should be, and also the extra around the harmonics. For the BRB and eccentricity fault they are very similar to the simulation without the subsea model. Estimation of amount of broken rotor bars are closer in this simulation. In the bearing fault the amplitude is much lower than without subsea model, the low amplitude will be difficult to detect in practical cases. A former study raised doubt on the usage of MCSA for bearing faults in a subsea context as a result of the low amplitudes [50]. In the stator fault it can be difficult to separate a stator fault from the healthy harmonics, although the faulted is at a higher amplitude. A filter would make this easier.

A drawback with the model are the reactance calculations which are dependent on inductance and rated frequency. Meaning that these are constant when a rated frequency is determined. If a VSD should be used, the model needs to be customized so that the reactance is dependent on the input frequency from the PWM, not rated frequency which it is now. However, this is a minor modification.

6 Conclusion

The aim of this study was to develop a dynamic model of the squirrel cage induction motor with its typical failures.

A strategic approach was used when developing the different models. This was done by looking at how the faults affect the performance of the motor and studying how to integrate it. First all the faulty models were developed separately before they were integrated to a generic model. Much of the modelling work are based on previous studies, but further developed. For the stator and rotor fault models this work involves solving the equations for transforming abc quantities to $qd0$ with possibilities to simulate failures in all phases, not just phase a as the work which it is based on. In the bearing fault model this work involves deriving equations and a method to simulate a specific type of bearing fault, not only general mechanical faults. The eccentricity model is the same as being described in the source which it is based on. The work in this model was to derive the mixed eccentricity equation and integrate it to Simulink. All these models were integrated to a generic model where also a graphical user interface(GUI) is developed. This releases the need for declaring variables in Matlab, making it easier to operate. The generic model was also tested in a subsea context with PWM source, cable model and transformers.

MCSA was used to validate the performance of the generic model. The results were in accordance with anticipated values, confirming the quality of the model. The only exception was the stator fault model which was missing a series of frequency components $f_{ss1} = \left(k \pm n \frac{1-s}{p} \right) f$. However, the stator fault did have another series of expected frequencies $f_{ss2} = 3kf$. This makes the generic model applicable in modelling all the four typical failures in the SCIM. In a subsea context the model gave satisfactory results, similar to earlier practical cases.

6.1 Future Work

There are some improvements that can be made on the model, making it more realistic. It should also be validated against other condition monitoring techniques, to clarify its performance.

To improve the model in the BRB case, the modifications of the rotor inductance can be included as explained in[10]. The BRB model also neglects end ring resistance, this could be included. If this is done, a simulation of cracked or broken end rings can be executed.

The eccentricity model does only vary the mutual inductance, which is not the case in reality. Both stator, rotor and mutual inductance are varying in a mixed eccentricity case, this can be included.

The stator model does not contain any of the expected frequencies from Equation 2.10. Further work could be to explain why these frequencies are absent and find other alternatives to model stator fault.

The bearing fault only modulates the load, a more realistic simulation will be modulating both load and inductance. Combining MWFA with load modulation can give a better performance of the model.

The subsea model are very simple and should be modified, for example; including mutual inductance and capacitance between the phases and ground in the cable, making a controller and include a filter.

Bibliography

[1] International Energy Agency. *World Energy Outlook 2016*. OECD Publishing, November 2016. ISBN 9264264949.

[2] OECD Publishing. *World Energy Outlook 2017 -*. OECD Publishing, Paris, November 2017. ISBN 9789264282056.

[3] P. C. Krause and C. H. Thomas. Simulation of symmetrical induction machinery. *IEEE Transactions on Power Apparatus and Systems*, 84(11):1038–1053, Nov 1965. ISSN 0018-9510.

[4] W.T. Thomson and I. Culbert. *Current Signature Analysis for Condition Monitoring of Cage Induction Motors: Industrial Application and Case Histories*. IEEE Press Series on Power Engineering. Wiley, Hoboken, NJ, 2017. ISBN 9781119029595.

[5] H.A. Toliyat, S. Nandi, S. Choi, and H. Meshgin-Kelk. *Electric Machines: modelling, Condition Monitoring, and Fault Diagnosis*. CRC Press, 2016. ISBN 9780849370274.

[6] R. O. Raad, T. Henriksen, H. B. Raphael, and A. Hadler-Jacobsen. Converter-fed subsea motor drives. *IEEE Transactions on Industry Applications*, 32(5):1069–1079, Sep 1996. ISSN 0093-9994.

[7] Arvind Singh, Bevon Grant, Ronald DeFour, Chandrabhan Sharma, and Sanjay Bahadoorsingh. A review of induction motor fault modelling. *Electric Power Systems Research*, 133:191 – 197, 2016. ISSN 0378-7796. URL http://www.sciencedirect.com/science/article/pii/S0378779615003946.

[8] Xianrong Chang, V. Cocquempot, and C. Christophe. A model of asynchronous machines for stator fault detection and isolation. *IEEE Transactions on Industrial Electronics*, 50(3):578–584, June 2003. ISSN 0278-0046.

[9] Shuo Chen and Rastko Živanović. Modelling and simulation of stator and rotor fault conditions in induction machines for testing fault diagnostic techniques. *European Transactions on Electrical Power*, 20(5):611–629, 2010. ISSN 1546-3109.

[10] P. M. Santos, M. B. R. Corrêa, C. B. Jacobina, E. R. C. da Silva, A. M. N. Lima, G. Didiery, H. Raziky, and T. Lubiny. A simplified induction machine model to study rotor broken bar effects and for detection. In *2006 37th IEEE Power Electronics Specialists Conference*, pages 1–7, June 2006.

[11] Shuo Chen. Induction machine broken rotor bar diagnostics using prony analysis / shuo chen, 04 2008. URL https://www.researchgate.net/publication/221958027_Estimation_of_frequency_components_in_stator_current_for_the_detection_of_broken_rotor_bars_in_induction_machines.

[12] Bindu S. and V. V. Thomas. Characteristic signature identification of air-gap eccentricity faults using extended d-q model for three phase induction motor. In *2015 International Conference on Condition Assessment Techniques in Electrical Systems (CATCON)*, pages 157–162, Dec 2015.

[13] Lane Maria Rabelo Baccarini, Benjamim Rodrigues de Menezes, and Walmir Matos Caminhas. Fault induction dynamic model, suitable for computer simulation: Simulation results and experimental validation. *Mechanical Systems and Signal Processing*, 24(1):300 – 311, 2010. ISSN 0888-3270. URL http://www.sciencedirect.com/science/article/pii/S088832700900199X.

[14] O. V. Thorsen and M. Dalva. modelling of converter-fed motor drives for analyzing motor transients. In *Conference Record of the 2001 IEEE Industry Applications Conference. 36th IAS Annual Meeting (Cat. No.01CH37248)*, volume 2, pages 1139–1146 vol.2, Sept 2001.

[15] L. Sivertsen, B.T. Hjertaker, T.E. Kjenner, and S. Stjernberg. Condition monitoring of subsea electrical equipment using motor current signature analysis. *EPE Journal*, 22 (1):28–36, 2012.

[16] S. Nandi and H. A. Toliyat. Condition monitoring and fault diagnosis of electrical machines-a review. In *Conference Record of the 1999 IEEE Industry Applications Conference. Thirty-Forth IAS Annual Meeting (Cat. No.99CH36370)*, volume 1, pages 197–204 vol.1, 1999.

[17] N. Tesla. A new system of alternate current motors and transformers. *Transactions of the American Institute of Electrical Engineers*, V(10):308–327, July 1888. ISSN 0096-3860.

[18] M. Mitolo and M. Tartaglia. Galileo farraris - a life dedicated to the electric sciences [history]. *IEEE Industry Applications Magazine*, 22(5):8–11, Sept 2016. ISSN 1077-2618.

[19] I. Boldea and S.A. Nasar. *The Induction Machine Handbook*. Electric Power Engineering Series. CRC Press, 2010. ISBN 9781420066685.

[20] P. C. Sen. *Principles of Electric Machines and Power Electronics*. John Wiley and Sons(WIE), 03 1989. ISBN 9780471617174.

[21] S. Bua, M. Dalva, and O.V. Thorsen. *Roterande elektriske maskiner*. Universitetsforlaget, 2007. ISBN 9788213025263.

[22] C.M. Ong. *Dynamic Simulation of Electric Machinery: Using MATLAB/SIMULINK*. Prentice Hall PTR, 1998. ISBN 9780137237852.

[23] N. Mohan, T.M. Undeland, and W.P. Robbins. *Power Electronics: Converters, Applications, and Design*. Number v. 1 in Power Electronics: Converters, Applications, and Design. John Wiley & Sons, 3rd edition, 2003. ISBN 9780471429081.

[24] P. Tavner. *Condition Monitoring of Rotating Electrical Machines*. Energy Engineering Series. Institution of Engineering and Technology, 2008. ISBN 9780863417412.

[25] G. B. Kliman, R. A. Koegl, J. Stein, R. D. Endicott, and M. W. Madden. Noninvasive detection of broken rotor bars in operating induction motors. *IEEE Transactions on Energy Conversion*, 3(4):873–879, Dec 1988. ISSN 0885-8969.

[26] W. T. Thomson and M. Fenger. Case histories of current signature analysis to detect faults in induction motor drives. In *Electric Machines and Drives Conference, 2003. IEMDC'03. IEEE International*, volume 3, pages 1459–1465 vol.3, June 2003.

[27] P. Vas. *Parameter Estimation, Condition Monitoring, and Diagnosis of Electrical Machines*. Monographs in Electrical and E. Clarendon Press, 1993. ISBN 9780198593751.

[28] Report of large motor reliability survey of industrial and commercial installations, part i. *IEEE Transactions on Industry Applications*, IA-21(4):853–864, July 1985. ISSN 0093-9994.

[29] O. V. Thorsen and M. Dalva. Methods of condition monitoring and fault diagnosis for induction motors. *European Transactions on Electrical Power*, 8(5):383–395, 1998. ISSN 1546-3109.

[30] W. T. Thomson. On-line mcsa to diagnose shorted turns in low voltage stator windings of 3-phase induction motors prior to failure. In *IEMDC 2001. IEEE International Electric Machines and Drives Conference (Cat. No.01EX485)*, pages 891–898, 2001.

[31] A. Stavrou, H. G. Sedding, and J. Penman. Current monitoring for detecting inter-turn short circuits in induction motors. *IEEE Transactions on Energy Conversion*, 16(1): 32–37, Mar 2001. ISSN 0885-8969.

[32] James W. Cooley and John W. Tukey. An algorithm for the machine calculation of complex Fourier series. *Mathematics of Computation*, 19:297–301, 1965. ISSN 0025–5718. URL: `http://cr.yp.to/bib/entries.html#1965/cooley`.

[33] M. Heideman, D. Johnson, and C. Burrus. Gauss and the history of the fast fourier transform. *IEEE ASSP Magazine*, 1(4):14–21, October 1984. ISSN 0740-7467.

[34] W. Bober and A. Stevens. *Numerical and Analytical Methods with MATLAB for Electrical Engineers*. Computational Mechanics and Applied Analysis. Taylor & Francis, 2013. ISBN 9781466579279.

[35] W. T. Cochran, J. W. Cooley, D. L. Favin, H. D. Helms, R. A. Kaenel, W. W. Lang, G. C. Maling, D. E. Nelson, C. M. Rader, and P. D. Welch. What is the fast fourier transform? *Proceedings of the IEEE*, 55(10):1664–1674, Oct 1967. ISSN 0018-9219.

[36] Richard Lyons. Windowing functions improve fft results, part. *EDN Network*, 06 1998. URL `https://www.edn.com/electronics-news/4383713/Windowing-Functions-Improve-FFT-Results-Part-I`.

[37] R. H. Park. Two-reaction theory of synchronous machines generalized method of analysis-part i. *Transactions of the American Institute of Electrical Engineers*, 48(3):716–727, July 1929. ISSN 0096-3860.

[38] H. C. Stanley. An analysis of the induction machine. *Electrical Engineering*, 57(12):751–757, Dec 1938. ISSN 0095-9197.

[39] G. Kron. *Equivalent Circuits of Electric Machinery*. General Electric series. J. Wiley & Sons, 1951.

[40] D. S. Brereton, D. G. Lewis, and C. C. Young. Representation of induction-motor loads during power-system stability studies. *Transactions of the American Institute of Electrical Engineers. Part III: Power Apparatus and Systems*, 76(3):451–460, April 1957. ISSN 0097-2460.

[41] P.C. Krause, O. Wasynczuk, S.D. Sudhoff, and IEEE Power Engineering Society. *Analysis of electric machinery and drive systems*. IEEE Press series on power engineering. IEEE Press, 2nd. edition, 2002. ISBN 9780471143260.

[42] B. Ozpineci and L. M. Tolbert. Simulink implementation of induction machine model - a modular approach. In *Electric Machines and Drives Conference, 2003. IEMDC'03. IEEE International*, volume 2, pages 728–734 vol.2, June 2003.

[43] F. Filippetti, M. Martelli, G. Franceschini, and C. Tassoni. Development of expert system knowledge base to on-line diagnosis of rotor electrical faults of induction motors. In *Conference Record of the 1992 IEEE Industry Applications Society Annual Meeting*, pages 92–99 vol.1, Oct 1992.

[44] S. Nandi, R. M. Bharadwaj, and H. A. Toliyat. Mixed eccentricity in three phase induction machines: analysis, simulation and experiments. In *Conference Record of the 2002 IEEE Industry Applications Conference. 37th IAS Annual Meeting (Cat. No.02CH37344)*, volume 3, pages 1525–1532 vol.3, Oct 2002.

[45] R. R. Schoen, T. G. Habetler, F. Kamran, and R. G. Bartfield. Motor bearing damage detection using stator current monitoring. *IEEE Transactions on Industry Applications*, 31(6):1274–1279, Nov 1995. ISSN 0093-9994.

[46] J.I. Taylor and Inc Vibration Consultants. *The vibration analysis handbook*. Vibration Consultants, 1994. ISBN 9780964051706.

[47] F. J. Harris. On the use of windows for harmonic analysis with the discrete fourier transform. *Proceedings of the IEEE*, 66(1):51–83, Jan 1978. ISSN 0018-9219.

[48] B. Corne, B. Vervisch, C. Debruyne, J. Knockaert, and J. Desmet. Comparing mcsa with vibration analysis in order to detect bearing faults. a case study. In *2015 IEEE International Electric Machines Drives Conference (IEMDC)*, pages 1366–1372, May 2015.

[49] William T Thomson and Ian Culbert. *Current signature analysis for condition monitoring of cage induction motors: industrial application and case histories*. Wiley-IEEE Press, Hoboken, NJ, 2017. URL https://cds.cern.ch/record/2248495.

[50] Tom Erik Kjenner. Tilstandsovervåkning av frekvensstyrt undervannsmotordrift ved strømanalyse. Master's thesis, University of Bergen, 06 2010.

[51] A. H. Bonnett. Analysis of the impact of pulse-width modulated inverter voltage waveforms on ac induction motors. In *Proceedings of IEEE Pulp and Paper Industry Conference*, pages 68–75, Jun 1994.

Appendices

A   Appendix A - Derivation of Equations

A.1   Change of resistance

$$\Delta r = r_r^* - r_r = \frac{(2N_s)^2}{N/3 - n}r_b - \frac{(2N_s)^2}{N/3}r_b$$

$$= \frac{N_b/3\left(2N_s^2\right)r_b - (N/3 - n)(2N_s)^2\,r_b}{N/3\,(N/3 - n)}$$

$$= \frac{n\,(2N_s)^2\,r_b}{N/3\,(N/3 - n)} = \frac{(2N_s)^2\,r_b}{N/3}\frac{n}{N/3 - n} = \frac{3n}{N - 3n}r_r$$

A.2   qd0 Transformations

A.2.1   Deriving $\boldsymbol{v}_s^{qd0}$

$$\boldsymbol{v}_s^{abc} = p\boldsymbol{\lambda}_s^{abc} + \boldsymbol{r}_s^{abc}\,\boldsymbol{i}_s^{abc}$$

$$\boldsymbol{v}_s^{abc} = p\left[\boldsymbol{T}_{qd0}(\theta)\right]^{-1}\boldsymbol{\lambda}_s^{qd0} + \boldsymbol{r}_s^{abc}\left[\boldsymbol{T}_{qd0}(\theta)\right]^{-1}\boldsymbol{i}_s^{qd0}$$

$$\left[\boldsymbol{T}_{qd0}(\theta)\right]\boldsymbol{v}_s^{abc} = \left[\boldsymbol{T}_{qd0}(\theta)\right]p\left[\boldsymbol{T}_{qd0}(\theta)\right]^{-1}\boldsymbol{\lambda}_s^{qd0} + \left[\boldsymbol{T}_{qd0}(\theta)\right]\boldsymbol{r}_s^{abc}\left[\boldsymbol{T}_{qd0}(\theta)\right]^{-1}\boldsymbol{i}_s^{qd0}$$

$$\boldsymbol{v}_s^{qd0} = \left[\boldsymbol{T}_{qd0}(\theta)\right]p\left[\boldsymbol{T}_{qd0}(\theta)\right]^{-1}\boldsymbol{\lambda}_s^{qd0} + \boldsymbol{r}_s^{qd0}\boldsymbol{i}_s^{qd0}$$

The time-derivate term $p\left[\boldsymbol{T}_{qd0}(\theta)\right]^{-1}\boldsymbol{\lambda}_s^{qd0}$ can be expressed as

$$p[\boldsymbol{T}_{qd0}(\theta)]^{-1}\boldsymbol{\lambda}_s^{qd0} = \begin{bmatrix} -\sin(\theta) & \cos(\theta) & 0 \\ -\sin(\theta - \frac{2\pi}{3}) & \cos(\theta - \frac{2\pi}{3}) & 0 \\ -\sin(\theta + \frac{2\pi}{3}) & \cos(\theta + \frac{2\pi}{3}) & 0 \end{bmatrix}\frac{d\theta}{dt}\boldsymbol{\lambda}_s^{qd0} + [\boldsymbol{T}_{qd0}(\theta)]^{-1}p\boldsymbol{\lambda}_s^{qd0}$$

calculating $\left[\boldsymbol{T}_{qd0}(\theta)\right]p\left[\boldsymbol{T}_{qd0}(\theta)\right]^{-1}\boldsymbol{\lambda}_s^{qd0}$

$$\frac{2}{3}\begin{bmatrix} \cos(\theta) & \cos(\theta - \frac{2\pi}{3}) & \cos(\theta + \frac{2\pi}{3}) \\ \sin(\theta) & \sin(\theta - \frac{2\pi}{3}) & \sin(\theta + \frac{2\pi}{3}) \\ \frac{1}{2} & \frac{1}{2} & \frac{1}{2} \end{bmatrix}\begin{bmatrix} -\sin(\theta) & \cos(\theta) & 0 \\ -\sin(\theta - \frac{2\pi}{3}) & \cos(\theta - \frac{2\pi}{3}) & 0 \\ -\sin(\theta + \frac{2\pi}{3}) & \cos(\theta + \frac{2\pi}{3}) & 0 \end{bmatrix}\frac{d\theta}{dt}\boldsymbol{\lambda}_s^{qd0} + p\boldsymbol{\lambda}_s^{qd0}$$

yields

$$\begin{bmatrix} 0 & 1 & 0 \\ -1 & 0 & 0 \\ 0 & 0 & 0 \end{bmatrix}\frac{d\theta}{dt}\boldsymbol{\lambda}_s^{qd0} + p\boldsymbol{\lambda}_s^{qd0}$$

substituting this back equals

$$\boldsymbol{v}_s^{qd0} = \omega\begin{bmatrix} 0 & 1 & 0 \\ -1 & 0 & 0 \\ 0 & 0 & 0 \end{bmatrix}\boldsymbol{\lambda}_s^{qd0} + p\boldsymbol{\lambda}_s^{qd0} + \boldsymbol{r}_s^{qd0}\boldsymbol{i}_s^{qs0}$$

where $\omega = \frac{d\theta}{dt}$

A.2.2 Deriving $\boldsymbol{v}_r^{qd0}$

$$\boldsymbol{v}_r^{abc} = p\boldsymbol{\lambda}_r^{abc} + \boldsymbol{r}_r^{abc}\boldsymbol{i}_r^{abc}$$

$$\boldsymbol{v}_r^{abc} = p\left[\boldsymbol{T}_{qd0}(\theta-\theta_r)\right]^{-1}\boldsymbol{\lambda}_r^{qd0} + \boldsymbol{r}_r^{abc}\left[\boldsymbol{T}_{qd0}(\theta-\theta_r)\right]^{-1}\boldsymbol{i}_r^{qd0}$$

$$\left[\boldsymbol{T}_{qd0}(\theta-\theta_r)\right]\boldsymbol{v}_r^{abc} = \left[\boldsymbol{T}_{qd0}(\theta-\theta_r)\right]p\left[\boldsymbol{T}_{qd0}(\theta-\theta_r)\right]^{-1}\boldsymbol{\lambda}_r^{qd0} + \left[\boldsymbol{T}_{qd0}(\theta-\theta_r)\right]\boldsymbol{r}_r^{abc}\left[\boldsymbol{T}_{qd0}(\theta-\theta_r)\right]^{-1}\boldsymbol{i}_r^{qd0}$$

$$\boldsymbol{v}_r^{qd0} = \left[\boldsymbol{T}_{qd0}(\theta-\theta_r)\right]p\left[\boldsymbol{T}_{qd0}(\theta-\theta_r)\right]^{-1}\boldsymbol{\lambda}_r^{qd0} + \boldsymbol{r}_r^{qd0}\boldsymbol{i}_r^{qd0}$$

The time-derivate term $p\left[\boldsymbol{T}_{qd0}(\theta-\theta_r)\right]^{-1}\boldsymbol{\lambda}_r^{qd0}$ can be expressed as

$$p[\boldsymbol{T}_{qd0}(\theta-\theta_r)]^{-1}\boldsymbol{\lambda}_r^{qd0} =$$
$$\begin{bmatrix} -\sin(\theta-\theta_r) & \cos(\theta-\theta_r) & 0 \\ -\sin(\theta-\theta_r-\frac{2\pi}{3}) & \cos(\theta-\theta_r-\frac{2\pi}{3}) & 0 \\ -\sin(\theta-\theta_r+\frac{2\pi}{3}) & \cos(\theta-\theta_r+\frac{2\pi}{3}) & 0 \end{bmatrix}\frac{d(\theta-\theta_r)}{dt}\boldsymbol{\lambda}_s^{qd0} + [\boldsymbol{T}_{qd0}(\theta)]^{-1}p\boldsymbol{\lambda}_s^{qd0}$$

calculating $\left[\boldsymbol{T}_{qd0}(\theta-\theta_r)\right]p\left[\boldsymbol{T}_{qd0}(\theta-\theta_r)\right]^{-1}\boldsymbol{\lambda}_r^{qd0}$

$$\frac{2}{3}\begin{bmatrix} \cos(\theta-\theta_r) & \cos(\theta-\theta_r-\frac{2\pi}{3}) & \cos(\theta-\theta_r+\frac{2\pi}{3}) \\ \sin(\theta-\theta_r) & \sin(\theta-\theta_r-\frac{2\pi}{3}) & \sin(\theta-\theta_r+\frac{2\pi}{3}) \\ \frac{1}{2} & \frac{1}{2} & \frac{1}{2} \end{bmatrix} \times$$
$$\begin{bmatrix} -\sin(\theta-\theta_r) & \cos(\theta-\theta_r) & 0 \\ -\sin(\theta-\theta_r\frac{2\pi}{3}) & \cos(\theta-\theta_r-\frac{2\pi}{3}) & 0 \\ -\sin(\theta-\theta_r+\frac{2\pi}{3}) & \cos(\theta-\theta_r+\frac{2\pi}{3}) & 0 \end{bmatrix}\frac{d(\theta-\theta_r)}{dt}\boldsymbol{\lambda}_r^{qd0} + p\boldsymbol{\lambda}_r^{qd0}$$

yields

$$\begin{bmatrix} 0 & 1 & 0 \\ -1 & 0 & 0 \\ 0 & 0 & 0 \end{bmatrix}\frac{d(\theta-\theta_r)}{dt}\boldsymbol{\lambda}_r^{qd0} + p\boldsymbol{\lambda}_r^{qd0}$$

Substituting this back equals

$$\boldsymbol{v}_r^{qd0} = (\omega-\omega_r)\begin{bmatrix} 0 & 1 & 0 \\ -1 & 0 & 0 \\ 0 & 0 & 0 \end{bmatrix}\boldsymbol{\lambda}_r^{qd0} + p\boldsymbol{\lambda}_r^{qd0} + \boldsymbol{r}_r^{qd0}\boldsymbol{i}_r^{qs0}$$

where $\omega-\omega_r = \frac{d(\theta-\theta_r)}{dt}$

A.2.3 Deriving of r_s^{qd0}

Deriving $[\boldsymbol{T}_{qd0}(\theta)]\boldsymbol{r}_s^{abc}[\boldsymbol{T}_{qd0}(\theta)]^{-1}$. Setting $\theta = 0$ yields

$$\boldsymbol{r}_s^{qdo} = \frac{2}{3}\begin{bmatrix} 1 & -\frac{1}{2} & -\frac{1}{2} \\ 0 & -\frac{\sqrt{3}}{2} & \frac{\sqrt{3}}{2} \\ \frac{1}{2} & \frac{1}{2} & \frac{1}{2} \end{bmatrix}\begin{bmatrix} r_s & 0 & 0 \\ 0 & r_s & 0 \\ 0 & 0 & r_s \end{bmatrix}\begin{bmatrix} 1 & 0 & 1 \\ -\frac{1}{2} & -\frac{\sqrt{3}}{2} & 1 \\ -\frac{1}{2} & \frac{\sqrt{3}}{2} & 1 \end{bmatrix}$$

$$\boldsymbol{r}_s^{qdo} = \frac{2}{3}\begin{bmatrix} r_s & -\frac{1}{2}r_s & -\frac{1}{2}r_s \\ 0 & -\frac{\sqrt{3}}{2}r_s & \frac{\sqrt{3}}{2}r_s \\ \frac{1}{2}r_s & \frac{1}{2}r_s & \frac{1}{2}r_s \end{bmatrix}\begin{bmatrix} 1 & 0 & 1 \\ -\frac{1}{2} & -\frac{\sqrt{3}}{2} & 1 \\ -\frac{1}{2} & \frac{\sqrt{3}}{2} & 1 \end{bmatrix}$$

$$\boldsymbol{r}_s^{qdo} = \begin{bmatrix} r_s & 0 & 0 \\ 0 & r_s & 0 \\ 0 & 0 & r_s \end{bmatrix}$$

A.2.4 Deriving of r_r^{qd0}

Deriving $[\boldsymbol{T}_{qd0}(\theta - \theta_r)]\boldsymbol{r}_r^{abc}[\boldsymbol{T}_{qd0}(\theta - \theta_r)]^{-1}$. Setting $\theta = 0$ yields

$$\boldsymbol{r}_r^{qd0} = \frac{2}{3}\begin{bmatrix} \cos(-\theta_r) & \cos\left(-\theta_r - \frac{2\pi}{3}\right) & \cos\left(-\theta_r\frac{2\pi}{3}\right) \\ \sin(-\theta_r) & \sin\left(-\theta_r - \frac{2\pi}{3}\right) & \sin\left(-\theta_r + \frac{2\pi}{3}\right) \\ \frac{1}{2} & \frac{1}{2} & \frac{1}{2} \end{bmatrix}\begin{bmatrix} r_r & 0 & 0 \\ 0 & r_r & 0 \\ 0 & 0 & r_r \end{bmatrix}$$

$$\begin{bmatrix} \cos(-\theta_r) & \sin(-\theta_r) & 1 \\ \cos\left(-\theta_r - \frac{2\pi}{3}\right) & \sin\left(-\theta_r - \frac{2\pi}{3}\right) & 1 \\ \cos\left(-\theta_r + \frac{2\pi}{3}\right) & \sin\left(-\theta_r + \frac{2\pi}{3}\right) & 1 \end{bmatrix}$$

Solving the trigonimetric equations yields

$$\boldsymbol{r}_r^{qd0} = \begin{bmatrix} r_r & 0 & 0 \\ 0 & r_r & 0 \\ 0 & 0 & r_r \end{bmatrix}$$

A.2.5 Deriving of L_{ss}^{qd0}

Deriving $[\boldsymbol{T}_{qd0}(\theta)]\boldsymbol{L}_{ss}^{abc}[\boldsymbol{T}_{qd0}(\theta)]^{-1}$. Setting $\theta = 0$ and $L_{sm} = L_{ss}\cos\left(\frac{2\pi}{3}\right) = -\frac{1}{2}L_{ss}$ yields

$$\boldsymbol{L}_{ss}^{qd0} = \frac{2}{3}\begin{bmatrix} 1 & -\frac{1}{2} & -\frac{1}{2} \\ 0 & -\frac{\sqrt{3}}{2} & \frac{\sqrt{3}}{2} \\ \frac{1}{2} & \frac{1}{2} & \frac{1}{2} \end{bmatrix}\begin{bmatrix} L_{ls} + L_{ss} & -\frac{1}{2}L_{ss} & -\frac{1}{2}L_{ss} \\ -\frac{1}{2}L_{ss} & L_{ls} + L_{ss} & -\frac{1}{2}L_{ss} \\ -\frac{1}{2}L_{ss} & -\frac{1}{2}L_{ss} & L_{ls} + L_{ss} \end{bmatrix}\begin{bmatrix} 1 & 0 & 1 \\ -\frac{1}{2} & -\frac{\sqrt{3}}{2} & 1 \\ -\frac{1}{2} & \frac{\sqrt{3}}{2} & 1 \end{bmatrix}$$

$$\boldsymbol{L}_{ss}^{qd0} = \begin{bmatrix} L_{ls} + \frac{3}{2}L_{ss} & 0 & 0 \\ 0 & L_{ls} + \frac{3}{2}L_{ss} & 0 \\ 0 & 0 & L_{ls} \end{bmatrix}$$

A.2.6 Deriving of L_{sr}^{qd0}

Deriving $[\boldsymbol{T}_{qd0}(\theta)]\boldsymbol{L}_{sr}^{abc}[\boldsymbol{T}_{qd0}(\theta-\theta_r)]^{-1}$. Setting $\theta = 0$ yields

$$\boldsymbol{L}_{sr}^{qd0} = \frac{2}{3}L_{sr}\begin{bmatrix} 1 & -\frac{1}{2} & -\frac{1}{2} \\ 0 & -\frac{\sqrt{3}}{2} & \frac{\sqrt{3}}{2} \\ \frac{1}{2} & \frac{1}{2} & \frac{1}{2} \end{bmatrix}\begin{bmatrix} \cos\theta_r & \cos\left(\theta_r+\frac{2\pi}{3}\right) & \cos\left(\theta_r-\frac{2\pi}{3}\right) \\ \cos\left(\theta_r-\frac{2\pi}{3}\right) & \cos\theta_r & \cos\left(\theta_r+\frac{2\pi}{3}\right) \\ \cos\left(\theta_r+\frac{2\pi}{3}\right) & \cos\left(\theta_r-\frac{2\pi}{3}\right) & \cos\theta_r \end{bmatrix}$$

$$\begin{bmatrix} \cos(-\theta_r) & \sin(-\theta_r) & 1 \\ \cos\left(-\theta_r-\frac{2\pi}{3}\right) & \sin\left(-\theta_r-\frac{2\pi}{3}\right) & 1 \\ \cos\left(-\theta_r+\frac{2\pi}{3}\right) & \sin\left(-\theta_r+\frac{2\pi}{3}\right) & 1 \end{bmatrix}$$

solving the first two matrices yields

$$\boldsymbol{L}_{sr}^{qd0} = \frac{2}{3}L_{sr}\begin{bmatrix} \frac{3}{2}\cos(\theta) & \frac{3}{2}\cos\left(\theta+\frac{2\pi}{3}\right) & \frac{3}{2}\cos\left(\theta-\frac{2\pi}{3}\right) \\ \frac{\sqrt{3}}{2}\left(\cos\left(\theta_r+\frac{2\pi}{3}\right)-\cos\left(\theta_r-\frac{2\pi}{3}\right)\right) & \frac{\sqrt{3}}{2}\left(\cos\left(\theta_r-\frac{2\pi}{3}\right)\cos(\theta_r)\right) & \frac{\sqrt{3}}{2}\left(\cos(\theta_r)-\cos\left(\theta_r+\frac{2\pi}{3}\right)\right) \\ 0 & 0 & 0 \end{bmatrix}$$

$$\begin{bmatrix} \cos(-\theta_r) & \sin(-\theta_r) & 1 \\ \cos\left(-\theta_r-\frac{2\pi}{3}\right) & \sin\left(-\theta_r-\frac{2\pi}{3}\right) & 1 \\ \cos\left(-\theta_r+\frac{2\pi}{3}\right) & \sin\left(-\theta_r+\frac{2\pi}{3}\right) & 1 \end{bmatrix}$$

Solving the trigonometric equations yields

$$\boldsymbol{L}_{sr}^{qd0} = \begin{bmatrix} \frac{3}{2}L_{sr} & 0 & 0 \\ 0 & \frac{3}{2}L_{sr} & 0 \\ 0 & 0 & 0 \end{bmatrix}$$

A.2.7 Deriving of L_{rs}^{qd0}

Deriving $[\boldsymbol{T}_{qd0}(\theta-\theta_r)]\boldsymbol{L}_{rs}^{abc}[\boldsymbol{T}_{qd0}(0)]^{-1}$. Setting $\theta = 0$ yields

$$\boldsymbol{L}_{rs}^{qd0} = \frac{2}{3}L_{sr}\begin{bmatrix} \cos(-\theta_r) & \cos\left(-\theta_r-\frac{2\pi}{3}\right) & \cos\left(-\theta_r\frac{2\pi}{3}\right) \\ \sin(-\theta_r) & \sin\left(-\theta_r-\frac{2\pi}{3}\right) & \sin\left(-\theta_r+\frac{2\pi}{3}\right) \\ \frac{1}{2} & \frac{1}{2} & \frac{1}{2} \end{bmatrix}$$

$$\begin{bmatrix} \cos(\theta_r) & \cos\left(\theta_r-\frac{2\pi}{3}\right) & \cos\left(\theta_r+\frac{2\pi}{3}\right) \\ \cos\left(\theta_r+\frac{2\pi}{3}\right) & \cos(\theta_r) & \cos\left(\theta_r-\frac{2\pi}{3}\right) \\ \cos\left(\theta_r-\frac{2\pi}{3}\right) & \cos\left(\theta_r+\frac{2\pi}{3}\right) & \cos(\theta_r) \end{bmatrix}\begin{bmatrix} 1 & 0 & 1 \\ -\frac{1}{2} & -\frac{\sqrt{3}}{2} & 1 \\ -\frac{1}{2} & \frac{\sqrt{3}}{2} & 1 \end{bmatrix}$$

Multiplying the two first matrices and solving the trigonometric equations yields

$$\boldsymbol{L}_{rs}^{qd0} = \frac{2}{3}L_{sr}\begin{bmatrix} \frac{3}{2} & -\frac{3}{4} & -\frac{3}{4} \\ 0 & -\frac{3\sqrt{3}}{4} & \frac{3\sqrt{3}}{4} \\ 0 & 0 & 0 \end{bmatrix}\begin{bmatrix} 1 & 0 & 1 \\ -\frac{1}{2} & -\frac{\sqrt{3}}{2} & 1 \\ -\frac{1}{2} & \frac{\sqrt{3}}{2} & 1 \end{bmatrix}$$

$$\boldsymbol{L}_{rs}^{qd0} = \begin{bmatrix} \frac{3}{2}L_{sr} & 0 & 0 \\ 0 & \frac{3}{2}L_{sr} & 0 \\ 0 & 0 & 0 \end{bmatrix}$$

A.2.8 Deriving of L_{rr}^{qd0}

Deriving $[T_{qd0}(\theta - \theta_r)]L_{rr}^{abc}[T_{qd0}(\theta - \theta_r)]^{-1}$. Setting $\theta = 0$ and $L_{rm} = L_{rr}\cos\left(\frac{2\pi}{3}\right) = -\frac{1}{2}L_{rr}$ yields

$$L_{rr}^{qd0} = \frac{2}{3} \begin{bmatrix} \cos(-\theta_r) & \cos\left(-\theta_r - \frac{2\pi}{3}\right) & \cos\left(-\theta_r + \frac{2\pi}{3}\right) \\ \sin(-\theta_r) & \sin\left(-\theta_r - \frac{2\pi}{3}\right) & \sin\left(-\theta_r + \frac{2\pi}{3}\right) \\ \frac{1}{2} & \frac{1}{2} & \frac{1}{2} \end{bmatrix} \begin{bmatrix} L_{lr} + L_{rr} & -\frac{1}{2}L_{rr} & -\frac{1}{2}L_{rr} \\ -\frac{1}{2}L_{rr} & L_{lr} + L_{rr} & -\frac{1}{2}L_{rr} \\ -\frac{1}{2}L_{rr} & -\frac{1}{2}L_{rr} & L_{lr} + L_{rr} \end{bmatrix}$$

$$\begin{bmatrix} \cos(-\theta_r) & \sin(-\theta_r) & 1 \\ \cos\left(-\theta_r - \frac{2\pi}{3}\right) & \sin\left(-\theta_r - \frac{2\pi}{3}\right) & 1 \\ \cos\left(-\theta_r + \frac{2\pi}{3}\right) & \sin\left(-\theta_r + \frac{2\pi}{3}\right) & 1 \end{bmatrix}$$

Solving the matrices yields

$$L_{rr}^{qd0} = \begin{bmatrix} L_{lr} + \frac{3}{2}L_{rr} & 0 & 0 \\ 0 & L_{lr} + \frac{3}{2}L_{rr} & 0 \\ 0 & 0 & L_{lr} \end{bmatrix}$$

B   Appendix B - Parameters

The parameter of the test motors used in the experimental studies are listed below, note that some of the parameters are estimated and noted with *.

B.1   Parameters of Siemens Test Motor

Table 16: Parameters of Siemens 4kW induction motor

Siemens	
Rated Power	$4kW$
Rated Voltage	$380V$
Rated Frequency	$50Hz$
Rated Current	$9.2A$
Rated* Torque	$26.62Nm$
Rated Speed	$1435rpm$
Rated* Power Factor	0.81
Pole Number	4
Moment of Inertia	$0.01kgm^2$
Amount of Stator Slots	36
Amount of Rotor Bars	28
Bearing Ball Diameter B_d	$9.52mm$
Bearing Pitch Diameter P_d	$53.1mm$
Bearing Contact Angle β	$0°$
Amount of Bearing Balls	9
Inner Stator Radius*	$48.1mm$
Inner Rotor Radius*	$47.0mm$
Stator* Resistance	1.57661Ω
Rotor* Resistance	0.83373Ω
Stator* Inductance	$8.11179mH$
Rotor* Inductance	$8.53798mH$
Magnetizing* Inductance	$162.50333mH$

B.2   Parameters Related to the Subsea Model

Table 17: Subsea cable parameters[14]

$240mm^2$ $50Hz$	
Length	$30km$
Rated Voltage	$12kV$
Series Resistance	$0.091[\Omega/km]$
Series Inductance	$0.27[mH/km]$
Shunt Capacitance	$0.57[\mu F/km]$

Table 18: Parameters of a typical subsea motor[14], some parameters are missing and therefore estimated, these are noted with*

Typical Subsea Motor	
Rated Power	$670kW$
Rated Voltage	$6kV$
Rated Frequency	$50Hz$
Rated Torque*	$4265.4Nm$
Rated Power Factor	0.8
Pole Number*	4
Moment of Inertia	$8kgm^2$
Amount of Rotor Bars*	60
Bearing Ball Diameter* B_d	$31.75mm$
Bearing Pitch Diameter* P_d	$180.00mm$
Bearing Contact Angle* β	0°
Amount of Bearing Balls*	9
Inner Stator Radius*	$250mm$
Inner Rotor Radius*	$247.5mm$
Stator Resistance	$0.01p.u$
Rotor Resistance	$0.0092p.u$
Stator Reactance	$0.11p.u$
Rotor Reactance	$0.11p.u$
Magnetizing Reactance*	$2.2p.u$

C Appendix C - Matlab FFT Script

```
%% FFT with Hann window
close
L = length(z); % Amount of samples
NFFT = 2^nextpow2(L); % Next to power of 2 from length
fahann = z. hann(L); % Applying hann window on data
hannfft=fft(fahann,NFFT)/L; % Using FFT on windowed data
Fs = L/(Length_in_seconds); % Sampling frequency
f = Fs/2 linspace(0,1,NFFT/2+1); % X values
maxfft=max(20 log10(2 abs(hannfft))); % Finding maximum,
% used to normalize
plot(f, 20 log10(2 abs(hannfft(1:NFFT/2+1)))-maxfft,'k')
% Plotting and normalizing with dB scale
xlabel('Frequency (Hz)')
ylabel('dB')
axis([0 200 -250 inf])
grid on
```